Laterally loaded piles in sloping ground

R.M. Verhoef

Master of Science Thesis

TU Delft Delft University of Technology

Faculty of Civil Engineering and Geosciences

Laterally loaded piles in sloping ground

Master of Science Thesis

For the degree of Master of Science in Civil Engineering at Delft University of Technology

R.M. Verhoef

February 26, 2015

Faculty of Civil Engineering and Geosciences · Delft University of Technology

Student

R.M. (Rianne) Verhoef
Balthasar van der Polweg 328
2628 AZ Delft
06 - 430 36 160
rianneverhoef@gmail.com

Assessment Committee

Chairman	Prof. Ir. A.F. van Tol	TU Delft
Daily Supervisor	Dr. Ir. W. Broere	TU Delft
Daily Supervisor	Ir. S. Azzouzi	ARCADIS
Supervisor	Dr. Ir. K.J. Bakker	TU Delft
External Supervisor	Ir. D.J. Jaspers Focks	Witteveen+Bos
External Supervisor	Ir. J.L. Bijnagte	Deltares

Abstract

The subject of this master's thesis stems from a lack of design rules in the current regulations for dolphins located in sloping ground. Dolphins are very common objects in Dutch waterways, of which a large part are located in sloping ground. The lack of design rules causes difficulties between clients and contractors, possible unfavourable designs, and a potential inefficient use of steel, the material of which dolphins are mostly constructed. In other words, a better understanding of the behaviour of a laterally loaded pile in sloping ground, as a dolphin can be schematized, may save money in the future.

The master's thesis starts with a literature review. The literature showed that previous studies already carried out research to laterally loaded piles in sloping ground. Four full scale tests have been conducted [1] [2] [3] [4], several model scale tests have been performed [5] [6] [7] and three studies carried out finite element analyses [8] [9] [10]. These studies all conclude that reduction of the confining soil, due to a sloping ground, decreases the lateral capacity of the pile. Parameters that influence the amount of capacity's decline are the slope angle, θ, the soil parameters, the pile properties and the roughness of the pile-soil interface. Moreover, in all full scale tests the formation of a gap was observed. This gap indicates that the size of the passive wedge and its offered resistance determine the pile-soil interaction. The method suggested by literature to account for sloping ground in engineering practice, is the reduction of the p-y curves by a multiplier. Several p-multipliers are suggested by the different studies [5] [3] [4] [10]. Georgiadis and Georgiadis are at the most advanced stage with their research, they have developed new p-y curves for the undrained lateral pile response in sloping ground [10].

To better qualify the influencing parameters within the pile-soil interaction of a laterally loaded pile in sloping ground, a parametric study has been conducted. The starting point for this analysis were the conditions of Dutch waterways, to which the varied parameters are connected as much as possible. First, the software programs had to be validated. Nimityongskul's full scale test [3] and Mezazigh's model test [5] have been modelled in D-Sheet Piling, D-Pile Group and Plaxis 3D. It has been demonstrated by this validation that the HSsmall model is most suitable in Plaxis 3D to model a laterally loaded pile. In contrast, the Mohr-Coulomb model is not suitable.

In the parametric study performed in Plaxis 3D two different soil profiles have been considered; a homogeneous profile consisting of medium dense sand and a layered profile of a clay layer underlain by a deeper sand layer. Two different slope angles with infinite slope have been assessed, 1:3 and 1:4, and 3 different soil parameter sets for both profiles. At the end, an analysis has been performed with a finite slope, where the pile is located at the crest, in the middle and at the toe of the slope.

The most important observation of this analysis is the fact that the capacity of a laterally loaded pile in a sand slope is much more affected by the angle of the slope than the capacity of a laterally

loaded pile in a clay slope. This difference can be explained by the fact that the strength of sand is stress-dependent and the cohesion of clay is not. The influence of the sloping ground is qualified with the help of normalised curves derived from the load-displacement curves and p-y curves. The normalised curves lead to specific p-multipliers for the conditions in Dutch waterways.

Finally, a design recommendation is proposed for laterally loaded piles in sloping ground. A flow chart with 4 design steps is recommended in Chapter 5. First, the original p-y curve for a laterally loaded pile in horizontal level ground need to be selected. Hereafter, an appropriate p-multiplier need to be defined with help of the normalised p-y curves obtained from the Plaxis 3D analysis. The original p-y curves can then be combined with the selected multiplier to form new p-y curves to determine the pile-soil interaction of piles located in sloping ground.

Preface

This publication is the product of my thesis study, which is the final stage of my master Geo-Engineering at the Faculty of Civil Engineering and Geosciences at Delft University of Technology.

The master's thesis, titled "Laterally loaded piles in sloping ground" was written at the office of ARCADIS in Rotterdam under the supervision of Ir. S. Azzouzi. I would like to express my gratitude to ARCADIS and Ir. S. Azzouzi for providing the resources and support during my stay at ARCADIS.

Furthermore I would like to thank all the members of my assessment committee, Prof. Ir. A.F. van Tol, Dr. Ir. W. Broere and Dr. Ir. K.J. Bakker of the TU Delft, Ir. S. Azzouzi of ARCADIS, Ir. D.J. Jaspers Focks of Witteveen+Bos and Ir. J.L. Bijnagte of Deltares.

The guidance and knowledge of the committee were of great value for this thesis.

Delft, February 2015
Rianne Verhoef

Table of Contents

List of Figures

List of Tables

Chapter 1

Introduction

1-1 Problem description

In the deltaic area of the Netherlands, characterized by the harbours and the inland waterways to supply Western-Europe, the banks along the waterways are full of dolphins. A large part of these dolphins are located in the slopes of banks. Nevertheless, there is a lack of design rules in the current regulations for dolphins located in sloping ground.

Dolphins have two functions; either they can be breasting dolphins to protect a structure (e.g. a pillar of a bridge), or mooring dolphins to secure a ship by ropes. A dolphin, loaded by an impact force or a mooring force, leads to a soil-structure interaction problem between a long vertical pile, which is laterally loaded, and the surrounding soil. Often, these dolphins are constructed in sloping ground. This changes the pile-soil interaction, particularly when the pile is loaded towards the slope. This is the case for mooring dolphins.

There is already a clear description of the problem of laterally loaded piles in horizontal surface level, for example L.C. Reese and M.F.Randolph had a great contribution with their research. However, the knowledge about laterally loaded piles in sloping ground is still limited. There has been done some research, but none led to clear design rules for laterally loaded piles on a slope or to design rules for dolphins in sloping ground in international guidelines.

It is important to expand the knowledge about dolphins in sloping ground, for several reasons. Understanding of the pile-soil behaviour of a laterally loaded pile in a slope contributes to a safer and more substantiated design of the dolphin (a). If regulations are developed in the future, the discussion between client and contractor about the design approach for each single dolphin will decline and uniformity in dolphin design will be achieved (b). Last, if more knowledge is available about the laterally loaded pile in a slope, a better pile design can be made. For the large dolphins, a large amount of steel is used. A reduction in steel, achieved by a better design, is also a large saving in money(c).

The lack of design rules was also encountered by CUR Committee 206 of SBRCURnet, which led to the start of this master's thesis. The SBRCURnet is an independent knowledge network for the construction industry in the Netherlands. The CUR publishes recommendations for the Dutch construction industry for among others the expertise geotechnical engineering [17].

1-2 Objective

The objectives formulated at the start of this project are:

- To give a review of present literature about laterally loaded piles in a slope
- To validate/ verify the Plaxis 3D model on test results found in literature
- To analyse the soil- structure interaction of a laterally loaded pile in sloping ground in Plaxis 3D by varying parameters
- To formulate a (simplified) design method for the pile-soil interaction of laterally loaded piles in a slope

1-3 Outline of the master's thesis

The structure of this master's thesis follows the order of the defined objectives. **Chapter 2** starts with a description of the available literature. In the first section the design methods for laterally loaded piles in horizontal surface level are regarded. This is followed by the analytical solutions that are derived to take the slope into account, these focus on the adoption of the passive wedge to determine the ultimate soil resistance. In the next sections the conducted tests, both full scale, model scale and finite element analyses, are discussed. Chapter 2 ends with an evaluation of the literature.

In **Chapter 3** the software programs D-Sheet Piling, D-Pile Group and Plaxis 3D are validated to determine their potential capability for the sensitivity analysis in the next chapter. The validation is carried out with the help of two full scale tests and one centrifuge test. It ends with an conclusion about the capabilities of the software programs.

In **Chapter 4** the performed parametric study in Plaxis 3D is presented. The chapter starts with a description of the organisation of the sensitivity analysis; the starting points and the varied properties are defined. Hereafter, the results of the load displacement curves are set out and discussed. The results contain among others the load-displacement curves, p-y curves and the normalised curves of both.

Chapter 5 compares first the results of the parametric study with the results found in literature. This is followed by design recommendations for laterally loaded piles in sloping ground.

The master's thesis ends with **Chapter 6**. The final conclusions are here presented together with the recommendations. The recommendations are split into the recommendations for future reserach regarding laterally loaded piles and recommendations for future research regarding dolphins.

Chapter 2

Literature review

2-1 Laterally loaded piles in horizontal ground surface

A laterally loaded pile is a typical soil-structure interaction problem. Both the deformation of the soil and the pile need to be elaborated to find a solution for this problem. If the lateral load is applied at the pile, this will induce a lateral deformation starting at the top of the pile. This deformation will induce moments and shear forces in the pile and mobilise lateral resistance of the soil. The soil will provide resistance against the deformation of the pile. Therefore, the lateral deflection and the soil resistance have an interdependent relationship.

Due to the lateral load, normal stresses in the soil will increase in front of the pile, and decrease behind the pile. This may cause a gap which arises between the back of the pile and the surrounding soil, as observed by Davidson [18] and later by Gabr and Borden [1]. Furthermore, the soil in front of the pile may fail and develop a passive wedge, which moves upwards. Further down along the pile shaft, the soil will fail by flowing around the pile, with no gap present any more. For these two failure mechanisms, schematized at the left part of Figure 2-1, different models are developed, which are described by Reese and van Impe [19] and by Fleming at al. [11]. These models are explained in Section 2-1-2 and 2-1-3. But first, the chapter starts with a derivation of the analytical behaviour of the pile under a lateral load, which can be considered as a beam.

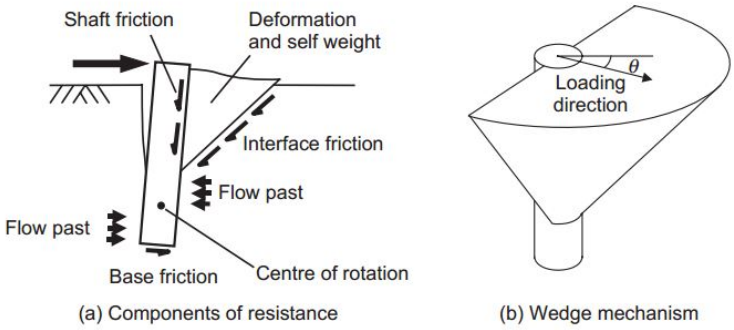

Figure 2-1: Collapse mechanism in the upper soil layer after Fleming et al. [11]

2-1-1 Beam model

In 1946 Hetenyi [20] determined that a pile subjected to a lateral load can be considered as a beam. He gives a derivation in his book for a differential equation, which provides a linear relationship between the pile deflection and the soil response. This relationship is defined in Equation 2-1, the derivation is enclosed in Appendix A. When the pile is only loaded laterally, the second term at the left side can be eliminated.

$$E_p I_p \frac{d^4y}{dx^4} + P_x \frac{d^2y}{dx^2} + E_{py} y = 0 \tag{2-1}$$

where
$E_p I_p$ = bending stiffness of the pile
y = lateral deflection of the pile
P_x = axial load on the pile
E_{py} = stiffness of the soil

In Figure 2-2 the response of the pile subjected to a lateral load is shown, with the corresponding mathematical relationships of Heteyeni. There are some limitations in the application of the above equation. To start with, the pile only can have a uniform cross section and consist of homogeneous and isotropic material. In addition, different soil layers can not be regarded. Furthermore, the soil must have a uniform modulus of subgrade reaction, which is not realistic. Last, the largest limitations are that only static situations can be considered, in which the proportional limit of the pile material can not be exceeded and that plasticity of the soil is not included in the model.

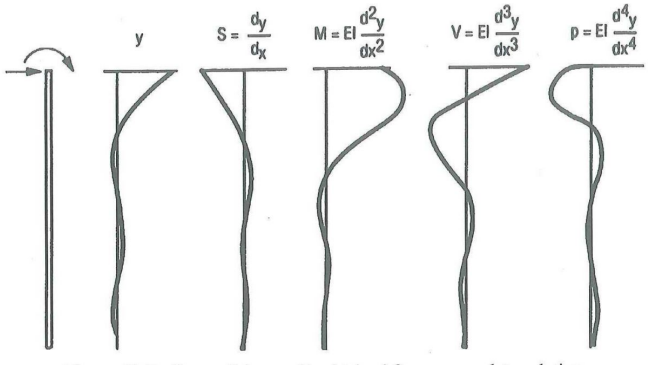

Figure 2-2: Response of a laterally loaded pile according to Heteyeni [12]

Nevertheless, Heteyeni's derivation formed the basis for the p-y cuves, which are nowadays used a lot in the engineering practice. In 1956 Reese and Matlock [21] extended the method by developing a solution that assumes a modulus of subgrade that increases with depth. Later, this was expanded to the nonlinear p-y method [12]. This method assigns a nonlinear spring (the subgrade modulus of the soil) to each soil layer. Over the years, a lot of full scale tests have been conducted on which the current p-y curves are calibrated. The p-y curves prescribed by the American Petroleum Institute (API) [22] are the standard in today's engineering practice. The software application D-Pile Group developed by Deltares [16] is also based on the p-y curves of the API.

2-1-2 Passive-wedge model

The passive-wedge model is based on the principle that normal stresses will increase in front of the pile due to the lateral load applied at the top of the pile. The increasing stresses cause the

soil to move up, and a passive wedge will develop as schematized in Figure 2-1. In this wedge, the resistance of the soil is provided by the normal force acting perpendicular to the bottom of the failure plane and the friction forces along the side planes of the failure wedge. The formation of the wedge will be confirmed in Section 2-3 by the tests of Gabr and Borden, Mirzoyan, Nimityongskul and Barker.

With the passive-wedge model one is able to determine the ultimate resistance of the soil against the laterally loaded pile. Since only the ultimate resistance can be derived, this is an ultimate strength model.

Clay

According to Reese, two different wedge types can be distinguished, one for clay and one for sand [19]. The passive wedge for clay can be found in Figure 2-3. The ultimate resistance of the soil, p_u, can be determined by solving the equilibrium for F_p by taking the weight of the wedge, W, and the forces on the sliding surfaces, F_s, F_n, F_t and F_f. If one then differentiates F_p with respect to H, the ultimate resistance of the soil can be determined using Equation 2-2.

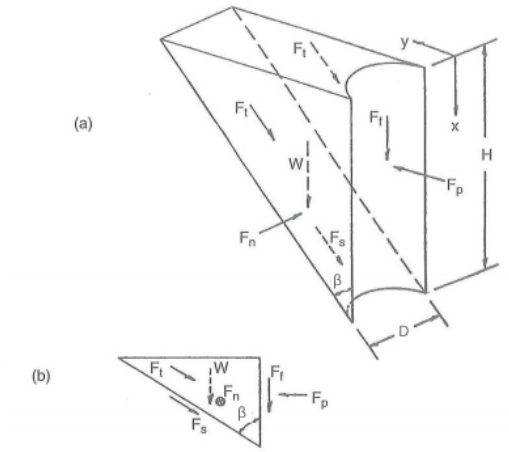

Figure 2-3: Assumed passive wedge-type failure for clay by Reese et al. [12]

$$p_u = c_a D[\tan\beta + (1+\kappa)\cot\beta] + \gamma DH + 2c_a H(\tan\beta\sin\beta + \cos\beta) \tag{2-2}$$

where

p_u	=	ultimate resistance near the surface per unit of length along the pile
c_a	=	average undrained shear strength over the depth H
β	=	angle of the inclined plane with the vertical
γ	=	unit weight of the soil
κ	=	reduction factor for shearing resistance along the face of the pile
D	=	diameter of the pile
H	=	depth below ground surface

Sand

The passive wedge for sand can be found in Figure 2-4. The force F_p can be obtained by solving the force equilibrium with the weight of the wedge, W, and the forces on the sliding surfaces, F_s, F_n, F_t and F_s, and subtracting the active force, F_a. If one then differentiates F_p with respect to

H, the ultimate resistance for the sand can be defined as:

$$p_u = \gamma H \Big[\frac{K_0 H \tan\phi \sin\beta}{\tan(\beta-\phi)\cos\Omega} + \frac{\tan\beta}{\tan(\beta-\phi)}(D + H\tan\beta\tan\Omega) + K_0 H \tan\beta(\tan\phi\sin\beta - \tan\Omega) - K_a D \Big] \tag{2-3}$$

where

ϕ	=	friction angle of the soil
K_0	=	coefficient of earth pressure at rest
K_a	=	minimum coefficient of active earth pressure
Ω	=	angle of the wedge

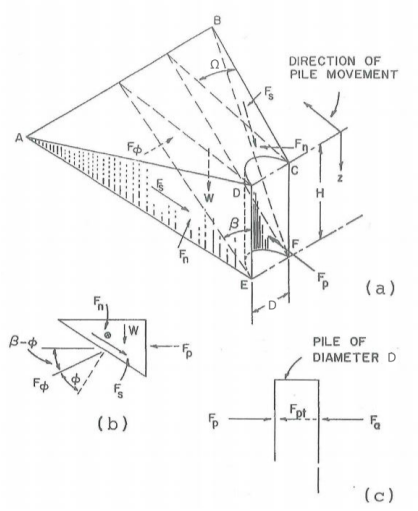

Figure 2-4: Assumed passive wedge-type failure for sand by Reese et al. [12]

The assumed passive wedges for clay and sand have different widths. The clay wedge has a width equal to the width of the pile. However, the sand wedge has an extension with two side flanks, which have an angle Ω. Field tests of Gabr and Borden [1] and Nimityongskul [3] show that for clay the wedge is definitely wider than the width of the pile. Therefore, the assumption for the width is not realistic and the amount of mobilised soil may be underestimated by the passive wedge of Reese et al. Furthermore, it is worth mentioning that in Reese's model for sand the active force F_a is substracted from the passive force, which means that Reese does assume that there exists no gapping for sand. In Section 2-3 will be demonstrated with the help of tests that this assumption is also incorrect.

2-1-3 Ultimate soil resistance at greater depth

Lower down the laterally loaded pile, the passive-wedge equilibrium is no longer valid any more. At greater depths, considerable larger ultimate soil resistances are developed by the soil than near to the ground surface. However, the limiting pressures are normally not reached, since in practice the pile will fail by the formation of a plastic hinge in the pile. Next, two different models to derive the ultimate soil resistance will be discussed, one developed by Randolph and Houlsby [23] and the other by Reese et al. [19].

Randolph and Houlbsy

To calculate the ultimate soil resistance at a greater depth below the soil surface, a limit analysis is developed by Randolph and Houlsby in 1984 as shown in Figure 2-5 [23], called the flow mechanism. In front of the pile an area of high mean stress will develop due to the lateral load subjected to the pile, at the back of the pile an a region of low stresses will occur. Consequently, the soil will flow around the pile from the front side to the back side.

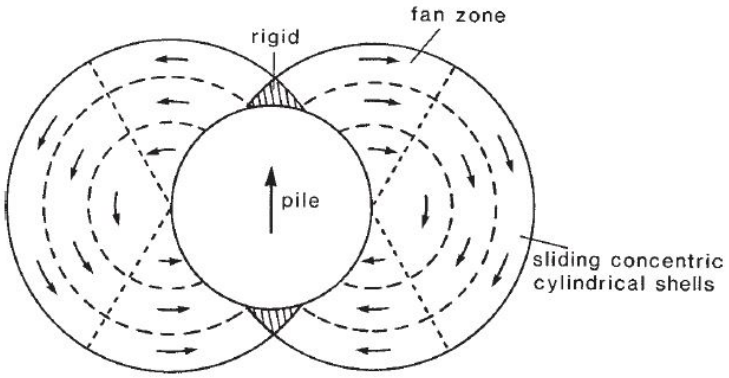

Figure 2-5: Flow mechanism for soil around laterally loaded pile by Randolph and Houlbsy [11]

Randolph and Houlbsy's model is developed for cohesive soils. The model assumes that there is a lower bound and an upper bound solution on the loads which will cause collapse with an associated flow rule. The lower bound solution can be obtained by finding the soil stresses at great depths which are in equilibrium with the applied load, but does not exceed the yield criterion of the soil. Randolph and Houlbsy's lower bound solution is defined in Equation 2-4.

$$\frac{P}{cD} = \pi + 2\Delta + 2\cos\Delta + 4\left[\cos\left(\frac{\Delta}{2}\right) + \sin\left(\frac{\Delta}{2}\right)\right] \tag{2-4}$$

Where Δ is a function of the cohesion, c, and adhesion, a; $\Delta = \arcsin(a/c)$. The function P/cD varies in value from $6 + \pi$ at $\Delta = 0$ to $4\sqrt{2} + 2\pi$ at $\Delta = \pi/2$ (i.e. from 9.14 to 11.94).

The upper bound solution is defined as:

$$\frac{P}{cD} = \pi + 2\Delta + 4\cos\psi(\sqrt{2} + \sin\psi) \tag{2-5}$$

where the angle ψ is equal to $\pi/4 - \Delta/2$.

Reese et al.

Reese et al. [12] developed a model for both clay and sand to determine the ultimate lateral resistance at greater depths. Also they acknowledge that as the maximum value of soil resistance will occur, the soil moves horizontally. To convert this into a formula, the limit equilibrium models plotted in Figure 2-6 were developed. A cylindrical pile is schematized with blocks of soil around it. When the pile moves as indicated in the Figure, block 5 is moved and stress is generated in that block to cause failure. The stresses are transmitted through block 4 and on around the pile to block 1. It is assumed that block 3 is not distorted, but on the sides of the block failure stresses develop.

For clay it is assumed that the developed resistance on each side of the pile is equal to $cD/2$. The ultimate resistance at greater depth for clay can then be defined as in Equation 2-6. For sand it is assumed that the states of stresses are as shown in Figure 2-6b. The ultimate resistance at greater depth for sand can then be defined as in Equation 2-7.

$$p_u \leq (\sigma_6 - \sigma_1 + c)/D \leq 11cD \tag{2-6}$$

$$p_u \leq K_a D\gamma H(\tan^8 \beta - 1) + K_0 D\gamma H \tan\phi \tan^4 \beta \tag{2-7}$$

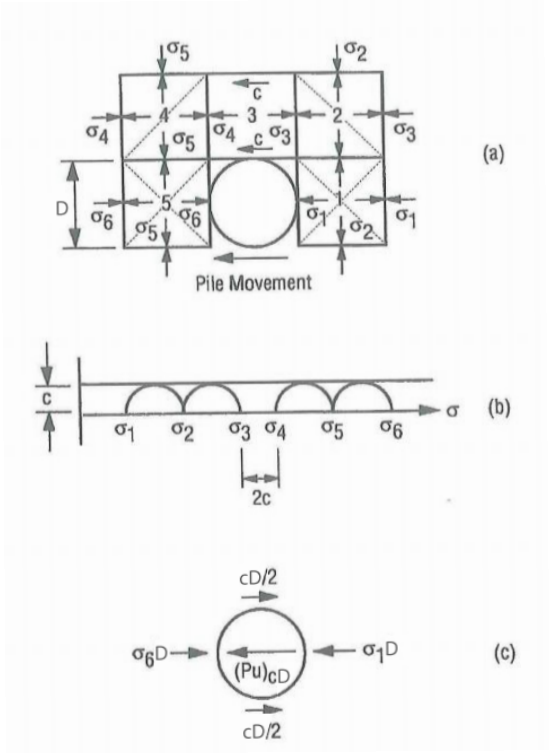

(a) Assumed mode of soil failure by lateral flow around a pile in clay by Reese et al.: (a) section through pile; (b) Mohr-Coulomb diagram; (c) forces acting on a section of a pile [12]

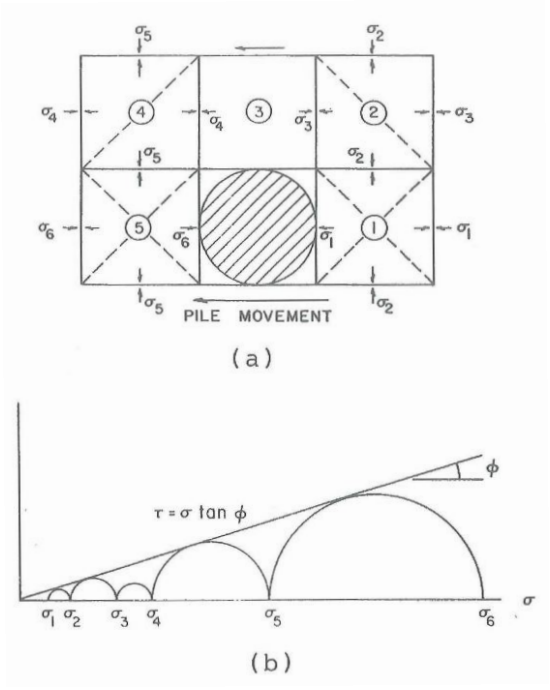

(b) Assumed mode of soil failure by lateral flow around a pile in sand by Reese et al.: (a) section through pile; (b) Mohr-Coulomb diagram [12]

Figure 2-6: Assumed mode of soil failure by lateral flow around a pile for sand and clay by Reese et al. [12]

2-1-4 Other methods used in engineering practice

Blum

The method of Blum is published in 1932 [24]. Since it is a very simple and quick method, it is more than eighty years later still used in the engineering practice for first estimates. The input parameters of the model are the maximum load on the pile, the diameter of the pile and the friction angle and volume weight of the soil, which give the output as the length of the pile. Due to the simplicity of the model, it has some limitations; it is an ultimate strength model which is only suitable for short rigid piles in homogeneous non-cohesive soils. As sketched in Figure 2-7 Blum considers the moment and force equilibrium at the theoretical penetration depth t_0, to

obtain the real penetration depth, the theoretical depth should be increased with 20%. Since it is an ultimate strength model, it is assumed that the full passive wedge is mobilised, plotted at the left side. The soil resistance is substituted by a point load in the model.

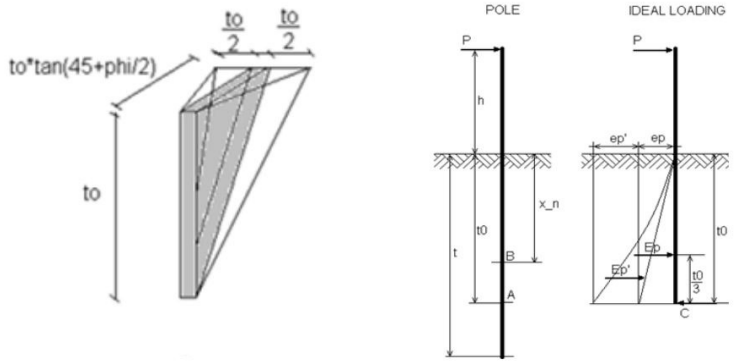

Figure 2-7: Model of Blum [13]

Brinch Hansen

The method of Brinch Hansen dates from 1961 [25]. It is, like Blum's model, an ultimate strength model, but it has more options. It can be used for layered soils and cohesive soils. However, it is not possible to calculate the deflection of the pile. In D-Pile Brinch Hansen's method is implemented to determine the lateral soil resistance by lateral earth pressure coefficients.

The resultant earth pressure, the passive pressure minus the active pressure, at depth D is calculated by Equation 2-8. Two factors influence the resultant earth pressure, e^D, the cohesion, c and the vertical effective overburden pressure, q. These quantities are multiplied by the corresponding earth pressure coefficients. The lateral earth pressure coefficients are determined for three different depths; at ground level, at moderate depth and at great depth.

$$e^D = qK_q^D + cK_c^D \tag{2-8}$$

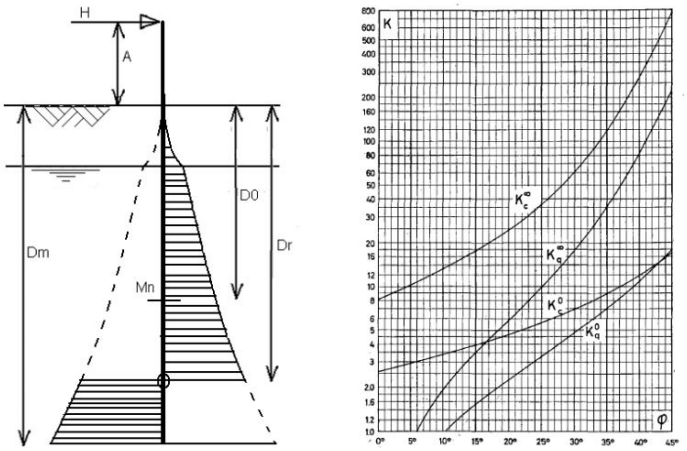

Figure 2-8: Model of Brinch Hansen and associated graph to obtain earth pressure coefficients [13]

Broms

Broms developed his method in 1964 [26]. The method uses the theory of subgrade reaction and it was for the first time possible to calculate the deflections and bending moments of the pile with an ultimate strength model. With a range of design charts obtained by Broms a suitable pile can be chosen. Deflections can only calculated for the "working load range", which is $0.3 - -0.5$ of the ultimate pile capacity. Broms assumes that for this range the soil behaves linearly elastic. Another simplification of the model is that for cohesive soils the subgrade modulus is assumed to be constant with depth. The method is validated by field tests; the calculated deflections are not very accurate. However, on ultimate lateral resistance the method for cohesive soil is reasonably accurate and for cohesionless soil it is conservative

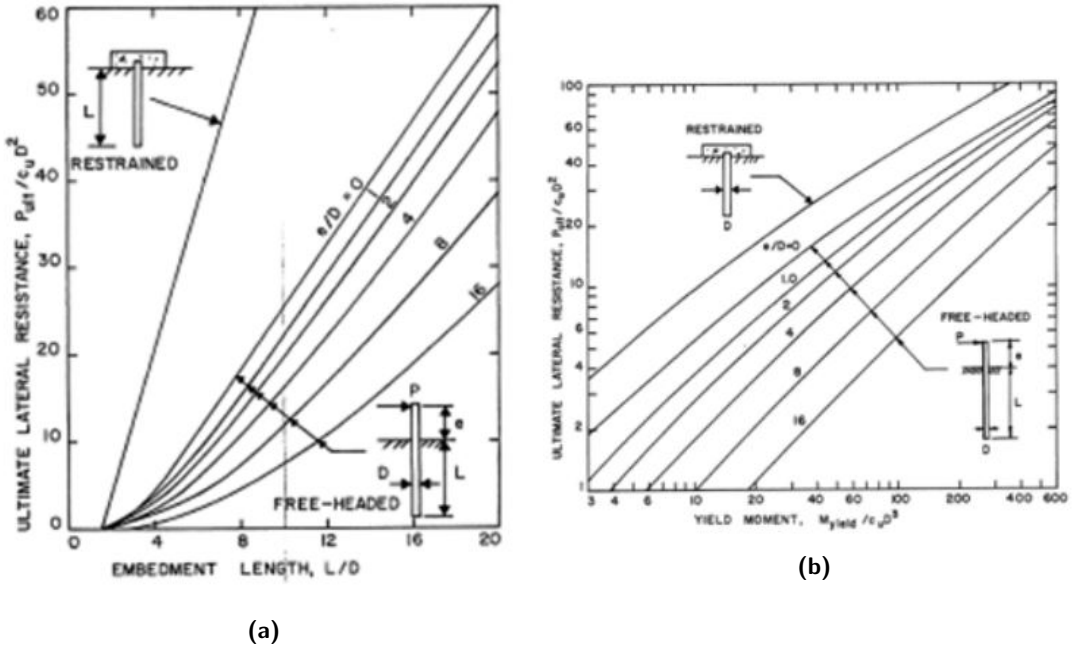

Figure 2-9: Design charts of Broms: ultimate resistance for cohesive soils related to (a) embedded length of pile (b) yield moment of pile

Complete overview and assessment of laterally loaded piles in level ground

The master's thesis of J. Ruigrok, "Laterally loaded piles", provides an overview and assessment of all available calculation methods for laterally loaded piles [13]. For a more extensive description of laterally loaded piles in horizontal surface level one is referred to this thesis.

2-2 Analytical solutions taking the slope into account

As stated in the introduction, the sloping ground may influence the soil-structure interaction between the pile and the surrounding soil significantly. The horizontal confining pressure is reduced at one side of the pile, which changes the passive wedge model. It is believed that the flow mechanism, to calculate the ultimate soil resistance at a greater depth, will not alter due to influence of the slope. However, it may develop lower down the pile than it would in horizontal surface level.

Already several researchers made modifications to the passive wedge model in sloping ground and derived the ultimate lateral resistance for that case. The first approach was done by Gabr and Borden in 1990 [1], they assumed a new failure wedge and derived hereby the ultimate resistance p_u. Hereafter Reese et al. [19] made a modification to their own strain-wedge model. Just recently, Mirzoyan tried to make a better approach [2].

2-2-1 Modification of Gabr and Borden

The passive wedge developed by Gabr and Borden is shown in Figure 2-10a. The model is appropriate for evaluating the ultimate soil resistance of laterally loaded piles in sloping ground consisting of cohesionless soil or soil that possess both cohesion and friction, a $c - \phi$ soil. As for the passive wedge model described in Section 2-1-2, only the ultimate soil resistance can be determined from this model, therefore it is an ultimate strength model.

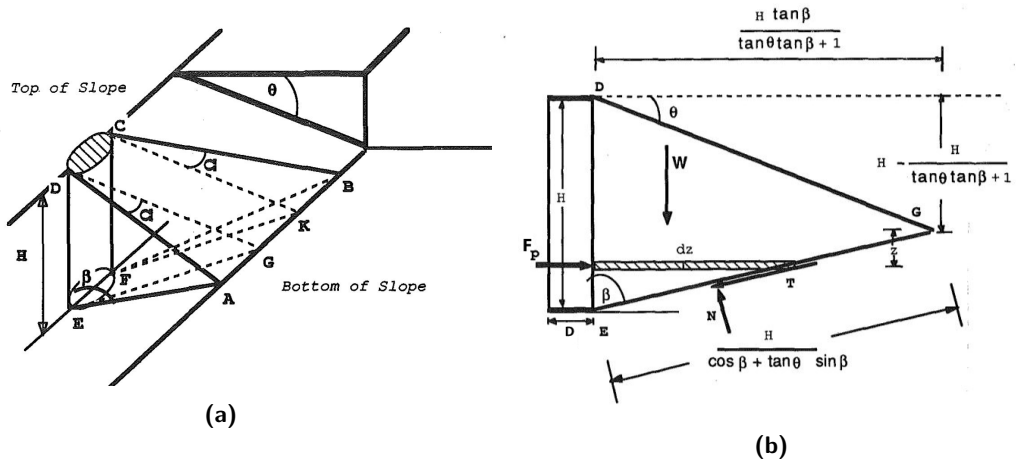

Figure 2-10: Assumed failure wedge with plane failure surface (a) and assumed wedge in equilibrium (b) of Gabr and Borden [1]

The derivation of the wedge equilibrium consists of two parts; the derivation of the resistance along the bottom plane EABF and the derivation of the resistance along the side planes EAD and FBC. Summing the active earth pressure at the back of the pile together with the lateral resistance from the two side planes and the front plane, the total lateral resistance can be expressed as defined in Equation 2-9. The complete derivation is enclosed in Appendix B.

$$p_u = \gamma H[H(S_{1\phi} + 3K_o S_{3\phi}) + DS_{2\phi} - K_a D] + c[H(S_{1c} + S_{3c}) + DS_{2c} - 2DK_a^{0.5}] \tag{2-9}$$

in which

H	=	depth below ground surface
K_o	=	coefficient of at-rest earth pressure
K_a	=	coefficient of active earth pressure
c	=	cohesion of the soil
D	=	diameter of the pile
$S_{1\phi} - S_{3\phi}$	=	parameter of Gabr and Borden
$S_{1c} - S_{3c}$	=	parameter of Gabr and Borden

For the angles β and Ω the values should be chosen such, that the critical failure wedge is obtained along which the total lateral resistance is the smallest.

Approaches for Ω will be covered further in Section 2-3.

2-2-2 Modification of Reese et al.

Reese has only published his modification of the formula to obtain the ultimate soil resistance, and not the derivation of the formula. The formula is shown for both clay and sand.

Clay

The ultimate resistance of clay near the ground surface if the pile is pushed downhill slope, which has an angle θ, is expressed as:

$$p_u = (2c_a D + \gamma DH + 2.83c_a H)\frac{1}{1+\tan\theta} \tag{2-10}$$

Sand

The ultimate resistance of the sand near the ground surface if the pile is pushed downhill, with an angle smaller than the friction angle, ϕ , is expressed as:

$$\begin{aligned} p_u =& \gamma H\Big[\frac{K_o H\tan\phi\sin\beta}{\tan(\beta-\phi)\cos\Omega}(4G_1^3 - 3G_1^2 + 1) + \frac{\tan\beta}{\tan(\beta-\phi)}(DG_2 + H\tan\beta\tan\Omega G_2^2) \\ &+ K_o H\tan\beta(\tan\phi\sin\beta - \tan\Omega)(4G_1^3 + 3G_1^2 + 1) - K_A D\Big] \end{aligned} \tag{2-11}$$

where

$$G_1 = \frac{\tan\beta\tan\theta}{\tan\beta\tan\theta + 1} \tag{2-12}$$

$$G_2 = 1 - D_1 \tag{2-13}$$

$$K_A = \cos\theta\frac{\cos\theta - (\cos^2\theta - \cos^2\phi)^{0.5}}{\cos\theta + (\cos^2\theta - \cos^2\phi)^{0.5}} \tag{2-14}$$

The modification of Reese et al. to the formula for clay, is easy to recognize; the soil resistance for horizontal ground is multiplied by the factor $\frac{1}{1+\tan\theta}$ to account for the slope. However, the modification for the sand formula is much more difficult to recognize.

2-2-3 Modification of Mirzoyan

Mirzoyan made a modification to the passive wedge model for his master's thesis. This model is only appropriate in cohesionless soils. In the model the distance, X, between the pile and the

crest of the slope can vary, which makes it also suitable for piles near sand slopes. However, it is not possible to position the pile in the slope.

The biggest difference between the derivation of Gabr and Borden, and Mirzoyan are the assumed planes that provide resistance. Mirzoyan assumes that the frictional resistance is only provided by the bottom plane FEAB, since it is the only plane of contact between the wedge and unaffected soil. While Gabr and Borden assume that also the two side flanks provide frictional resistance. The assumed failure wedge by Mirzoyan is schematized in Figure 2-11.

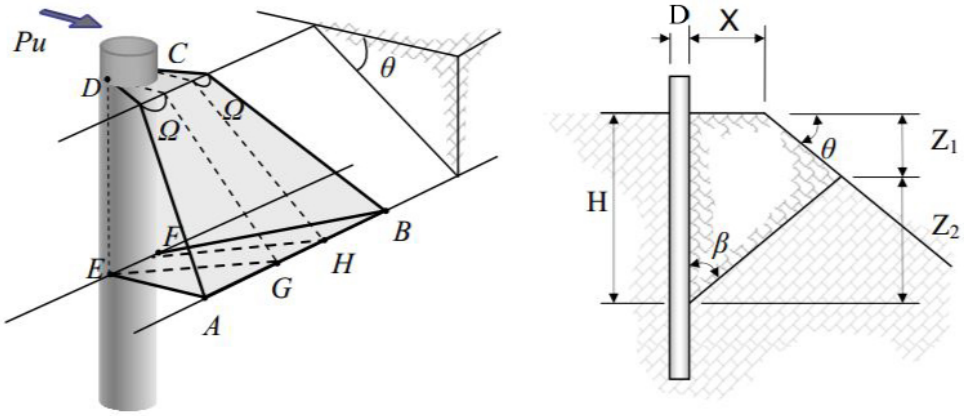

Figure 2-11: Assumed failure wedge by Mirzoyan [2]

The ultimate resistance of the soil, p_u, can be derived from the equilibrium of the wedge. The weight, W, the normal force, N, and the friction force, T, are acting on the failure wedge. From these forces, the force that resists the lateral movement of the soil can be derived as defined in Equation 2-15.

$$F_p = N\cos\beta + N\tan\phi\sin\beta = \frac{W(\cos\beta + \tan\phi\sin\beta)}{\sin\beta - \tan\phi\cos\beta} \tag{2-15}$$

The ultimate resistance per unit length, p_{ult}, can be obtained by differentiating Equation 2-15 with respect to the depth H. Due to the discontinuous geometry of the wedge, two equations are derived:

$$p_{ult} = \frac{\gamma H(bJ_5 + HJ_6)}{\tan(\beta - \phi)} \tag{2-16}$$

for $0 < H \leq (X/\tan\beta)$

and

$$p_{ult} = \frac{\gamma(X + HJ_3)(DJ_3J_5 + (DJ_5^2 + J_6(X + HJ_3)))}{(J_3 + J_5)^2\tan(\beta - \phi)} \tag{2-17}$$

for $H > (X/\tan\beta)$

where

H	=	depth below ground surface
γ	=	unit weight of the soil
D	=	diameter of the pile
X	=	distance between pile and crest of the slope
β	=	angle of the inclined plane with the vertical
ϕ	=	internal friction angle of the soil
$J3, J5, J6$	=	parameters of Mirzoyan

The complete derivation is enclosed in Appendix C.

2-2-4 Comparison of the modifications

To finish this chapter, some remarks should be made about the assumptions of the modifications and the differences between the models.

- Gabr and Borden have developed a failure wedge that is equal for cohesive and cohesionless soil. This is in contradiction with Reese et al., who developed different failure wedges for both situations. As discussed in Chapter 2-1 the difference between the wedges of Reese et al. is the width of the failure wedge, i.e. the amount of soil that is mobilised. Reese assumes that in cohesive soil a smaller amount of soil is mobilised.
- Gabr and Borden take the active pressure into account for their solution, Reese et al. takes it only into account for sand, while Mirzoyan neglects it to determine the ultimate resistance of the soil.
- Another difference between the derivation of Gabr and Borden and Mirzoyan are the assumed planes that provide frictional resistance. Mirzoyan assumes that only the bottom plane provides friction, while Gabr and Borden and Reese et al. suppose that also the side flanks provide frictional resistance.
- It is considered for all the models that the soil is homogeneous and isotropic, and has no water table. This is not realistic for the conditions one will encounter in the field.

With help of a spreadsheet a comparison has been made between the four failure wedges of Gabr and Borden, Rees et al., Mirzoyan and Reese et al. horizontal. This was done for both sand and clay. The selected values for the comparison are shown in Table 2-1, the results are plotted in Figure 2-12.

Based on the graphs shown in Figure 2-12 several observations can be made. Sand supplies much more resistance than clay does; for the selected values the difference is a factor 9. However, if one takes the slope into account, the reduction of the ultimate soil resistance is much more for sand than for clay. Which indicates that sand is much more sensitive for sloping ground than clay according to these models.

The difference in Figure 2-12 between the analytical solution for sand between Mirzoyan and Reese et al. has two reasons. First, Reese et al. assumes that the active force should be taken into account. By tests is demonstrated that the active force does not play a role, so this can be considered as wrong. Moreover, the difference is caused by the assumed friction planes. Mirzoyan assumes that there is only friction along the bottom plane, since this the only plane of contact between the wedge and unaffected soil and really provides friction.

Last, some changes has been made to the spreadsheet and a comparison between the analytical solutions for $\theta = 0$ has been conducted. The graphs for Reese et al. horizontal, Reese et al. slope and Mirzoyan corresponded with each other for that case. Unfortunately, Gabr and Borden show for both sand and clay large deviations. If one makes another modification, a pile diameter of 0.1

m in combination with horizontal level ground, all the graphs for clay correspond to each other. However, for sand the graph of Gabr and Borden still shows a large deviation. It can be concluded that the solution of Gabr and Borden for cohesive soil is only reliable for small pile diameters (up to 0.5 m) and that the solution of Gabr and Borden is absolutely not suitable for cohesionless soil.

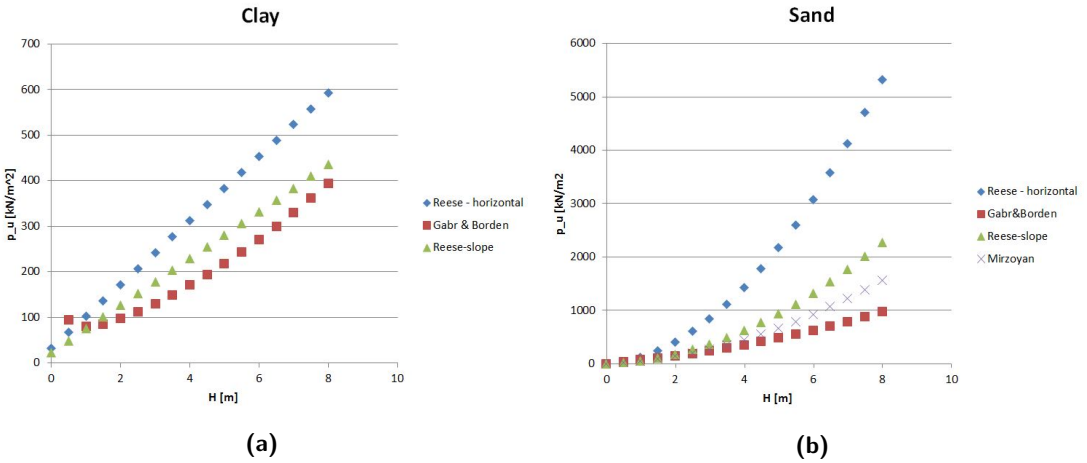

Figure 2-12: Comparison of the ultimate soil resistance derived from the failure wedges

	c $[kPa]$	ϕ [°]	D $[m]$	γ $[kN/m^3]$	θ [°]	β [°]	Ω [°]	K_a [-]	K_0 [-]
Clay	20	17.5	0.8	17	20	45	13.125	0.54	0.70
Sand	0	32.5	0.8	20	20	65	24.375	0.30	0.46

Table 2-1: Values of sand and clay used for comparison of the failure wedges

2-3 Tests found in literature

Different studies have been performed to examine the effect of the slope on the lateral capacity of the soil. In some of these studies, tests were part of the research. In this chapter, the results of these tests, both full scale and small scale will be described.

2-3-1 Gabr and Borden (1990)

Besides their derivation of the analytical solution for the passive wedge model of piles in a slope, Gabr and Borden have also executed five load tests on piers in the field to validate their analytical solution [1]. One test was performed in cohesionless soil, and four tests were performed in c-ϕ soil. The pier in cohesionless soil was constructed at the crest of the slope, which had a gradient of 3.5:1 (15.9°). The four piers in the c-ϕ soil were installed in the slope, which had a gradient of 2.2:1 (22.3°).

Observations

For both the pier in cohesionless soil and the piers in c-ϕ soil, it was observed that a gap arose behind the pile. This gap opened already at small load levels, and got wider as higher loads were applied. The soil did not collapse into the gap.

Results

The five tested piles showed different maximum load capacities, this was attributed to the different soil strengths and cohesion at the locations.

The accuracy of the predicted values with the model derived in Section 2-2-1 varies, but underestimates the capacity in all cases. The best approach, for pier 1, which was the pier in cohesionless soil, underpredicts the response by less than 10 %, assuming Ω equal to $\phi/2$. The other piers fluctuated between an underprediction of 10% and 25% these values. If one ignores the slope, the predicted behaviour is estimated 30% to 45% too high. Underestimation of the ultimate soil resistance may be attributed to the fact that the model of Gabr and Borden takes the active forces into account, which is not realistic since a gap behind the pile appears.

Parametric study

Gabr and Borden executed a parametric study based on the model described in Section 2-2-1. They varied the slope angle, θ, the internal friction angle, ϕ, and the cohesion, c. Figure 2-14a and 2-14b clearly show that the the slope reduction factor, Ψ, defined as $P_u(slope)/P_u(flat)$, only slightly depends on the internal friction angle, ϕ. However, Ψ decreases from 0.6-0.7 to 0.45-0.55 as a soil changes from a cohesionless soil with a ϕ of 30° to a cohesive soil with a ϕ of 30° and a cohesion of 1 tsf (=95.76 kPa).

Since it was concluded in Section 2-2-4 that the analytical solution of Gabr and Borden was not suitable for a soil without cohesion, the above parametric study is not based on a valuable solution. Moreover, it was concluded as a result of Figure 2-12 that sand is much more sensitive for a slope than clay, which will also be confirmed further in this thesis. Figures 2-13 and 2-14, are in contradiction to this, since they show the opposite. Therefore, Gabr and Borden's graphs and conclusions derived from their parametric study should be considered as unreliable.

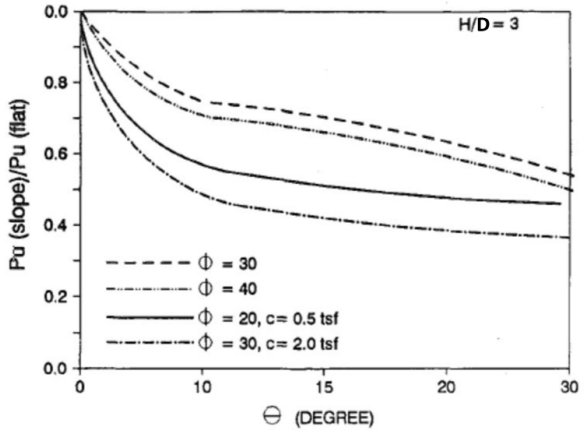

Figure 2-13: Ultimate resistance reduction factor Ψ as function of ground surface slope angle θ after Gabr and Borden [1]. (1 tsf = 95.76 kPa)

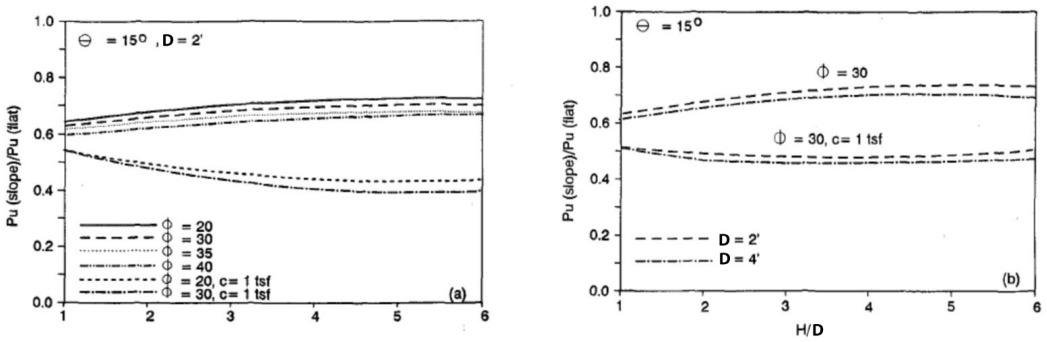

(a) **(b)**

Figure 2-14: Ultimate resistance reduction factor Ψ as function of the H/D ratio after Gabr and Borden [1]. (1 tsf = 95.76 kPa, 2' = 0.61m, 4' = 1.22m)

2-3-2 Mezazigh and Levacher (1998)

Mezazigh and Levacher performed 59 centrifuge tests, to study the effect of slopes or the proximity of slopes on p-y curves.. Their purpose was to find coefficients that can be applied to the existing p-y curves for horizontal ground. The location of the tested piles was either at horizontal surface (reference tests) or at distances t from the slope ranging between 0 and 12 times the diameter of the pile (t/D=0 to 12). Furthermore, they considered two different slopes, 2H:1V (26.6°) and 3H:2V (33.7°).

Results

The data shows good repeatability between the different tests. The displacements of the pile installed at the crest of the slope (2:1) were 1.7 times higher than for the reference pile at the same load level. For a slope of 3:2, a factor of 4.2 was measured. Moreover, the effect of the sloping ground was negligible from a distance $t/D = 6$ for the 2:1 slope. For the steeper slope of 3:2, this was not negligible until $t/D = 12$. Last, it was observed that the maximum moment increases as the pile approaches the slope. The point of the maximum moment lowers along the

pile as the slope becomes steeper and the pile becomes closer to the slope.

Based on the 59 centrifuge tests Mezazigh and Levacher propose the multiplier, r, to take the slope into account. This multiplier reduces the p-y curve as defined in Equation 2-18. The p-y curves of the tested piles were determined with the help of 20 pairs of strain gauges.

$$P(t/D) = rP(t/D) \cdot P_{ref} \tag{2-18}$$

The multiplier r can be expressed as:

$$\begin{cases} r = \frac{17-15\tan\beta}{100} \cdot \frac{t}{D} + \frac{1-\tan\beta}{2} & if \quad t \leq t_{lim} \\ r = 1 & if \quad t > t_{lim} \end{cases} \tag{2-19}$$

where

$$t_{lim} = 4D(6\tan\beta - 1) \tag{2-20}$$

and

β	=	angle of the slope
t	=	distance from the crest to the centre of the pile
D	=	diameter of the pile

It should be marked that the multiplier r does not depend on any soil property according to Mezazigh and Levacher. The multiplier only depends on the normalised position of the pile, and the angle of the slope. This may be caused by the fact that only two different sands were tested, which could have made it impossible, due to the little variance, to couple this information to a multiplier. Another observation is that Mezazigh and Levacher do not mention anything about along which length of the pile the multiplier should be applied. One could question whether the slope still influences the p-y curves at greater depth. Moreover, it is remarkable that the multiplier defined in Equation 2-19, does not correspond to the graph in Figure 2-15b. Filling in an slope angle of 1:2 does not equal the coefficients 0.661 and 0.472 in the graph. However, the drawn trendlines do correspond to test results. These observations are confusing, but are unfortunately not explained by the article of Mezazigh and Levacher. The multiplier was validated by Mezazigh and Levacher by comparing the experimental curves with curves computed by PILATE, which is a program for the analysis of a single pile [27]. It was concluded that the error always remains less then 10%.

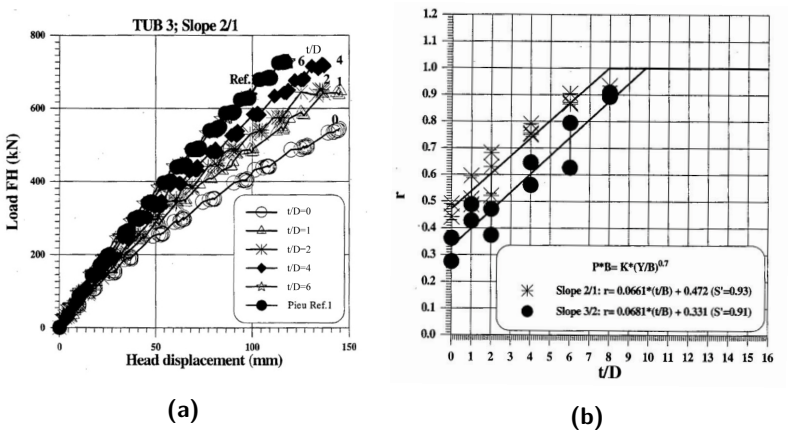

(a) **(b)**

Figure 2-15: Effect of the proximity of the slope on the loading curves (a) and coefficient r versus relative distance t/D to the slope (b), after Mezazigh and Levacher [5]

2-3-3 Chae et al. (2004)

Chae et al. conducted model tests in dry Onahama sand on short piles, which had a constant embedment depth/diameter (D/B) ratio of 5. The adjacent slope had an angle of 30°. The piles were installed at distances 4D, 2D and 0D from the crest of the slope and one reference pile was installed in horizontal ground. The test are combined with a 3D Finite Element (FE) analysis.

Results

The load displacement curves of the tests are shown in Figure 2-16. It is remarkable that the results of the tests (reffered to as experimental results in the graph) and the results of the FE analysis (referred to as analytical results in the graph) widely differ for the piles in horizontal ground and at a distance of 4D from the crest. However, for the 2D pile and the pile at the crest the experimental and analytical results do agree. Chae et al., do not give an explanation for this discrepancy, but it seems that their developed 3D finite element model is not appropriate for the whole modelling process.

Therefore, it is reasonable that the values for the load ratio, ψ, obtained from the experimental result are more realistic than the values obtained from the analytical result. The load ratios of the analytical result give a distorted view. Both values can be found in Figure 2-17. Due to these deviations, one should conclude that these values should be used with caution.

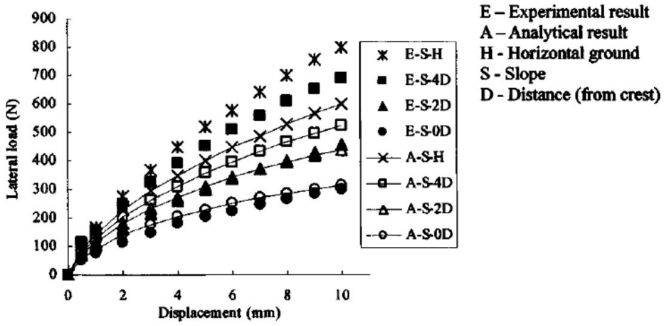

Figure 2-16: Loading curves derived from the analytical and experimental results after Chae et al. [6]

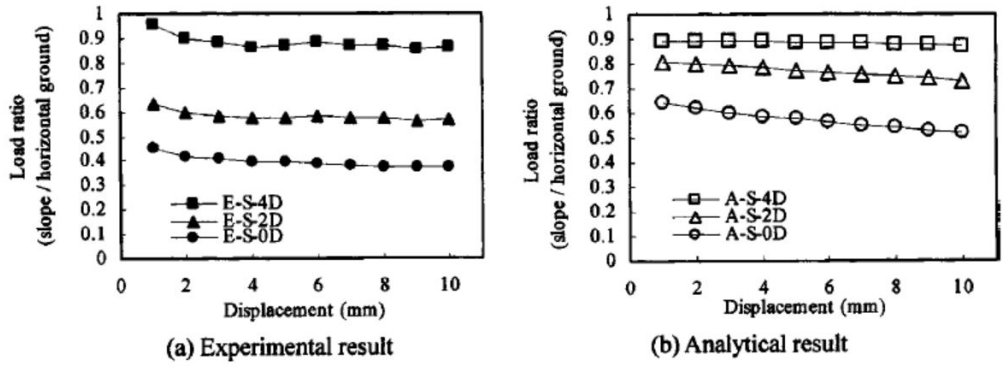

Figure 2-17: Load ratios for the experimental results and the analytical results after Chae et al. [6]

2-3-4 Mirzoyan (2007)

Mirzoyan conducted three field tests; one pile in a horizontal profile, one pile at the crest of the slope and one pile at a distance of 3D from the crest. The slope had an angle of 30°. The upper 2.5 meter of the soil layer was a sand fill consisting of a well graded clean sand, underlain by alternating layers of silts, clays and sands.

Observations

Corresponding to the observations of Gabr and Borden, Mirzoyan observed a gap behind the pile. The gap remained open throughout the whole test, suggesting that the soil behind the pile has little influence on the pile response for the depth of the gap. It was also noticed that the pile did not move back to its original position, after the load was completely removed. Mirzoyan attributed this to yielding of the pile, since the gap behind the pile remained open.

Results

The load deflection curve of Mirzoyan's test is shown in Figure 2-18. The load ratio, ψ, the load on the pile in a sloped profile to the load on the pile in a horizontal profile, is for the pile located at the crest 0.8 and for the pile at a distance from 3D of the crest 0.91. These values are significant higher than suggested by earlier research. For instance, Gabr and Borden found a value of about 0.6 for the pile at the crest. From the graphs of Mezazigh and Levacher a value of about 0.45 can be derived. An explanation suggested by Mirzoyan for the stiffer behaviour could be that the slope was only cut 1.8m horizontally and 1.1m vertically, which made the effect of the sloping ground smaller.

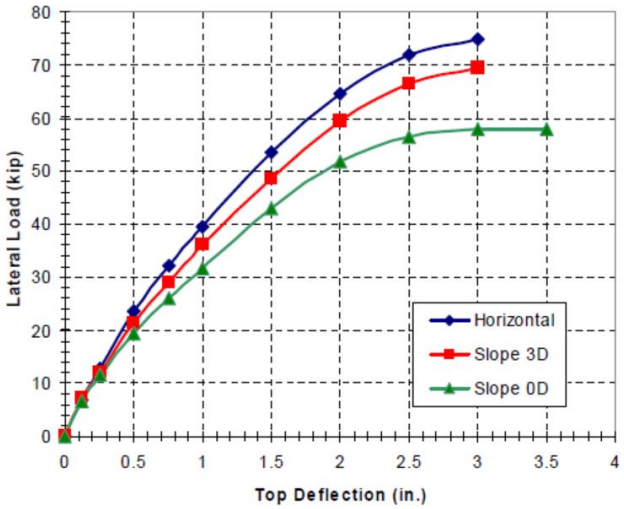

Figure 2-18: Effect of the proximity of the slopes on loading curves after Mirzoyan [2]. (1 kip = 4.45kN, 1 inch = 2.54 cm)

Moreover, it was observed that the slope had little influence on the location of the maximum bending moment. However, this could be caused by the lack of sufficient strain gauges at the location of the maximum moment. Last, it was observed that the maximum moment increases when the pile is located closer to the slope for the same applied load.

Shear failure of the soil

Mirzoyan paid a lot of attention to the shear failure patterns visible at the soil surface in order to

investigate the shear failure angle, Ω. It is difficult to determine this exactly, since the lines were not fully visible. However, it could be noticed that Ω did decrease as the applied load increased, suggesting that the shear failure angle is dependent on the deflection of the pile.

Figure 2-19 shows the failure pattern, which became visible at the loading test for the pile at the crest. The shear angle is about 29° on the south side of the pile and about 33° at the north side of the pile. This would indicate that Ω is about 75% of the angle of internal friction. However, it should be mentioned that this is only based on one test.

The failure pattern of the test executed at a distance of 3D from the crest of the slope, showed a shear angle of about 21° on the south side and 24° at the north side. This suggest that Ω is about half of the angle of internal friction at 3B from the crest. This value is more frequently suggested in literature.

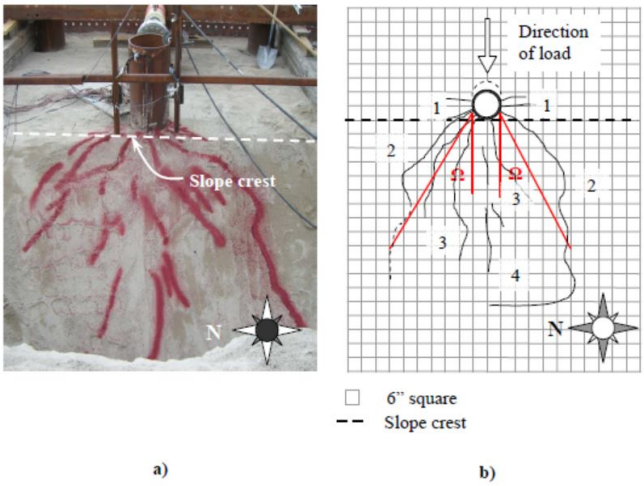

Figure 2-19: Failure pattern for the pile at the crest, the numbering is the sequence of appearing of the cracks , after Mirzoyan [2]

2-3-5 Nimityongskul (2010)

Nimityongskul conducted a series of full scale tests at the test site of the Oregon State University for his dissertation [3]. This included two tests in horizontal ground, four tests at a distance 8D, 4D, 2D and 0D from the crest of the slope, and one test in the slope at a distance -4D from the crest. The first soil layer, which was 10D thick, consisted of cohesive soil, in which a slope was excavated of 2:1 (26.6°) to a depth of 2.75m. This layer was underlain by alternating layers of sand and clay. The embedded length of the tested piles was 7.9m.

Observations

Only for the pile in horizontal level ground and the 8D pile heaving was observed in front of the pile. Moreover, behind all the test piles gaps were observed. The failure pattern due to shear failure started with a major crack in front of the pile in the loading direction, then major cracks with an angle of about 45° perpendicular to the loading direction occurred. This pattern is different than observed by Mirzoyan, which is shown in Figure 2-19. That pattern started with cracks perpendicular to the loading direction and was followed by cracks in front of the pile. Differences could be explained by the difference in soil (cohesive versus cohesionless) or to the randomness of the soil properties as stated by Nimityongskul. Furthermore it was observed that the cracks

started at lower displacements for the 0D and -4D pile than for the piles at greater distance to the crest.

Results

Based on the load displacement curves and the curvature and rotation profiles of the pile tested in horizontal ground and the 8D pile, it can be concluded that the effect of the slope is insignificant for the 8D pile. For the pile located at a distance 4D from the crest, the slope has a significant effect on the load-displacement curve. This can be seen in Figure 2-20a and 2-20b.

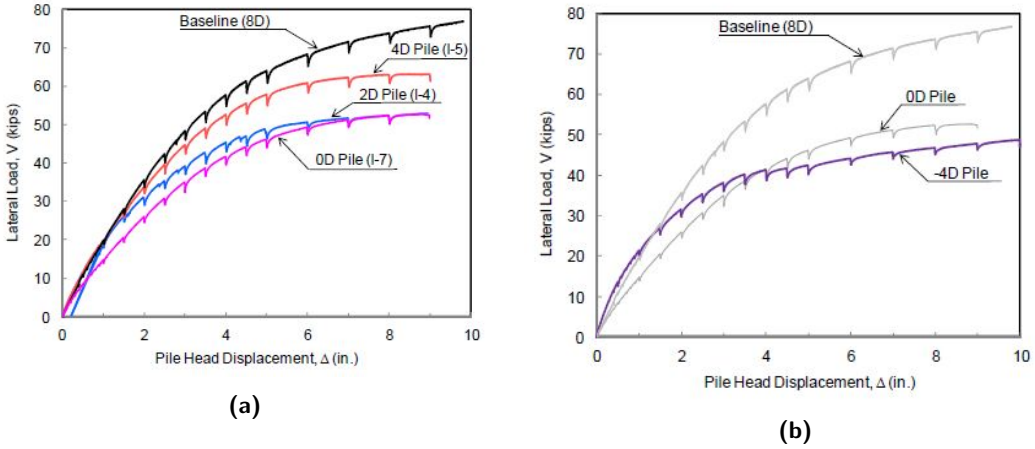

Figure 2-20: Load displacement curves for (a) the 8D, 4D, 2D and 0D piles and (b) the -4D pile after Nimityongskul [3]. (1 kip = 4.45 kN, 1 inch= 2.54 cm)

Based on the back-calculated p-y curves, Nimityongskul proposes a p-multiplier to account for the slope. This was done by normalizing the back-calculated p-y curves with the p-y curves for the pile in horizontal ground. Since Nimityongskul observed that the effect of the slope on p-y curves is larger as the displacements increase and becomes steady at larger soil displacements, he developed a p-multiplier which depends on the soil displacement. The result is shown in Figure 2-21. The p-multiplier of Nimityongskul is based on seven p-y curves at a distance one to seven feet below the ground surface. The p-multiplier is only valid until 7 feet (=2.13m, =7D) beneath the soil surface, below a distance of 7D Nimityongskul considers the multiplier to be equal to 1.

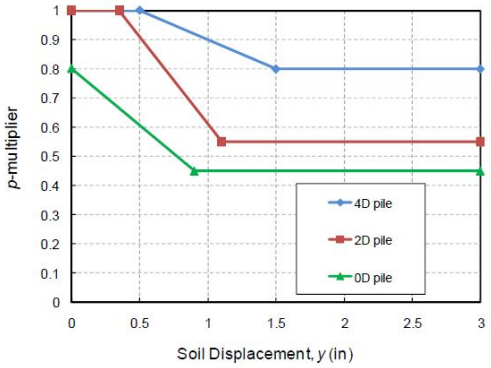

Figure 2-21: Proposed p-multipliers by Nimityongskul [3]. (1 inch = 2.54 cm)

2-3-6 Sivapriya and Gandhi (2011)

Sivapriya and Gandhi conducted a series of small scale tests in silty clay [7]. Due to the small scale, a lot of parameters could be varied. The clay had a shear strength of 30 kPa and 50 kPa and three different slopes were constructed, 1:2, 1:2.5 and 1:3. The piles were located at the crest, at a distance of one radius of the crest in the slope (referred to as -1R), and at a distance of two radius of the crest in the slope (referred to as -2R).

Results

As expected, the load displacement curve for the soil strength of $s_u = 50$ kPa had a higher capacity than for $s_u = 30$ kPa. The load displacement curves for the slope of 1:2 are shown in Figure 2-22a and 2-22b. It was also observed that the bending moment and the depth of the bending moment increases as the lateral load increases. The phenomena is accounted to the fact that the soil in front of the pile fails, leaving the top of the pile unsupported. This leads to lowering of the depth of the maximum bending moment. For the pile in horizontal ground, at the crest, and at a distance -1R from the crest, the maximum bending is obtained at 0.4L of the pile. For the pile located at -2R from the crest, the maximum bending moment is observed at 0.5L. This is in contradiction with the findings of Mirzoyan. However, Mirzoyan already questioned his results and attributed it to the use of too little strain gauges.

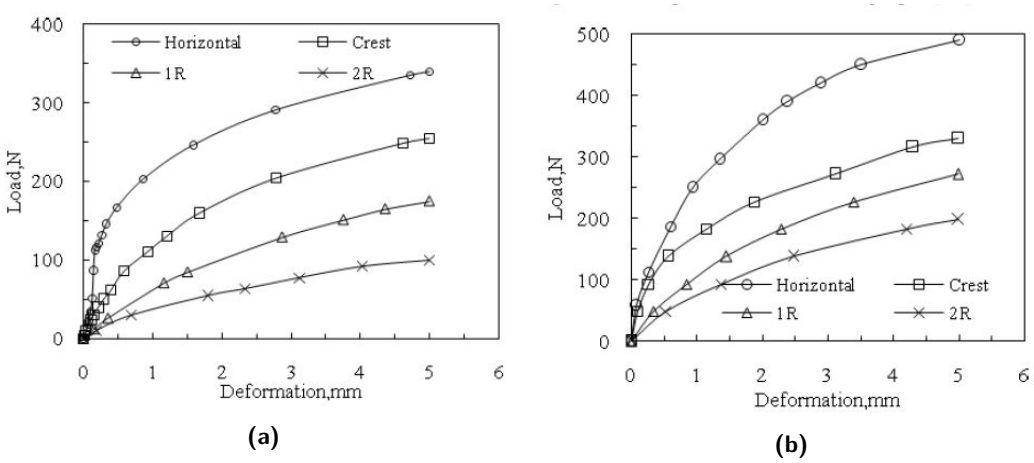

Figure 2-22: Load displacements curve for a 1:2 slope with a shear strength of (a) 30kPa and (b) 50kPa by Sivapriya and Gandhi [7]

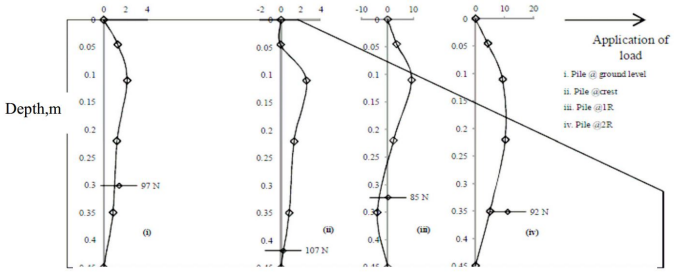

Figure 2-23: Effect of the slope on the bending moments along the pile by Sivapriya and Gandhi [7]

2-3-7 Barker (2012)

Also Barker conducted full scale tests at the test site of the Oregon State University [4]. For this series of tests an embankment was constructed on the original surface level which had an slope of 1:2. The embankment consisted of a cohesionless structural backfill, underlain by alternating clay and sand layers. Two of the tests were performed in horizontal ground and five tests at a distance of 8D, 4D, 2D, 0D and -4D of the crest of the slope. The stratification of the soil consisted of a constructed embankment of cohesionless structural backfill underlain by alternating clay and sand layers.

Observations

For the pile in horizontal ground and the 8D pile, Barker observed ground heaving in front of the pile, which increased as the displacements increase. Behind the pile large gaps appeared, this was attributed to the apparent cohesion of the sand, due to capillarity. For the piles closer to the crest of the slope, or in the slope, the failure wedges were clearly visible, as shown in Figure 2-24. As the piles moved further down from the slope, the shear failure angle, Ω, increased. Based on these passive failure wedges, Barker recommends a shear failure angle of 70% of the internal friction angle, ϕ, which is smaller than Mirzoyan proposed in his study (75%).

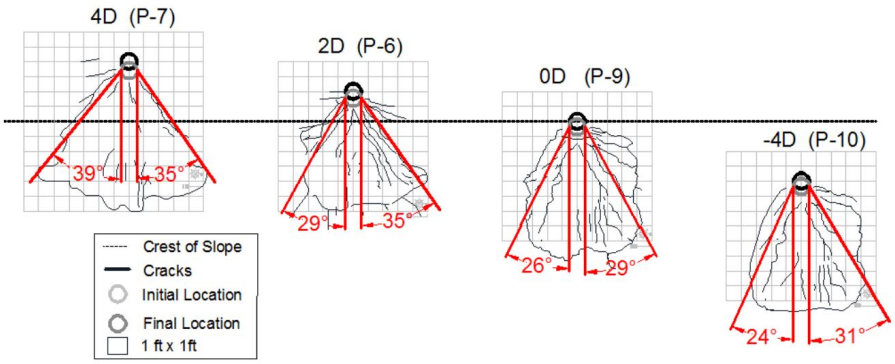

Figure 2-24: Failure wedges with shear failure angle, Ω, after Barker. [4]

Results

The loading curves for all tested piles are shown in Figure 2-25. The pile located on 8D of the crest of the slope, reacts stiffer at small displacements than the pile in horizontal ground, but the maximum capacity is equal. Therefore, Barker considered it as comparable curves and concluded that the effect of the slope for the 8D pile is insignificant. Untill the pile reaches the crest of the slope, the initial stiffness for small displacements (up to 2.5 inch) is the same. From a displacement of 2.5 inch the proximity of the slope has an effect. For the piles at the crest and in the slope, the initial stiffness is considerable lower.

P-multiplier

By analysing the back-calculated p-y curves of the field test, Barker has suggested p-multipliers as plotted in Figure 2-26. These p-multipliers depend on the distance to the slope and the depth below soil surface. It gives a clear recommendation for p-multiplier along the length of the pile. Beneath a depth of 10D the multiplier is equal to one and is the slope considered to not influence the p-y curve any more. Barker indicates that his multiplier is between 5% and 25% too conservative. The conservatism increases with the depth and with the distance behind the crest.

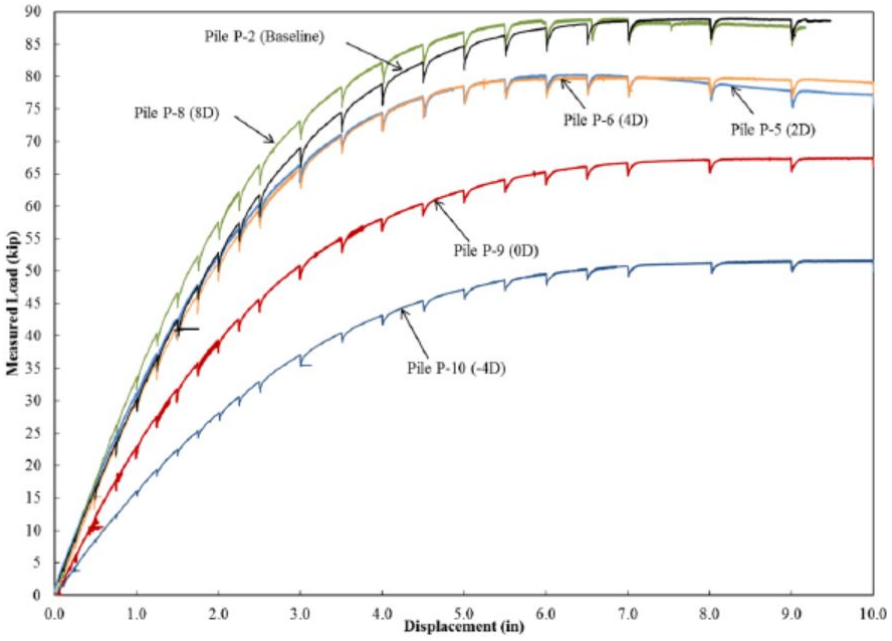

Figure 2-25: The effect of the proximity of the slope on the loading curves after Barker [4]. (1 kip = 4.45 kN, 1 inch = 2.54 cm)

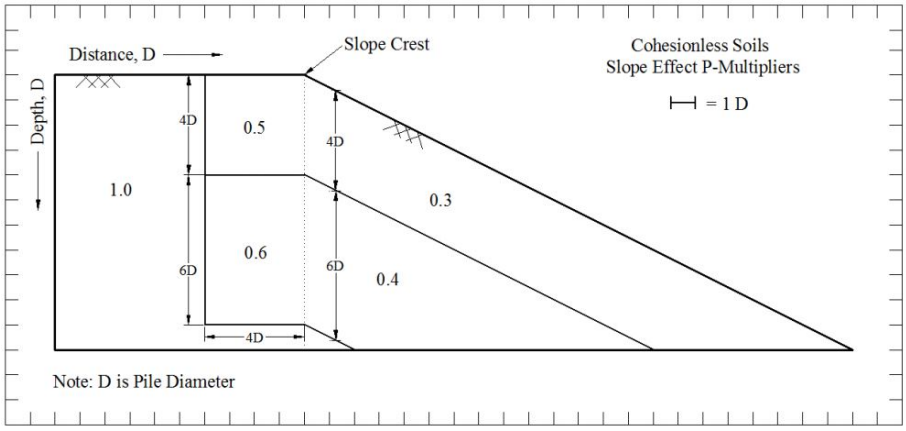

Figure 2-26: Recommended p-multipliers by Barker for a generalized cohesionless slope [4].

2-4 Finite Element analyses to determine the effect of the slope

2-4-1 Chen and Martin (2001)

Chen and Martin used the finite difference program $FLAC^{3D}$ to perform their study to the effect of the slope on the lateral response of piles. The soil was modelled as an elastic-plastic material, using the Mohr-Coulomb model and the pile was modelled as a non-yielding elastic continuum. Interface elements were used to make it possible to model a gap. The soil resistance, p_u, was obtained by summing together the normal forces acting on the interface nodes with the shear drag forces around the pile shaft.

To verify the finite element model, first two tests of laterally loaded piles in level ground published by Matlock [28] and Reese [29] were modelled in $FLAC^{3D}$. Hereafter, the slope was added to the model. For the analysis a c-ϕ soil was used.

Results

The analysis started with an examination of the effect of the slope angle on the p-y curves, which is shown in Figure 2-27a. In addition, the effect of the slenderness on the p-y curves was evaluated. The results can be found in Figure 2-27b; if the pile becomes more slender the soil has a lower ultimate resistance. Hereafter, a study to the effect of the pile location with respect to the slope was adopted. The results are shown in Figure 2-28a. Chen and Martin stated that the effect of the slope could be neglected from distances larger than 6D if the slope angle is smaller than 45°, since the effect on the p-y curve was smaller than 10%.

Last, Chen and Martin conducted a parametric study. They varied the pile properties and the soil properties, after which they evaluated the results. The remarkable results are shortly discussed here. To start with, the influence of the pile bending stiffness is very small. One would expect that stiffer piles have a smaller deflection at the same load level, what provokes less soil resistance. From Figure 2-28b it can be concluded that it has not that much effect on the p-y curves. In contrast, it does have a significant effect on the load displacement curve.
Moreover,the shape of the pile has a considerable influence on the lateral resistance, p_u. This is caused by the fact that square piles induce a wider wedge than circular piles and therefore mobilise more soil resistance. The effect is shown in Figure 2-29a. Last, the effect of the properties of the interface between the pile and the soil is also significant. This is shown in Figure 2-29b.

2-4-2 Begum and Mutukkumaran (2008)

The study of Begum and Mutukkumaran covered a two-dimensional, plain strain FE analysis of a pile on the crest of the slope [9]. The constitutive soil model used for the FE analysis was an elasto-plastic model with the Mohr-Coulomb failure criterion, the pile soil interface was modelled with contact elements using interface condition. The considered variations in the FE analysis are slopes of 1V:1.5H and 1V:2H, relative densities of sand of 30%, 45% and 70% and L/D (embedded length/diameter) ratios of 25 and 30. The validation of the FE model was based on a small scale test by comparing the bending moments. The margin of error was 20% for the bending moment in the pile.

Results

With respect to earlier research, the results confirm the previous conclusions about the behaviour of piles located on the crest of the slope. The steeper the slope, the lower the lateral load capacity. As the slope increases, the moment and the depth of the moment below the ground surface increases as well. The increase of the slope from horizontal to 1:2, increases the maximum bending moment by 28–30%. Increase of the slope from 1:2 to 1:1.5, increases the maximum bending moment around

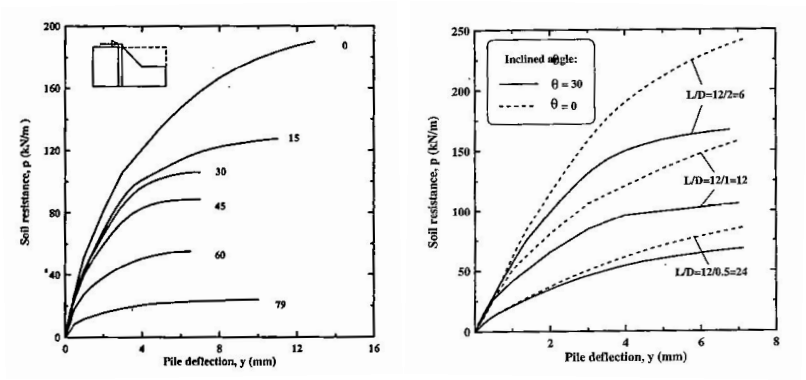

(a) **(b)**

Figure 2-27: The effect on the p-y curves of (a) the angle of the slope and (b) slenderness of the pile after Chen and Martin [8]

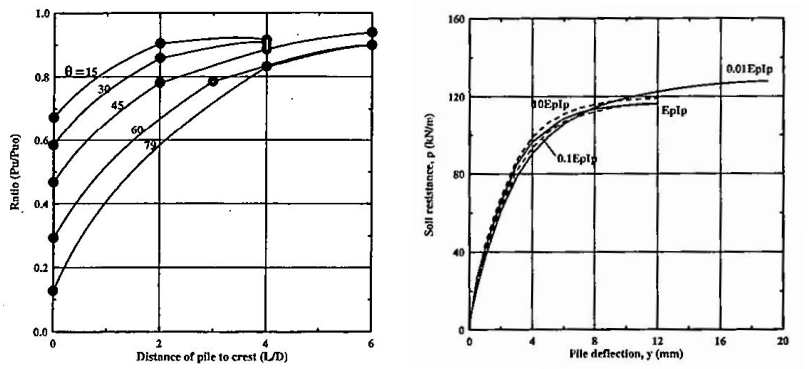

(a) **(b)**

Figure 2-28: (a)Effect of the pile location with respect to the slope and (b) effect of the pile bending stiffness on the p-y reaction curves after Chen and Martin [8]

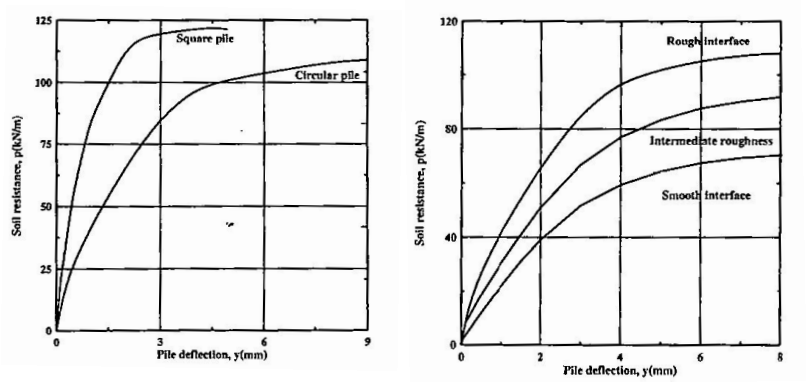

(a) **(b)**

Figure 2-29: The effect on the p-y curves of (a) the pile shape and (b) the interface roughness after Chen and Martin [8]

9–14%. The effects of the slope on the load-displacement curves and the maximum bending moments are shown in Figures 2-30 and 2-31.

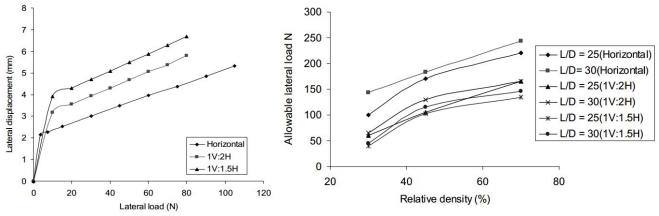

Figure 2-30: Effect of the slope on the load-displacement curve (L) and effect of the density and slope angle on the allowable lateral load (R) after Begum and Mutukkumaran [9]

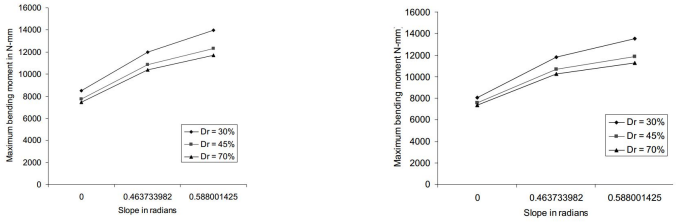

Figure 2-31: Effect of slope on the maximum bending moment for a pile with L/D ratio of 25 (L) and for a pile with L/D ratio of 30 (R) after Begum and Mutukkumaran [9]

2-4-3 Georgiadis and Georgiadis (2010, 2011)

Georgiadis and Georgiadis conducted a finite element analysis in Plaxis 3D Foundation for piles in sloping ground which consists of cohesive soils. Their main purpose was to find the variation of the initial slope of the p-y curve, K_i and the variation of the ultimate lateral resistance, p_u, with respect to the ground inclination under undrained lateral loading conditions in clay soils. The soil was modelled as a linear elastic-perfectly plastic material. In order to allow a gap between the pile and the surrounding soil, a thin zone of 10 cm around the pile that was assigned to have zero tensile strength. To obtain the p-y curves out of the analysis, the shear force, Q, versus depth, z were plotted in a graph and differentiated to a p-z curve (lateral resistance versus the depth). This was done by a curve-fitting computer program to determine the best approach. Hereafter, the p-z curves were combined with y-z curves to gain the desired p-y curves [10].

Results

In their parametric study Georgiadis and Georgiadis found some new conclusions with respect to previous research:

- The slope height did not have much influence on the ultimate resistance, the analyses showed almost identical p-y curves
- The effect of the slope on the shear force is rather limited compared to the effect on the lateral displacement of the pile
- The shorter the pile, the greater the increase in deflection when varying the slope angle; this effect is shown in Figure 2-32

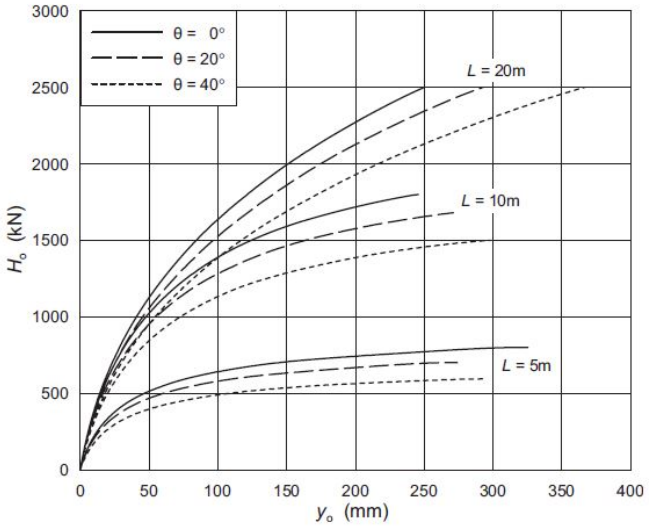

Figure 2-32: Effect of slope angle and length of the pile on the pile head displacement after Georgiadis and Georgiadis [10]

Development of p-y curves in the slope

Since the effect of the slope is larger for the ultimate soil resistance, p_u than for the initial stiffness, K_i, Georgiadis and Georgiadis tried to establish a relationship for those two separately.

To take the variation of the slope into account for the ultimate soil resistance, they suggested a modification based on their analysis of the factor N_p. This is the lateral bearing capacity factor:

$$N_p = N_{pu} - (N_{pu} - N_{po}\cos\theta)e^{-\lambda(z/D)/(1+\tan\theta)} \tag{2-21}$$

where
N_{pu} = ultimate lateral bearing capacity factor for deep lateral flow of soil
N_{po} = bearing capacity factor at the surface for horizontal gound
λ = non-dimensional factor

N_{po} varies from 2 for a fully smooth ($\alpha = 0$) to 3.5 for a fully rough ($\alpha = 1$) pile-soil interaction:

$$N_{po} = 2 + 1.5\alpha \tag{2-22}$$

The value of the non-dimensional factor varies from 0.55 to 0.4:

$$\lambda = 0.55 - 0.15\alpha \tag{2-23}$$

The ultimate bearing capacity factor can be computed with the formula proposed by Randolph and Houlbsy [23]:

$$N_{pu} = \pi + 2\Delta + 2\cos\Delta + 4\Big(\cos\frac{\Delta}{2} + \sin\frac{\Delta}{2}\Big) \tag{2-24}$$

where

$$\Delta = \sin^{-1}\alpha \tag{2-25}$$

To take the variation of the slope into account for the initial stiffness, Georgiadis and Georgiadis propose the formula:

$$\mu = \frac{K_{i\theta}}{K_{io}} = \cos\theta + \frac{z}{6D}(1 - \cos\theta) \tag{2-26}$$

At a depth of z=6D and lower, $K_{i\theta}$ becomes equal to K_{io}.

Now the adopted factors N_p and K_i for a slope θ are derived, they can be used in the p-y curves for undrained analysis for laterally loaded piles in clayey soils:

$$p = \frac{y}{(1/K_i) + (y/p_u)} \tag{2-27}$$

where

$$p_u = N_p c_u D \tag{2-28}$$

To validate this developed method, the new p-y curves are used as input in the software program LPILE [30]. LPILE is a software program for the analysis of piles and drilled shafts under lateral loads, which uses the p-y method. In contrast to D-Pile Group, it is possible in LPILE to consider sloping ground. The LPILE software is used particularly in the USA.

Three field tests were recalculated in LPILE by Georgiadis and Georgiadis, two reported by Matlock [28] and one reported by Wu et al. [31]. This resulted in a small discrepancy (error within 15%) between the measured and the predicted load-displacement curve, the general shape of the curves was however very similar.

Development of p-y curves near the slope (2011)

After their successful study in 2010 which resulted in an adopted p-y curve for the undrained analysis of laterally loaded piles in clayey soils, Georgiadis and Georgiadis extended their study to the response of piles near slopes [14]. The aim was to find appropriate p-y curves for the undrained response in clay of piles near the slope. This was achieved by modification of the ultimate lateral soil resistance, p_u, and the initial stiffness, K_i, which are the parameters in the p-y curve for undrained analysis in clay as defined in Equation 2-27.

To adopt p_u for the vicinity of the slope, another modification of the factor N_p is proposed:

$$N_p = N_{pu} - (N_{pu} - N_{pc})e^{(-\lambda\alpha_\theta(z-z_c)/D)} \tag{2-29}$$

where

$$\alpha_\theta = 1 - \frac{\sin\theta(1+\sin\theta)}{2} \tag{2-30}$$

$$z_c/D = 8.5 - 10\log_{10}(8 - b/D) \tag{2-31}$$

and

z_c	=	critical depth above which the presence of the slope has no influence on factor N_p
z	=	depth below ground surface
b	=	distance from the crest of the slope

To account for the effect of the slope on the initial stiffness Georgiadis and Georgiadis consider the sketch in Figure 2-33. The depth z is replaced by the virtual depth $(z + z_1)$ where z_1 is defined as:

$$z_1 = (b - D/2)\tan\theta \tag{2-32}$$

Filling this in, the equation for the reduction factor of the initial stiffness K_i becomes:

$$\mu = \frac{K_i}{K_{io}} = \cos\theta + \frac{1-\cos\theta}{6D}\left[\frac{z}{D} + \left(\frac{b}{D} - 0.5\right)\tan\theta\right] \leq 1 \tag{2-33}$$

Now the adopted N_p and K_i for a pile at a distance of the crest are derived, they can be used for the p-y curves for undrained analysis for laterally loaded piles in clayey soils:

$$p = \frac{y}{(1/K_i) + (y/p_u)} \tag{2-34}$$

where

$$p_u = N_p c_u D \tag{2-35}$$

Georgiadis and Georgiadis have not validated the new proposed p-y curves in their article.

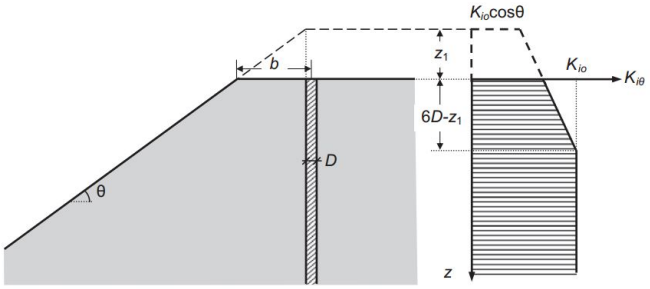

Figure 2-33: Effect of θ and b on initial p-y stiffness $K_{i\theta}$ after Georgiadis and Georgiadis [14]

2-4-4 Georgiadis et al. (2013)

In 2013 Georgiadis et al. published a research which focussed on short rigid piles instead of long flexible piles near clay slopes [15]. The difference in the design process between these piles is that the failure mechanism of long flexible piles is dominated by the yielding of the pile, while the failure of rigid piles is governed by the lateral resistance of the soil.

As an alternative for the solution that can be obtained with the p-y curve defined in Equation 2-27, charts for $H_u/c_u D^2$ versus L/D were determined.

Based on the equation for N_p the lateral earth pressure diagram of piles in level ground have been obtained, which is schematized in Figure 2-34a. With help of the force equilibrium (Equation 2-36) and moment equilibrium (Equation 2-37), the two unknowns, the rotation depth and the lateral bearing capacity can be derived:

$$H_u = \int_0^{z_0} p_u dz - \int_{z_0}^{L} p_u dz \tag{2-36}$$

$$eH_u = \int_{z_0}^{L} z p_u dz - \int_0^{z_0} z p_u dz \tag{2-37}$$

where

H_u	=	lateral bearing capacity [kN]
e	=	height of load application above surface level [m]
z_0	=	depth of rotation [m]
L	=	embedded pile length [m]

The solution of these simultaneous equations is:

$$\alpha_1(z_0/D)^2 + \alpha_2(z_0/D) + \alpha_3 e^{-\lambda(z_0/D)} + \alpha_4(z_0/D)e^{-\lambda(z_0/D)} + \alpha_5 = 0 \tag{2-38}$$

where

$$\alpha_1 = N_{pu}, \quad \alpha_2 = N_{pu}(e/D), \quad \alpha_3 = 2(N_{pu} - N_{po})(1/\lambda + e/D), \quad \alpha_4 = 2(N_{pu} - N_{po})/\lambda$$

$$\alpha_5 = -N_{pu}\left(\frac{L^2}{2D^2} + \frac{eL}{D^2}\right) - \frac{N_{pu} - N_{po}}{\lambda}\left[\frac{e}{D} + \frac{1}{\lambda} + \left(\frac{L}{D} + \frac{1}{\lambda} + \frac{e}{D}\right)e^{-\lambda L/D}\right]$$

The z_0/D ratio from Equation 2-38 can be introduced into the lateral force equilibrium to obtain the non-dimensional lateral bearing capacity:

$$\frac{H_u}{c_u D^2} = N_{pu}\left(2\frac{z_0}{D} - \frac{L}{D}\right) + \frac{N_{pu} - N_{po}}{\lambda}\left(2e^{-\lambda z_0/D} - e^{-\lambda L/D} + 1\right) \tag{2-39}$$

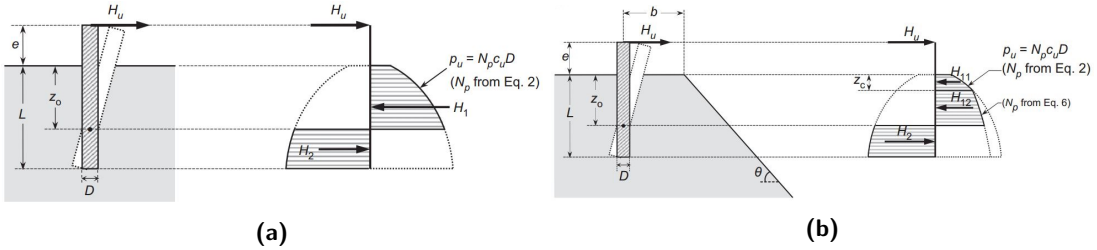

Figure 2-34: Lateral earth pressure for piles (a) in level ground and (b) near sloping ground after Georgiadis et al. [15]

Slope

With the help of the same mathematical procedure, the non-dimensional lateral bearing capacity near the clay slope can be determined. The lateral earth pressure diagram is shown in Figure 2-34b, the corresponding equations for the force and moment equilibrium are defined as:

$$H_u = \int_0^{z_c} p_u dz + \int_{z_c}^{z_0} p_u dz - \int_{z_0}^{L} p_u dz \tag{2-40}$$

$$eH_u = \int_{z_0}^{L} z p_u dz - \int_{z_c}^{z_0} z p_u dz - \int_0^{z_c} z p_u dz \tag{2-41}$$

The solution of these simultaneous equations is:

$$\alpha_1(z_0/D)^2 + \alpha_2(z_0/D) + \alpha_3 e^{-\lambda(z_0/D)} + \alpha_4(z_0/D)e^{-\lambda(z_0/D)} + \alpha_5 e^{-\lambda\alpha_\theta(z_0/D)} + \alpha_6(z_0/D)e^{-\lambda\alpha_\theta(z_0/D)} + \alpha_7 = 0 \tag{2-42}$$

where

$$\alpha_1 = N_{pu}, \quad \alpha_2 = 2N_{pu}(e/D), \quad \alpha_3 = (N_{pu} - N_{po})(1/\lambda + e/D)/\lambda, \quad \alpha_4 = (N_{pu} - N_{po})/\lambda$$

$$\alpha_5 = \frac{N_{pu} - N_{pc}}{\lambda\alpha_\theta}\left(\frac{1}{\lambda\alpha_\theta} + \frac{e}{D}\right)e^{\lambda\alpha_\theta(z_c/D)}, \quad \alpha_6 = \frac{N_{pu} - N_{pc}}{\lambda\alpha_\theta}e^{\lambda\alpha_\theta(z_c/D)}$$

$$\alpha_7 = -N_{pu}\left(\frac{L^2}{2D^2}+\frac{Le}{D^2}\right)-\frac{N_{pu}-N_{po}}{\lambda}\left(\frac{1}{\lambda}+\frac{e}{D}\right)-\frac{N_{pu}-N_{po}}{\lambda}\left(\frac{L}{D}+\frac{1}{\lambda}+\frac{e}{D}\right)e^{-\lambda(L/D)}$$
$$-\frac{N_{pu}-N_{pc}}{\lambda\alpha_\theta}\left(\frac{z_c}{D}+\frac{1}{\lambda\alpha_\theta}+\frac{e}{D}\right)+\frac{N_{pu}-N_{po}}{\lambda}\left(\frac{z_c}{D}+\frac{1}{\lambda}+\frac{e}{D}\right)e^{-\lambda(z_c/D)}$$

The z_0/D ratio from Equation 2-42 can be introduced into the lateral force equilibrium to obtain the non-dimensional lateral bearing capacity:

$$\frac{H_u}{c_u D^2} = c_1(z_0/D)^2 + [c_2 + c_3(z_0/D)]e^{-\lambda(z_0/D)} + [c_4 + c_5(z_0/D)]e^{\lambda\alpha_\theta(z_0/D)} + c_6 \tag{2-43}$$

where

$$c_1 = -N_{pu}(D/e), \quad c_2 = -(N_{pu}-N_{po})(D/e)/\lambda^2, \quad c_3 = -(N_{pu}-N_{po})(D/e)/\lambda$$
$$c_4 = -\frac{N_{pu}-N_{pc}}{\lambda^2\alpha_\theta^2}(D/e)e^{\lambda\alpha_\theta(z_c/D)}, \quad c_5 = -\frac{N_{pu}-N_{pc}}{\lambda\alpha_\theta}(D/e)e^{\lambda\alpha_\theta(z_c/D)}$$

$$c_6 = \frac{D}{e}\Big[\frac{N_{pu}}{2}\left(\frac{L}{D}\right)^2+\frac{N_{pu}-N_{po}}{\lambda^2}+\frac{N_{pu}-N_{po}}{\lambda^2}\left(\lambda\frac{L}{D}+1\right)e^{-\lambda(L/D)}$$
$$-\frac{N_{pu}-N_{po}}{\lambda^2}\left(\lambda\frac{z_c}{D}+1\right)e^{-\lambda(z_c/D)}+\frac{N_{pu}-N_{pc}}{\lambda\alpha_\theta}\left(\frac{z_c}{D}\right)+\frac{N_{pu}-N_{po}}{\lambda^2\alpha_\theta^2}\Big]$$

Georgiadis et al. have validated the charts $H_u/c_u D^2$ versus L/D by comparing these with lateral bearing capacity from field tests, only 2 tests were conducted on the crest of the slope, 23 tests in level ground. The result is shown in Figure 2-35. It is observed that the results from the proposed new method agree well with the field test results. It is a significant improvement compared with Broms' method.

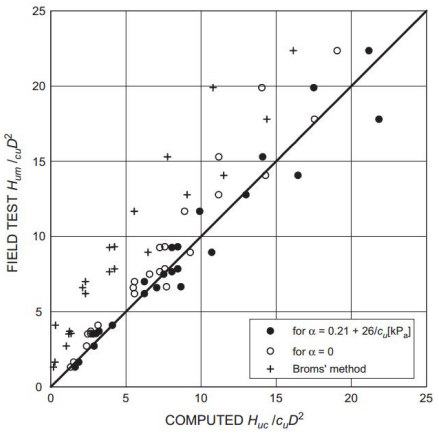

Figure 2-35: Comparison of computed and measured bearing capacities in pile load tests by Georgiadis et al. [15]

2-5 Evaluation of the literature

Overview

To compare the literature described in the previous sections, an overview has been made of all the tests. For each test the characteristics are given (kind of test, soil properties, pile properties) with the associated determined values for the ultimate lateral load capacity ratio, ψ, defined as $F_u(slope)/F_u(hor)$. This overview can be found in Table 2-2 and has been made visual in Figure 2-36 for clay tests and in Figure 2-37 for sand tests.

There are some derived values for ψ in Table 2-2 that should be regarded with caution. For instance, the values of Gabr and Borden. The ultimate load capacity at level ground is derived from an analytical solution and the value of the ultimate load capacity at the slope is determined from the full scale test. This means that the reliability of the load capacity ratio of Gabr and Borden depends on the accuracy of the analytical solution. Also, the value of Chae et al. founded from the FEM is questionable, since the model did not correspond for the pile in level ground with the results of the small scale test. This gives a distorted view of the ultimate load capacity ratio, ψ, derived from the FEM. The value determined from the small scale test is considered to be more reliable.

If one observes the graphs in Figures 2-36 and 2-37, a clear pattern can not be recognized. This may be attributed to the different parameters used in each study such as the slope angle, soil parameters, pile properties and the different methods (i.e. full scale models, small scale models and FEM).

Moreover, it was attempted to find a correlation for sand between the ratio of the slope angle and the friction angle on one hand and the load ratio, ψ, on the other hand. Unfortunately, a clear correlation was not visible and has not been found.

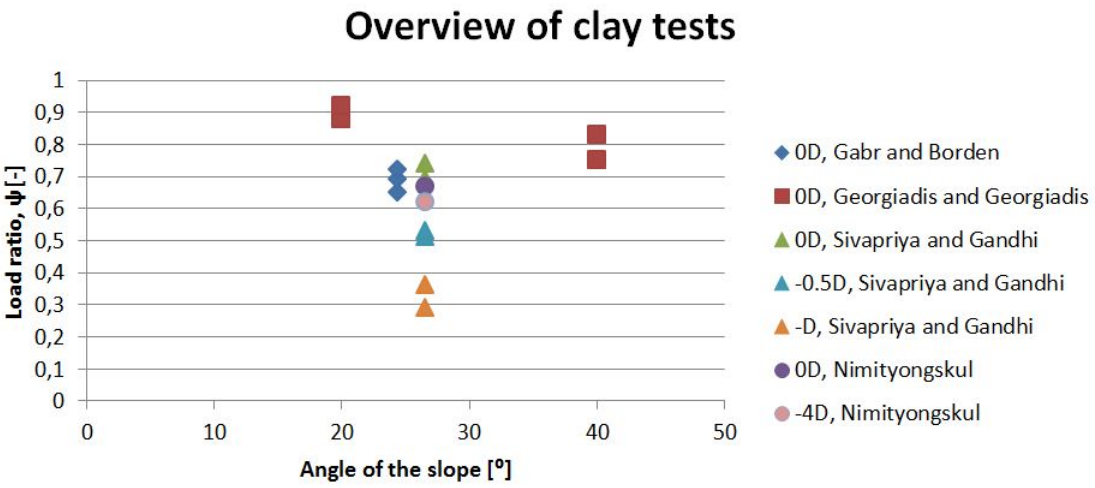

Figure 2-36: Overview of the ultimate lateral load capacity ratios of clay tests from literature

Researchers	**Soil type**	D_r [%]	ϕ [°]	c [kPa]	D [m]	L [m]	Test type	θ [°]	X_{lim}	$Pos.$	ψ
Gabr and Borden	Sand c-ϕ soil	-	40 25	0 62	0.76	2.13	FST FST	15.9 24.4	-	0D	0.67 0.65-0.75
Mezazigh and Levacher	Fine sand	81	-	-	0.018	0.3	SST	26,6	6-7D	0D	0,65
Chae et al.	Sand	90	47.5	-	0.1	0.5	SST FEM	30 30	-	0D	0,4 0,6
Muthukkumaran & Begum	Sand		30 40 45 30 40 45 30 40 45 30 40 45		0.02546 0.02456 	0.636 0.7638 	2D FEM 2D FEM 	1:2 1:1.5 1:2 1:1.5 	- - 	0D 0D 	0.6 0.59 0.73 0.35 0.59 0,59 0.46 0.72 0.67 0.32 0,69 0.56
Georgiadis & Georgiadis	Clay			70* 	1	5, 10	FEM	20 40		0D	0.88, 0.92 0.75, 0.83
Sivapriya and Gandhi	Clay	-	-	30* 50* 	0.016	0.45	SST	26.5	-	0D -1R -2R 0D -1R -2R	0.74 0.51 0.29 0.69 0.53 0.36
Mirzoyan	Top layer clean sand	-	-	-	0.32	13.4	FST	30	-	0D	0.78
Barker	Top layer cohesive	-	-	-	0.32	7.9	FST	26.5	8D	0D -4D	0.76 0.59
Nimityongskul	Top layer cohesionless	-	-	-	0.32	7.9	FST	26.5	8D	0D -4D	0.67 0.62

Table 2-2: Overview of tests from literature

D_r = density of the soil; ϕ = internal friction angle of the soil; c_u = undrained shear strength of the soil; D = diameter of the pile; L = embedded length of the pile; θ = angle of the slope; X_{lim} = distance from crest at which the slope has no significant influence on lateral load capacity of the pile; $Pos.$ = position of the pile with respect to the crest of the slope(- is from the crest towards the slope, + is from the crest away); Ψ = ratio of the ultimate lateral resistance, p_u; ψ = ratio of the lateral load capacity; FST = Full scale test; FEM= Finite Element Method; SST = Small Scale Test, * values are undrained shear strength

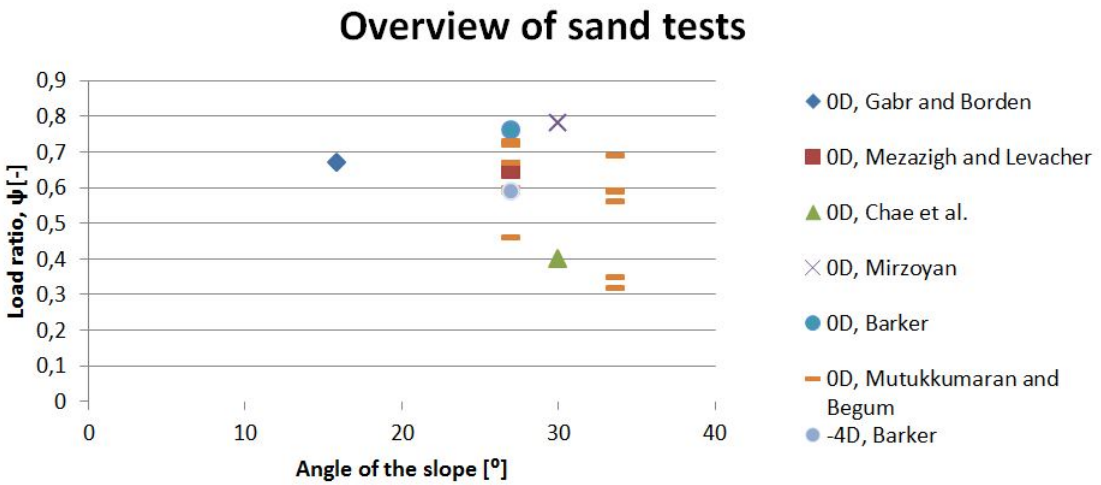

Figure 2-37: Overview of the ultimate lateral load capacity ratios of sand tests from literature

Influencing parameters

Based on the literature review it can be concluded that the parameters listed below influence the ultimate load capacity of the laterally loaded pile in a slope:

- The slope angle, θ.
- The location of the pile on the slope, expressed as distances D from the crest of the slope.
- The kind of soil. A sandy soil has a much higher load capacity than a clayey soil. In contrast, if one accounts for the slope, the load ratio for clay is higher than for sand.
- The pile properties. A larger pile diameter and pile length means a higher load capacity of the pile.
- The roughness of the pile-soil interface. The rougher the pile, the higher the load capacity.

Observations

Besides the measurements during the tests from which the overview table has been derived, there were also observations at the ground surface. Regarding the existence of the gap and the failure pattern, it can be concluded that:

- All studies agree about the fact that a gap arises between the back of the pile and the surrounding soil due to the applied lateral load. This gap appears both in cohesive and cohesionless soil, opens further as the load increases, and does not collapse or fill up the gap. The existence of the gap is attributed to the cohesive properties of the soil or to the apparent cohesion in sand, due to capillarity. The gap suggests that over the length of the gap no active pressure does contribute to the pile-soil interaction.
- Mirzoyan, Nimityongskul and Barker paid attention to the soil failure pattern of the passive wedge. It was observed that failure wedge angle, Ω decreases as the pile location moves to the crest and as the applied load increases. Suggested values for Ω are: 0.75ϕ (Mirzoyan) and 0.7ϕ (Barker).

Multipliers

To adopt the p-y curve for the sloping ground 4 different methods were developed. Two methods are suitable for sand and two are suitable for clay.

- Mezazigh and Levacher suggested a multiplier r for the p-y curve applicable for sand. The multiplier depends on the angle of the slope and the distance to the crest. One difficulty of the multiplier is the lack of information about over which depth the multiplier should be used. Another limitation is that the formula of the multiplier does not correspond to test results, unfortunately Mezazigh and Levacher do not explain these uncertainties.
- Barker suggested to divide the slope into zones; to each zone a multiplier is assigned. This multiplier is obtained from the p-y curves back-calculated from the full scale test. Below a depth of 10D beneath ground surface the multiplier is considered to be equal to 1. The easy applicability of this method is a great advantage.
- Nimityongskul realised that the effect of the slope on the p-y curves increases as the displacements increase. Therefore, he developed a multiplier which depends on the soil displacements for clayey soils. The multiplier is obtained from the back-calculated p-y curves of the first 7D below ground surface, below this depth Nimityongskul considers that the p-y curves are not changed with respect to a pile in horizontal ground surface.
- Georgiadis and Geoargiadis have done the most thorough and successful study to develop p-y curves for sloping ground. The developed p-y curves are designed for undrained loading in clay. By performing a parameter study in Plaxis 3D, both the variation of the initial stiffness and the variation of the ultimate soil resistance is examined. The new p-y curves were used as input in the program LPILE to recalculate three tests from literature, the results were satisfying. The error was within 15%, the general shape of the calculate load-displacement curves was very similar to the measured curves.

Chapter 3

Software validation

Now the literature review has been completed, tests are selected to validate the software applications. The applications used in this master's thesis are D-Sheet Piling, D-Pile Group and Plaxis 3D. D-Sheet Piling and D-Pile Group are selected, since these programs are most frequently used in the Dutch engineering practice. Plaxis 3D is selected for its extensive modelling options, which has among others the advantages to take the continuity of the soil into account and examine the in-situ stress conditions. All programs have the feasibility to model a laterally loaded pile, the aim of this chapter is to determine how capable they are in modelling the behaviour of a laterally loaded pile.

In Appendix E a discussion about the three software programs and their properties is enclosed. This chapter contains an explanation of the tests selected from literature including the test results from the modelling programs. The chapter will finish with a conclusion about the capabilities of the software applications.

3-1 Full scale test - Nimityongskul

For his dissertation, "Effects of Soil Slope on Lateral Capacity of Piles in Cohesive Soils", Nimityongskul conducted a series of full scale tests [3]. In contrast to what the title suggests, the tests were not conducted in entirely cohesive soil. The first layer, which has a thickness of 10D, is a cohesive clay layer, followed by alternating sand and clay layers. However, Nimityonskul qualifies it as cohesive soil, since the literature shows that the lateral response of the piles depends mainly on the soil properties of the soil layers in the first 8D-10D [19] [32] [33].

Site description

The tests are conducted at the test site of the Oregon State University campus. This site has been used for geotechnical research since 1972, as a consequence a lot of information is available about the geotechnical circumstances. In addition to this, also four extra boreholes, three Cone Penetration Tests, and two Dilatometer Tests were executed.

The top layer of the site is referred to as the **upper cohesive soil layer** and extends to a depth of 3m. This layer consists of stiff to very stiff cohesive soil. It can be represented as a layer with uniform average and upper bound undrained shear strength of 76.6 kN/m^2 and 114.9 kN/m^2

respectively and it has an average unit weight of 18.1 kN/m^3. This layer is underlain by a layer of dense, poorly graded sand with silt and gravel which is encountered from -3 m to -4 m relative to ground surface. The average corrected blow count of the layer, N_1, is 33, the internal friction angle of the sand is 40° and the average unit weight is 20.6 kN/m^3. The layer is referred to as the **upper sand layer**. Below this is a stratum of medium stiff, high plasticity sandy silt, which has a thickness of 1.5m. This layer is referred to as the **lower cohesive layer**. The undrained shear strength and unit weight are qualified to be the same as the upper cohesive layer. Hereafter a layer of medium dense to dense, well-graded sand with silt and gravel is found, it extends to a depth of -7m below ground surface. The internal friction angle is suggested to be 45°. This layer is referred to as the **lower sand layer**. Below this sand layer is a layer of stiff to very stiff, blue-gray, high plasticity sily clay, which extends to a depth of approximately -23m. The undrained shear strength is estimated to be 167.6 kN/m^2 and it has an average unit weight of 17.5 kN/m^2. This layer is referred to as the **blue-gray clay layer**. The water table varies throughout the year, but was -2.1m below ground surface during the tests. In Table 3-1 an overview of the stratification can be found. Other relevant information from the site investigation can be found in appendix D.

The slope on the testing site has been constructed by excavation. A soil layer of 3.5m has been excavated, the constructed slope had an angle of 26.5°.

Soil layer	Height top $[m]$	γ_{unsat} $[kN/m^3]$	$\gamma_{sat}[kN/m^3]$	s_u $[kN/m^2]$	ϕ [°]
Upper cohesive layer	0	18.1	18.3	114.9	-
Upper sand layer	-3	20.4	20.6	-	40
Lower cohesive layer	-4	18.1	18.3	114.9	
Lower sand layer	-5.5	20.4	20.6		45
Blue gray clay layer	-7	17.3	17.5	167.6	

Table 3-1: Stratification of the soil at the test site of Nimityongskul

Test set-up

The testing program included two tests in horizontal ground and tests at distances 8D, 4D, 2D, 0D and -4D from the crest of the slope. Also, one battered pile was tested, but this will not be considered in this thesis.

All the test piles had an outer diameter of 323.85 mm and a wall thickness of 9.5 mm. The total length of the piles was 9.1 m, the embedded length was 7.9 m.

The test piles were loaded by a hydraulic actuator. Therefore, reaction piles were required to provide reaction for the test piles, these were coupled with a horizontal beam. A sketch of the test set-up can be found in Figure D-1a in Appendix D.

The test piles were loaded by steps to obtain load-displacement curves. For each step, the pile was loaded until a target displacement was reached and maintained for 5 to 10 minutes to allow the pile to stabilize. Hereafter, the procedure was repeated and the next displacement increment was applied. The loading continued until it was determined that the maximum load capacity of the test pile was reached.

To register the test, several instruments were used. Strain gauges, tiltmeters, load cells and linear potentiometers were installed on the pile to determine the behaviour of the pile during the test. An overview can be found in Figure D-1b in Appendix D. At each level, two gauges were installed on each side of the tested pile to measure tension and compression of the pile. The tiltmeters were used to record pile rotation during testing. The linear string potentiometers measured the lateral pile head displacement. Four load cells were used to record the applied lateral load. Instruments were not installed in the surrounding soil, so soil stresses were not registered. However, gridlines were drawn on the ground surface to observe the ground movement with photos during the test.

3-1-1 Modelling Nimityongskul's test

D-Sheet Piling

The input parameters for D-Sheet Piling of Nimityongskul's test are presented in Table 3-2. Undrained conditions for clay are simulated, since for the cohesion the undrained shear strength is entered in combination with $\phi = 0$. For the modulus of Ménard, the correlation in Appendix E-1 is used. For clay, the modulus of Ménard is 2 á 3 times the cone resistance. From the CPT in appendix D is determined that the average cone resistance for the upper cohesive layer is 2000 kN/m^2, therefore E_{Menard} is chosen as 4000 kN/m^2. The results from this analysis can be found in Figure 3-1. It can be concluded that the results of D-Sheet Piling and Nimityongskul agree considerably well. It should be mentioned that the correspondence of the results depend largely on the chosen value for E_{menard} for the upper soil layer. The value of 4000 kN/m^2 provides similarity between the graphs and corresponds to the correlation in Appendix E-1.

Soil layer	γ_{unsat} $[kN/m^3]$	γ_{sat} $[kN/m^3]$	c $[kN/m^2]$	ϕ [°]	E_{menard} $[kN/m^2]$
Upper cohesive layer	18.1	18.3	114.9	0	4,000
Upper sand layer	20.4	20.6	0	40	8,500
Lower cohesive layer	18.1	18.1	114.9	0	3000
Lower sand layer	20.4	20.6	0	45	20,000
Blue gray clay layer	17.3	17.3	167,9	0	15,000

Table 3-2: Input parameters for D-Sheet Piling for Nimityongskul's test

D-Pile Group

The input parameters for D-Pile Group are presented in Table 3-3. As for D-Sheet Piling, undrained conditions are simulated for the clay layers, by filling in the undrained shear strength for the cohesion and no internal friction angle. For the clay layers J is considered as 0.5, and ϵ_{50} as 0.005, ϵ_{50} is determined from the correlation in appendix E-2. The ϵ_{50} is decreased for the upper cohesive layer, to simulate more realistic the stiffer behaviour of the upper layer due to dehydration of the clay.

The result of the analysis is shown in Figure 3-1. The results do not correspond as good as the results of D-Sheet do, this is caused by the difficult upper cohesive layer. The upper side of the clay layer is dehydrated, which makes it very stiff. It was attempted to simulate this behaviour by increasing ϵ_{50} to 0.001, but the results of D-Sheet remain more satisfying.

Soil layer	γ_{unsat} $[kN/m^3]$	γ_{sat} $[kN/m^3]$	c $[kN/m^2]$	ϕ [°]	J [-]	$\epsilon_{50\%}$ [-]
Upper cohesive layer	18.1	18.3	114.9	-	0.5	0.001
Upper sand layer	20.4	20.6	-	40	-	-
Lower cohesive layer	18.1	18.3	114.9	-	0.5	0.005
Lower sand layer	20.4	20.6	-	45	-	-
Blue gray clay layer	17.3	17.3	167,9	-	0.5	0.005

Table 3-3: Input parameters for D-Pile Group for Nimityongskul's test

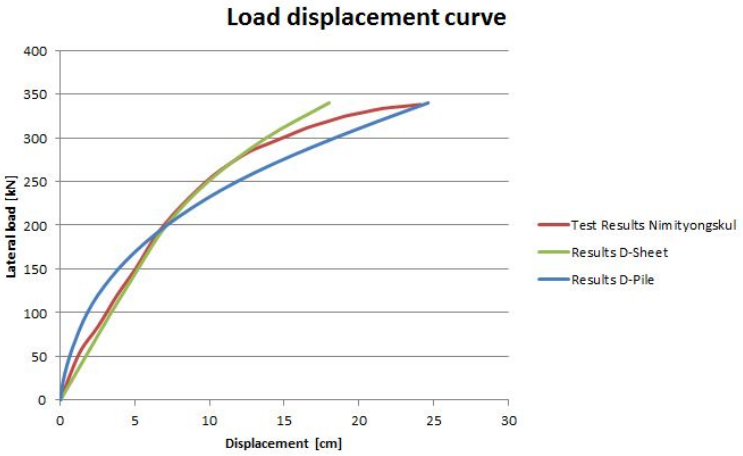

Figure 3-1: Load displacement curves of Nimityongskul, D-Sheet and D-Pile at 0.9m above surface level

Plaxis 3D

For the sand layers, only the internal friction angle was available from the information of Nimityongskul. Therefore, the other input parameters for the $HSsmall$ model for sand were derived from the correlation developed by Brinkgreve et al. [34]. The input parameters for the clay layer are determined iteratively with the stress strain curves of the undrained traxial tests and the soil test function of Plaxis. The stiffness of the clay layers is considerable higher than common in the Netherlands. However, also other correlations indicate these high values. Meigh and Corbet give as correlation between the oedometer stiffness and cone resistance $E_{oed} = (5 \text{ á } 8) * q_c$. The cone resistance can be determined from the CPT in appendix D. The q_c for the upper cohesive layer has a maximum value of 5 MPa and an average value of 2 MPa, for the lower cohesive layer is the cone resistance around 1 MPa, and the blue-gray clay layer has a cone resistance around 9 MPa. So these values result in the same range of stiffness's. An overview of the input parameters is given in Table 3-4.

To prevent numerical problems, it was required to model the soil within the pile as drained. When the soil was modelled as undrained, within the pile unexplainable very high water-overpressures were built up, which were unrealistic. During the calculation this led constantly to a numerical error. Moreover, since a laterally loaded pile can be considered as symmetrical problem, only half of the problem is modelled. The results of the load-displacement curves are plotted in Figure 3-2. As can be observed, modelling only half of the problem is justified since the results agree considerably well.

If one observes Figure 3-2 it is remarkable to note that the load-displacement curve of the pile located in the slope behaves stiffer initially then the pile located at the crest. This contradicts to the expectation, but Plaxis 3D simulates the behaviour satisfying. However, this phenomenon can be explained by the different heights of load application above surface level. Since it was impossible for Nimityongskul to move down the hydraulic actuator for the pile located at the slope, this pile had a higher load of application and hence a different embedded length. Since the failure mechanism of Nimityongskul's full scale test was the yielding of the pile, the test results and Plaxis results can only be compared for the elastic part of the test. It is not possible to model plastic yielding of a plate material in Plaxis 3D.

Plaxis 3D is capable of modelling this behaviour over the elastic part of the pile. For the pile located at the crest and the slope, the load displacement curves agree considerably well. For the pile in horizontal level ground the results deviate slightly off, but are still with an acceptable range.

		Upper cohesive layer	Upper sand layer	Lower cohesive layer	Lower sand layer	Blue-gray clay layer
		HS small Undrained A	HS small Drained	HS small Undrained A	HS small Drained	HS small Undrained A
γ_{unsat}	$[kN/m^3]$	18.1	20.4	18.1	20.4	17.3
γ_{sat}	$[kN/m^3]$	18.3	22	18.3	22	17.5
E_{50}^{ref}	$[kN/m^2]$	40,000	60,000	18,000	80,000	80,000
E_{oed}^{ref}	$[kN/m^2]$	20,000	60,000	9000	80,000	40,000
E_{ur}^{ref}	$[kN/m^2]$	120,000	180,000	54,000	240,000	240,000
m	[-]	1	0.3880	1	0.25	1
$c^{`}$	$[kN/m^2]$	60	0.5	40	0.5	70
ϕ	[°]	20	40	20	45	25
Ψ	[°]	-	3	-	3	
$\gamma_{0.7}$	[-]	0.1E-03	0.1E-03	0.1E-03	0.065E-03	0.1E-03
G_0^{ref}	$[kN/m^2]$	50,000	128,000	22,500	152,000	100,000
R_{inter}	[-]	0.9	0.8	0.7	0.8	0.7

Table 3-4: Input parameters for Plaxis 3D for Nimityongskul's test

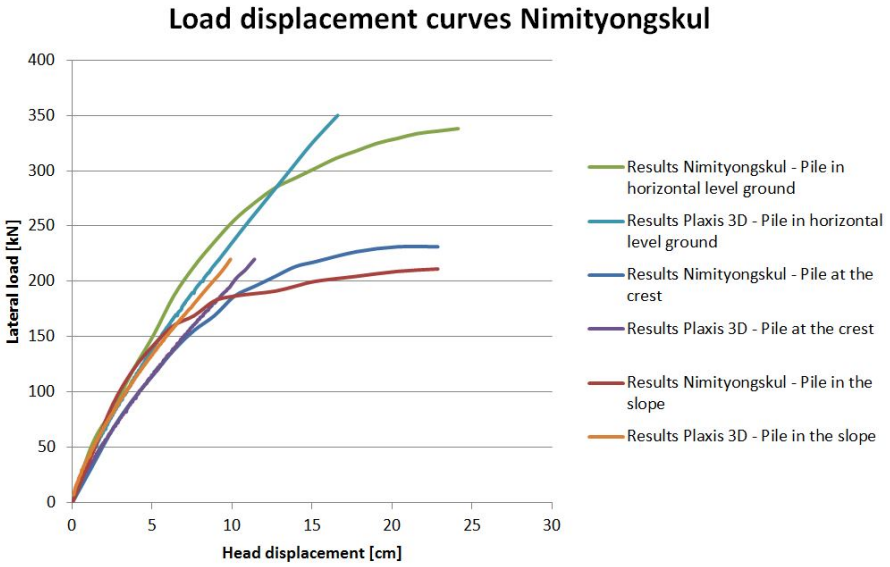

Figure 3-2: Comparison of the load-displacement curves measured by Nimityongskul for the pile in level ground, at the crest of the slope (0D Pile) and in the slope (-4D Pile)

Plaxis 3D by Nimityongksul

Besides the conducted Plaxis calculations in this thesis, Nimityongskul himself conducted also Plaxis calculations after the execution of the full scale test. Instead of the *HSsmall* model, he used the Mohr Coulomb soil model. The results are worth mentioning.

Nimityongskul used a previous version of Plaxis 3D, Plaxis 3D Foundation - V2.2 [35]. The choice for the MC model was substantiated by positive experiences of Brown and Shie [36] and Georgiadis and Geoargiadis [10] for simulating soil behaviour of clay during undrained loading. The Mohr Coulomb model has two main differences compared to the *HSsmall* model. In the MC model, the yield surface is not affected by the plastic straining and the stiffness of the soil is not stress dependent. Nimityongskul determined the input parameters from the UU traxial test results. To consider undrained loading conditions, Nimtyongskul selected $c^{`} = s_u$ and $\phi = 0$. An overview of

the input parameters is presented in Table 3-5.

The load displacement curves of Nimityongskul analysis' are plotted in Figure 3-4. For the pile in level ground the results agree considerably well over the elastic part. As the pile tends to yield (around 40kip/ 180kN), Plaxis calculates stiffer behaviour. This is caused by the fact that it is impossible to model plasticity of the pile in Plaxis 3D. From Figure 3-4b can be concluded that Plaxis models the behaviour of the pile located at the crest of the slope a lot more inaccurate. The load-displacement curve of Plaxis is much stiffer than the measured results. Nimityongskul attributes this to the fact that the material model does not account for softening due to dilatation and de-bonding. Hereby, the soil behaves stiffer than in reality. To obtain equal behaviour of Plaxis 3D and the test results, Nimityongskul had to decrease the original parameters to $0.45 s_u$ and $0.6 E_{50}$.

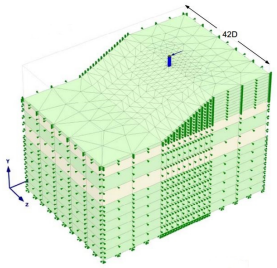

Figure 3-3: Plaxis 3D model of Nimityongskul [3]

		Upper cohesive layer	Upper sand layer	Lower cohesive layer	Lower sand layer	Blue-gray clay layer
		Mohr Coulomb Undrained A	Mohr Coulomb Drained	Mohr Coulomb Undrained A	Mohr Coulomb Drained	Mohr Coulomb Undrained A
γ_{unsat}	$[kN/m^3]$	18.1	20.4	18.1	20.4	17.3
γ_{sat}	$[kN/m^3]$	18.1	20.4	18.1	20.4	17.3
E_{ref}	$[kN/m^2]$	7565	28728	7565	28728	7565
c_{ref}	$[kN/m^2]$	114.9	0	114.9	0	167.6
ν	[-]	0.495	0.35	0.495	0.35	0.495
ϕ	[°]	0	40	0	45	0
Ψ	[°]	0	0	0	0	0
R_{inter}	[-]	0.7	0.7	0.7	0.7	0.7

Table 3-5: Input parameters for Plaxis 3D by Nimityongskul

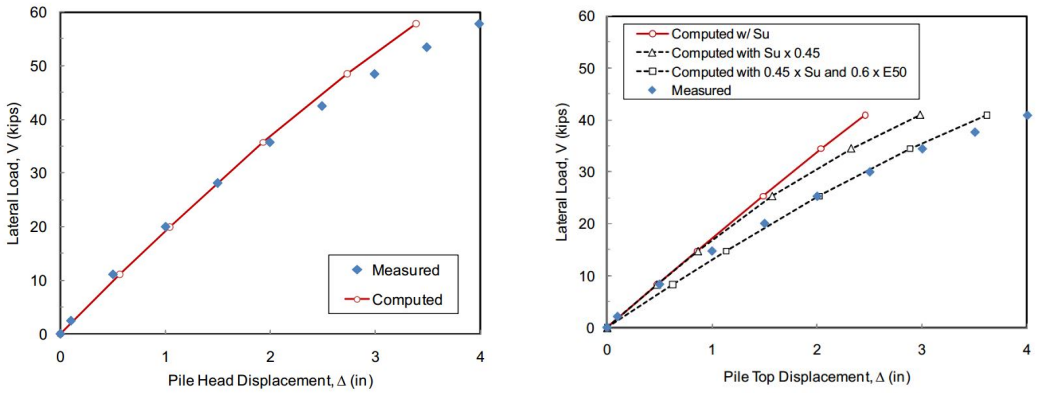

Figure 3-4: Load displacement curves of the pile (a) located in level ground and (b) located at the crest of the slope after Nimityongskul [3](1 kip = 4.45 kN, 1 inch = 2.54 cm)

3-2 Full scale test - Barker

Also Barker conducted full scale tests for his master's thesis, "Effects of Soil Slope on the Lateral Capacity of Piles in Cohesionless Soils" at the testing site of the Oregon State University. Likewise for Barker, the test was not in entirely cohesionless soil. By constructing a 10D thick embankment of cohesionless soil on the existing test site, Barker assumes that the pile behaves as it would in entirely cohesionless soil. This statement is based on literature that shows that the lateral response of the piles depends mainly on the soil properties of the soil layers in the first 8D-10D [19] [32] [33].

Site description

An embankment consisting of a cohesionless structural backfill was constructed on the original ground surface with a height of 3 meter and a slope of 26.5°. In compacted lifts with each a relative compaction of at least 95%, an embankment was built with an internal friction of 43° and an average unit weight of 19.95 kN/m^3. After construction of the embankment, three mud rotary borings were drilled. These boring were consistent with the boring logs performed by Nimityongskul, therefore the lower layers are considered to have the same soil properties and depths in this analysis. Hence, the soil stratification is considered to be as shown in Table 3-6.

Barker assumes that the consolidation caused by construction of the embankment did not affect the stress and strength of the native soils. Also, the effects of new hydrological condition were not considered, so the water table will be -5.1 meter beneath the new surface level.

Soil layer	**Height top** $[m]$	γ_{unsat} $[kN/m^3]$	$\gamma_{sat}[kN/m^3]$	s_u $[kN/m^2]$	ϕ [°]
Cohesionless backfill	0	19.95	19.95	-	43
Upper cohesive layer	-3	18.1	18.3	114.9	-
Upper sand layer	-6	20.4	20.6	-	40
Lower cohesive layer	-7	18.1	18.3	114.9	-
Lower sand layer	-8.5	20.4	20.6	-	45
Blue gray clay layer	-10	17.3	17.5	167.6	-

Table 3-6: Stratification of the soil on the test site of Barker

Test set-up
Barker conducted 10 full scale lateral load tests; two piles in horizontal ground surface, 3 battered piles and five piles at distances of 8D, 4D, 2D, 0D and -4D of the crest of the slope. The battered piles will not be considered in this thesis.

All the test piles had an outer diameter of 323.85 mm, a wall thickness of 9.5 mm and a length of 9.1 m, the embedded length of the piles was 7.9 m.

The testing set-up was identical to the set-up of Mirzoyan. The pile was loaded by a hydraulic actuator and 15 piles with a horizontal beam were used as reaction. To register the pile during the test strain gauges, tiltmeters, linear string potentiometers and load cells were installed. To observe the soil behaviour, gridlines were drawn on ground surface and photos were taken.

Also, the loading procedure was equal to Nimityongskul's. For each step, the pile was loaded till a target displacement was reached to obtain the load-displacement curves. After a target displacement was reached, this was maintained for 5 to 10 minutes. The loading procedure was repeated until it was determined that the maximum load capacity of the tested pile was reached.

3-2-1 Modelling Barker's test

Since from site investigation was concluded that the native soil layers were not effected by construction of the embankment, only an extra sand layer was added above the native soil layers in D-Sheet Piling, D-Pile Group and Plaxis 3D. All the other parameters remained the same in the models. The piles were installed closed-ended, to allow installing of the measurement devices. This means that there are significant installation effects, which affects the sand. Unfortunately, no extra CPT's have been executed after installing of the pile, so the correct parameters of the sand backfill are unknown.

D-Sheet Piling

The input parameters for the new structural backfill layer are presented in Table 3-7. The cone resistance of the structural backfill layer is unknown, this makes it difficult to determine the Modulus of Ménard. Since it is a very compacted layer, due to the installation effects, the value of 25,000 kN/m^2 is selected as value for E_{Menard}. The result of the analysis is plotted in Figure 3-5. As can be seen, the pile in D-Sheet reacts significant less stiff than the tested pile. This is explained by the installation effects of the pile. Only when an internal friction of 55° is entered, the slope of D-Sheet load-displacement curve has the same slope as the load-displacement curve of the test results.

Soil layer	γ_{unsat} $[kN/m^3]$	γ_{sat} $[kN/m^3]$	c $[kN/m^2]$	ϕ [°]	$E_{menard}[kN/m^2]$
Structural backfill	19.9	19.9	0	43	25,000

Table 3-7: Input parameters for D-Sheet Piling for the structural backfill layer for Barker's test

D-Pile Group

It is not possible in D-Pile Group to model a soil which has an internal friction angle of 43°with the standard API p-y curve. Therefore the correct API p-y curve for sand has been calculated with the help of a spreadsheet. The value for k, the initial modulus of subgrade reaction have been interpolated from Table E-1, the other parameters for the p-y curve are determined with the formulas defined in Appendix E-2.

The results of the analysis in D-Pile are plotted in Figure 3-5. The load displacement curve of D-Pile agrees well with the curve of D-Sheet, nevertheless with respect to Barker's test results the

	ϕ [°]	Ψ [°]	E_{50}^{ref} $[kN/m^2]$	E_{oed}^{ref} $[kN/m^2]$	E_{ur}^{ref} $[kN/m^2]$	m [-]	$\gamma_{0.7}[-]$	G_0^{ref} $[kN/m^2]$
Structural backfill	43	3	72,000	72,000	216,000	0.31	0.8E-04	142,000

Table 3-8: Input parameters for the structural backfill layer in Plaxis 3D for the test of Barker

pile-soil interaction is considerable weaker. Also this is explained by the installation effects of the pile. Since the soil is already very compacted (compaction > 95%), the area which is effected by the pile installation is very large. Therefore, in a large area the soil parameters must be much higher than indicated by the standard soil parameter correlations.

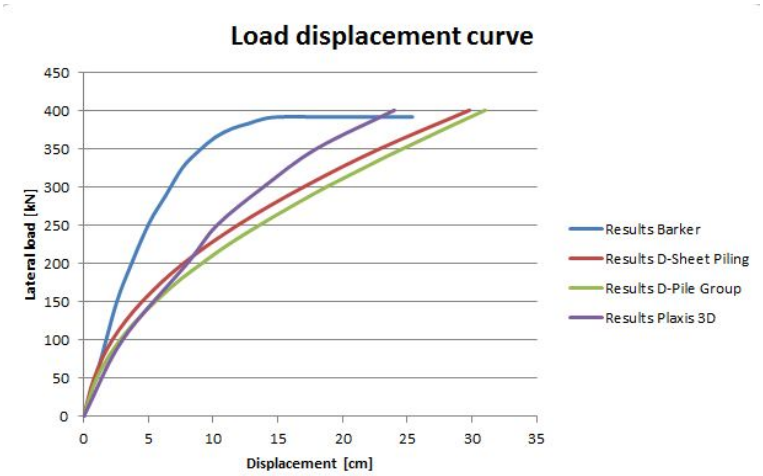

Figure 3-5: Load displacement curves of Barker, D-Sheet, D-Pile and Plaxis 3D at 0.9m above surface level

Plaxis 3D

The input parameters for the structural backfill layer were, as for the other sand layers, determined from the correlation developed by Brinkgreve et al. [34]. With an internal friction angle of 43°, this leads to the parameters presented in Table 3-8.

As can be seen in Figure 3-5 the pile-soil interaction is stiffer than in D-Sheet and in D-Pile for loads higher than 250kN. Nevertheless, also the results of Plaxis 3D are considerable weaker than Barker's test results. Also this is attributed to the fact that it is impossible to model installation effects in Plaxis 3D. The large effect of the installation of the pile is explained by the already high compacted sand layer.

Since the results of this test are not satisfying in any model program, there is not put effort in modelling the slope and the piles in the slope for this test. Therefore, a third test from literature is selected to validate the programs for sand layers. The centrifuge test of Mezazigh and Levacher is explained in the next section.

3-3 Centrifuge test - Mezazigh and Levacher

Mezazigh and Levacher conducted 59 laterally loaded pile tests with centrifuge modelling, this method was preferred for the large amount of tests that can be executed relative to full scale tests. The aim of the testing program was to study the effect of a slope on the p-y curves near sloping ground in dry sand.

Test set-up
The sand used in the centrifuge test was a fine white Fontainebleau sand. Two different densities were regarded, 58% giving a unit weight of 15.5 kN/m^3 and 81% giving a unit weight of 16.1 kN/m^3 . The density deviation in the containers was less than 1% obtained by an automatic hopper that constructed the sand mass by raining.

All the test piles were AU4G aluminium tubes with an outside diameter of 18mm, a wall thickness of 1.5mm an embedded length of 300mm and a total length of 380mm. Having a centrifugal acceleration of 40g, this simulates a prototype pile with a length of 12 m and a diameter of 0.72 m. The flexural stiffness of the pile, E_pI_p, is 514 MNm^2. The pile was instrumented with strain gauges placed 15mm apart. Three displacement sensors DP1, DP2 and DP3 were positioned 0, 20 and 65mm (0, 0.8m and 2.6m)above surface level.

For the centrifuge tests containers were used of 1200mm x 800mm. Within these containers for each series of tests first three reference tests were performed in a horizontal surface, hereafter the slopes were cutted. Two different slopes were tested, 2:1 (26.6°) and 3:2 (33.7°) with a slope height of 350mm. The lateral load was applied at 40mm (1.6m) above surface level by a steel cable.

3-3-1 Modelling Mezazigh and Levacher's test

D-Sheet Piling

The input parameters for D-Sheet Piling are presented in Table 3-9. The modulus of Ménard was estimated based on the correlation for sand in Appendix E-1. The load-displacement curve of D-Sheet is very sensitive for the value of the modulus of Ménard, for the current values the load displacement curves agree most. The correlation of Brinkgreve et al. [34] was used to estimate the internal friction angle with the help of the relative density.

The load displacement curves are plotted in Figure 3-6. As can be seen the agreement between the curves is reasonable, for a relative density of 81 % the behaviour is somewhat stiffer, for a density of 58% the curves corresponds even better.

	γ_{unsat} $[kN/m^3]$	γ_{sat} $[kN/m^3]$	c $[kN/m^2]$	ϕ [°]	$E_{menard}[kN/m^2]$
Fontainebleau sand for D=81%	16.1	16.1	0	38	9000
Fontainebleau sand for D=58%	15.5	15.5	0	35	8000

Table 3-9: Input parameters for D-Sheet Piling for the test of Mezazigh and Levacher

D-Pile Group

The input parameters for D-Pile Group are also determined by the correlation of Brinkgreve et al. [34]. The value of the cone resistance does not influence the results of D-Pile Group for a laterally loaded pile.

The load displacement curves of D-Pile Group are also plotted in Figure 3-6. It is clear that the correlation of Brinkgreve et al. [34], which determined the unit weight, the internal friction angle

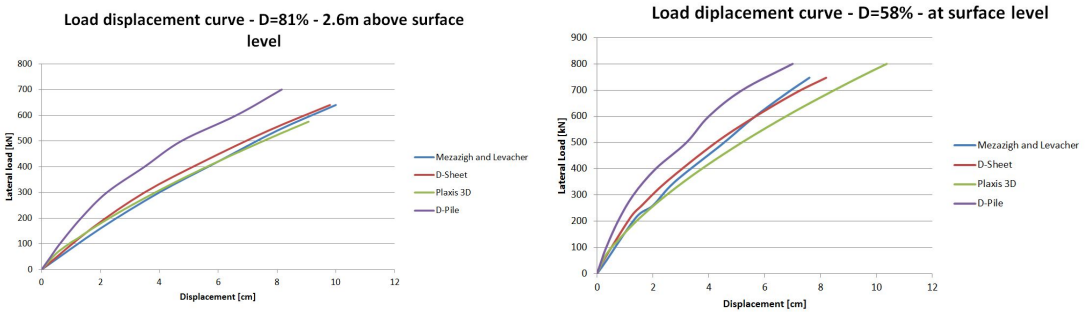

Figure 3-6: Load displacement curves of Mezazigh and Levacher for (a) D=81%, 2.6m above surface level and (b) D=58%, at surface level

and indirectly K_0, is much less appropriate for D-Pile Group than it is for D-Sheet Piling. The load-displacement curve reacts too stiff.

	γ_{unsat} $[kN/m^3]$	γ_{sat} $[kN/m^3]$	ϕ [°]	K_0[-]	q_c $[kN/m^2]$
Fontainebleau sand for D=81%	16.1	16.1	38	0.38	12,000
Fontainebleau sand for D=58%	15.5	15.5	35	0.43	10,000

Table 3-10: Input parameters for D-Pile Group for the test of Mezazigh and Levacher

Plaxis 3D

The parameters for the *HSsmall* model are determined with the correlations of Brinkgreve et al. [34] and presented in Table 3-11. Based on the load displacement curves plotted in Figure 3-6, it can be concluded that this correlation is excellent for a relative density of 81%, the load displacement curves agree considerably well. For a relative density of 58% the correlation is less suitable. However, the load displacement curve is still within an acceptable margin for smaller displacements, when a load is applied of 700 kN, the error is 25%. Beneath this load, the error is smaller.

Hereafter, the pile on the crest of the slope is modelled in sand with a relative density of 81%. Exactly the same soil parameters are used, only the pile is relocated. The load displacement curves are plotted in Figure 3-7 and the results correspond very well.

Relative density		Fontainebleau sand 81%	Fontainebleau sand 58%
Material model		HS small	HS small
Drainage type		Drained	Drained
γ_{unsat}	$[kN/m^3]$	16.1	15.5
γ_{sat}	$[kN/m^3]$	16.1	15.5
E_{50}^{ref}	$[kN/m^2]$	48,000	34,800
E_{oed}^{ref}	$[kN/m^2]$	48,000	34,800
E_{ur}^{ref}	$[kN/m^2]$	144,000	104,400
m	[-]	0.45	0.519
$c^{`}$	$[kN/m^2]$	0.5	0.5
ϕ	[°]	38	35
Ψ	[°]	3	3
$\gamma_{0.7}$	[-]	1.2E-04	1.42E-04
G_0^{ref}	$[kN/m^2]$	114,000	99,440
R_{inter}	[-]	0.8	0.8

Table 3-11: Input parameters for Plaxis 3D for the test of Mezazigh and Levacher

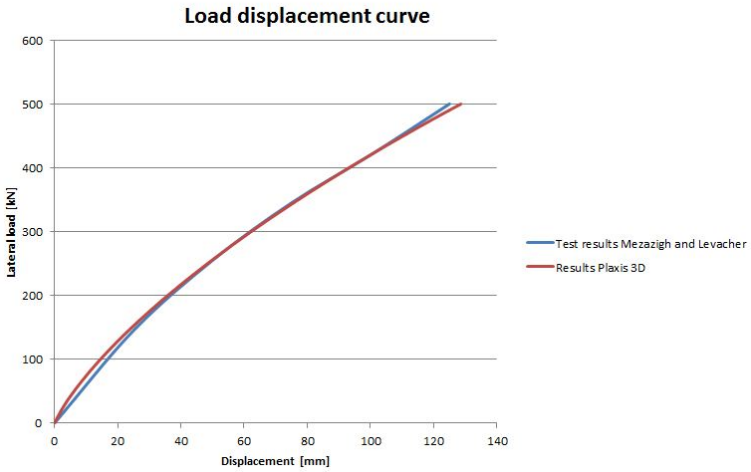

Figure 3-7: Load displacement curves of Mezazigh and Levacher and Plaxis 3D of the pile installed at the crest of sand slope with D=81%

3-4 Conclusion

In the previous sections different tests from literature were modelled with the software programs D-Sheet Piling, D-Pile Group and Plaxis 3D. With regard to D-Sheet Piling and D-Pile Group, D-Sheet Piling performs much better than D-Pile Group using the correlations of Brinkgreve et al. [34] for sand and about equal for undrained conditions of clay. Moreover, it was concluded that the results of D-Sheet Piling are largely influenced by the modelus of Ménard.

Plaxis 3D is the best performing modelling program. It is capable of modelling a laterally loaded pile in both level ground and sloping ground. The test of Mezazigh and Levacher showed that correlations of Brinkgreve et al. are suitable to determine the parameters for the $HSsmall$ model. In general, the analysis of a sand slope is less time-consuming than an analysis of a clay slope.

It is more difficult to validate Plaxis 3D for a laterally loaded pile on a clay slope, the parameters for the $HSsmall$ model are more difficult to determine and a lot more numerical problems arise

during the calculation process. However, after some effort, one could see in Figure 3-2 that Plaxis 3D is highly capable of modelling laterally loaded piles located at the crest and at the slope.

By comparing the Plaxis results of Nimityongskul, who used the Mohr Coulomb model, with the Plaxis results of this thesis, it becomes clear that the *HSsmall* model is much more appropriate than the Mohr Coulomb model to model a pile on a slope. The Mohr Coulomb model seems to be able to model the behaviour of a laterally loaded pile located in level ground. However, for the pile located at the crest, the Mohr Coulomb model underestimates consequent largely the displacements of the pile installed at the crest.

All the load-displacement curves show that it is appropriate to model only half of the laterally loaded pile in Plaxis 3D, since it is a symmetrical problem. This will save a lot of calculation time during the parametric study. The disadvantage of Plaxis 3D is the inability to model plastic yielding of the pile. Therefore, the parametric study in the next chapter has been set up such that the failure mechanism is caused by soil failure.

Chapter 4

Parametric study

4-1 Analysis in Plaxis 3D

To investigate the sensitivity of a laterally loaded pile to sloping ground, a parametric study is performed. Based on the validation presented in Chapter 3, it is decided to execute this analysis in Plaxis 3D. Advantages of Plaxis 3D are that the program is able to take the continuity of the soil into account, it contains the *HSsmall* model, which is able to model soil hardening and stress dependent stiffness, and another advantage is that the in-situ stress conditions can be examined. Moreover, it had the best performance in the previous chapter.

Two different soil profiles are considered for the parametric study; a homogeneous profile consisting of medium dense sand (I) and a layered profile of a clay layer underlain by a deeper sand layer (II). These profiles are selected, since they appear a lot in the deltaic waterways of the Netherlands. This choice ensures that the results are useful for the engineering practice in the Netherlands. Both soil profiles are sketched in Figure 4-1. The properties that are varied to investigate the sensitivity to the slope are the soil properties, the slope angle and the loading direction. The varied properties are discussed in the next paragraphs. An overview of the performed calculations in Plaxis 3D is given in Table F-1 in Appendix F.

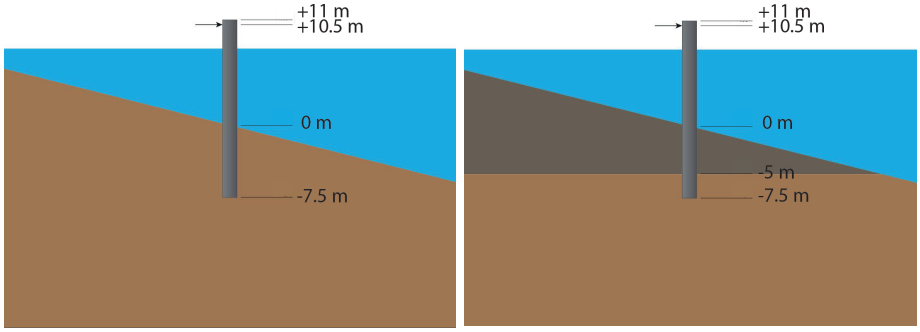

Figure 4-1: Sketch of the considered profiles for the parametric study in Plaxis 3D (a) of profile I and (b) of profile II

Variation of properties

The variation of the sand properties is related to variation of the internal friction angle, ϕ. The values 30°, 35°, and 40°are selected for ϕ. For each ϕ, a corresponding relative density is determined and from here the parameters for the $HSsmall$ model are obtained. This is based on the correlations developed by Brinkgreve et al. [34], which has proven its value in the previous chapter. The parameterset for $\phi = 35$ is considered as the standard soil profile for sand, the parameterset for $\phi = 30$ as variation 1 and the parameterset for $\phi = 40$ as variation 2. An overview of the soil properties for sand are shown in Table 4-1.

The variation of the clay properties is related to variation of the cohesion, c. The values 2 kPa, 6 kPa and 10 kPa are selected for the cohesion. Corresponding to the cohesion a cone resistance, q_c is selected, which is linked to the E^{ref}_{oed}, chosen as $4.5q_c$. Other relations used to determine parameters for the $HSsmall$ model are $E^{ref}_{50} = 2E^{ref}_{oed}$, $E^{ref}_{ur} = 3E^{ref}_{50}$ and $E^{ref}_{ur} = 2.4G^{ref}_{0}$. The properties of the deeper sand layer in profile II are constant throughout the analysis, and are equal to the standard parameter set with $\phi = 35$.

For clay the drainage type *undrained* is selected. This can be justified since the load on the dolphin can be assumed as short term and the permeability of clay is too small for any outflow of water. However, for sand *drained* is selected as drainage type. Therefore, the results of the parametric study for sand are only valid for mooring dolphins. When a breasting dolphin is loaded by the impact of a ship, this happens so fast that the sand must be considered as undrained. However, during undrained moddeling of the soil, the value of the dilation angle plays a large role, which is not validated in the previous chapter. Moreover, undrained modelling of sand is much more time-consuming and challenging in Plaxis 3D. For these reasons, only drainage type *drained* is considered, which makes the study only valid for mooring dolphins. However, particular mooring dolphins are located in sloping ground in the Dutch waterways, so the study is still broadly applicable.

For the tested pile constant properties are selected. The pile has a total length of 18.5 meter, with an embedded length of 7.5 meter. This short embedded length is due to the fact that the maximum moment in the pile should be lower than the maximum yielding moment of the pile to force the analysis to fail on soil failure. The diameter of the pile is 1.5 meter, the thickness is 20 mm and the Young's modulus is defined as 210 GPa.

Sloping ground

Two different slope angles are considered in the Plaxis 3D analysis; 1:3 and 1:4. The most common tested slope in literature is 1:2. For this master's thesis slope angles of 1:3 and 1:4 are selected, since these appear most often in the harbour of Rotterdam, moreover it is a good addition to the existing literature. The performed analyses in Plaxis 3D have an infinite slope, i.e. the slope continues till it does not influence the result of the analysis anymore. At the end, a final analysis with a finite slope is conducted, where the pile is located at the crest, in the middle and at the toe of the slope. This is sketched in Figure 4-2.

Soil parameters sand		**standard**	**variation 1**	**variation 2**
Model type		HSsmall	HSsmall	HSsmall
Drainage type		drained	drained	drained
RD	$[-]$	56	30	96
γ_{unsat}	$[kN/m^3]$	17.2	16.2	18.8
γ_{sat}	$[kN/m^3]$	19.9	19.5	20.5
c	$[kN/m^2]$	0.5	0.5	0.5
ϕ	$[degree]$	**35**	**30**	**40**
ψ	$[^\circ]$	5	0	10
E_{50}^{ref}	$[kN/m^2]$	33,600	18,000	57,600
E_{oed}^{ref}	$[kN/m^2]$	33,600	18,000	57,600
E_{ur}^{ref}	$[kN/m^2]$	100,800	54,000	172,800
m	$[-]$	0.595	0.6763	0.47
$\gamma_{0.7}$	$[kN/m^2]$	0.000144	0.00017	0.000104
G_0^{ref}	$[kN/m^2]$	98,080	80,400	125,280
R_{inter}	$[-]$	0.85	0.85	0.85

Table 4-1: Sand parameters for the parametric study

Soil parameters clay		**standard**	**variation 1**	**variation 2**
Model type		HSsmall	HSsmall	HSsmall
Drainage type		undrained	undrained	undrained
γ_{unsat}	$[kN/m^3]$	17	14	19
γ_{sat}	$[kN/m^3]$	17	14	19
c	$[kN/m^2]$	**6**	**2**	**10**
ϕ	$[degree]$	20	20	20
ψ	$[^\circ]$	0	0	0
E_{50}^{ref}	$[kN/m^2]$	9000	4500	13500
E_{oed}^{ref}	$[kN/m^2]$	4500	2250	6750
E_{ur}^{ref}	$[kN/m^2]$	27000	13500	40500
m	$[-]$	1	1	1
$\gamma_{0.7}$	$[kN/m^2]$	0.00054	0.00018	0.00091
G_0^{ref}	$[kN/m^2]$	11,250	5,625	16,875
R_{inter}	$[-]$	0.7	0.7	0.7

Table 4-2: Clay parameters for the parametric study

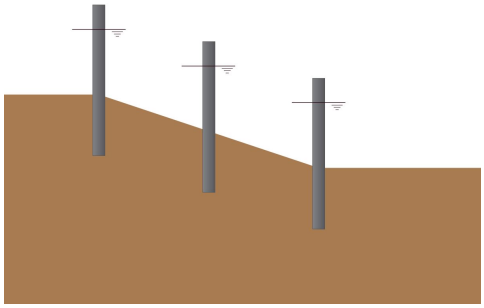

Figure 4-2: Sketch of Plaxis 3D analysis: pile located at different positions along slope

Principles of the analysis

To ensure that the results of the Plaxis 3D calculations can be compared, some principles are defined which must be satisfied in each analysis.

- Plaxis 3D is not capable to model plastic yielding of the pile. Therefore it is important that the Plaxis analysis fails on failure of the soil, while the bending moment in the pile stays smaller than the yielding moment. For this reason, the embedded length of the pile is only 7.5 m.
- To safe calculation time, only half of the model is modelled in Plaxis 3D. In the previous chapter it is proven that this leads to sufficient accurate results.
- To compare the results of each analysis, the embedded length of the pile, the height of the waterline above surface level and the point of force application is constant for each calculation.
- Unfortunately, it is not possible to obtain the bending moments directly from the plate material of which the pile is made. Therefore, to obtain the bending moments in the pile a beam is positioned on the side of the pile. This beam has a flexural rigidity 10,000 times smaller than the plate material pile has, in this way it does not hinder the movement of the pile.

4-2 Results

In this section the results of the Plaxis 3D analysis are included. It contains a discussion on the load-displacement curves, the results of the piles located at different positions along the slope are presented, and the section ends with a consideration of the p-y curves obtained from the Plaxis 3D analysis.

Load-displacement curves

The load-displacement curves for sand and clay are shown in Figure 4-3 and 4-4 respectively. The curves have been obtained from the listed calculations in Appendix F. If one examines the graphs it is immediately clear from this analysis that a laterally loaded pile in a sand slope is much more effected by the slope than a laterally loaded pile in a clay slope. This can be explained by the fact that the strength of sand is stress-dependent and the cohesion of clay, in contrast, is not stress-dependent. When the passive wedge then reduces by the slope, the effect for sand is much larger than for clay. The reduction in capacity for clay is mostly affected by decreasing of the

wedge and slightly influenced by the reduction of the strength, since the clay did have a small angle of internal friction, ϕ, of 20°. However, the lateral load capacity of sand is both affected by the reduction of the wedge and by a much larger reduction of the strength, since ϕ of sand had a value between 30° and 40°. The effect is clearly demonstrated by the load-displacement curves.

For a better interpretation of the load-displacement curves and to identify influencing parameters, all load-displacement curves of the piles in sloping ground have been normalised to the load-displacement curves of the piles in horizontal level ground, to obtain the load ratios, ψ. The load ratio ψ is defined as $F_{lateral,slope}/F_{lateral,hor}$.

The normalised load-displacement curve have been derived with the help of the Matlab curve fitting tool [37]. First, all the curves have been approached with the help of a Piecewise Cubic Hermit Interpolating Polynomial (PCHIP). This means that at the prescribed values the approached function is continuous, between the prescribed values the function is approached by a third order polynomial. After approaching functions for the load displacement curves, the normalised curves can be evaluated by dividing the load displacement curve in sloping ground by the load displacement curve in horizontal level ground, which leads to the load ratio, ψ. It should be realised that the normalised cures can not be considered as exact values, but it can be regarded as a good approximation.

If one examines the load-displacement curves in Figure 4-5 and 4-6 it is noticeable that in the first quarter of the graph the load ratios can vary considerably, especially for clay. One would expect that the load ratios have about the same shape; the ratio should start in (0,1) and then decrease non-linear. The variation in ratio can be explained by the error of the approximation, this error is increased in the first part of the graph. The initial stiffness of the load displacement curves is for all soil parameters sets almost similar and independent of the slope angle. Therefore, in the first part two numbers are divided which are close to each other. Hence, a small approximation error in this part is by the fraction increased to a larger error in the normalised curves. The approached ratio of clay could be improved by improving the output data of Plaxis 3D. By studying the output, the output intervals during the first 20 cm the are relatively large. By manually adopting the step size, the output intervals can be decreased and the clay ratio be improved.

If Figure 4-5 is inspected, one can identify patterns, which are in agreement with studies from literature. For a sloping ground with an angle of 1:4 the load ratio is approximated between 0.75 and 0.85, for an angle of 1:3 the load ratio is approached between 0.65 and 0.75. The load ratio decreases as the internal friction angle increases, this is in line with the stress-dependence of sand. If the passive wedge changes by the existence of a sloping ground, it effects most the pile located in sand with the largest internal friction angle. This effect is visible after a head displacement of 18 cm.

In Figure 4-6 a pattern related to the cohesion can not be recognized. The ratio depends mainly on the slope angle. For a slope angle of 1:4, the load ratio is approached between 0.93 and 0.96. For a slope angle of 1:3, the load ratio varies between 0.85 and 0.92, disregarding the discontinuities in the first 20 cm. Based on Figures 4-5 and 4-6 the most important conclusion is that the size of the slope angle has the largest effect on the reduction of the lateral load capacity. The soil parameters are subordinate.

After completion of all calculations the bending moment of the dolphin has been checked. The bending moment stayed throughout the whole analysis beneath the plastic moment, which means that all the performed Plaxis 3D calculations have been failed on soil failure. In Figures F-36 and F-37 in Appendix F-2 an example of soil failure is shown.

In Figures 4-7 and 4-8 the load ratios from the Plaxis 3D analysis are added to the overview of the load ratios found in literature. The results are a valuable addition, since this range of slope angles is not tested much yet. The values from the Plaxis 3D analysis fall within a logical range compared to the values from literature. However, a clear pattern is not visible in both Figures. The variation in these graphs can among others be attributed to the variations of the parameters used in the studies, such as cohesion, friction angle, embedded pile length and modelling method.

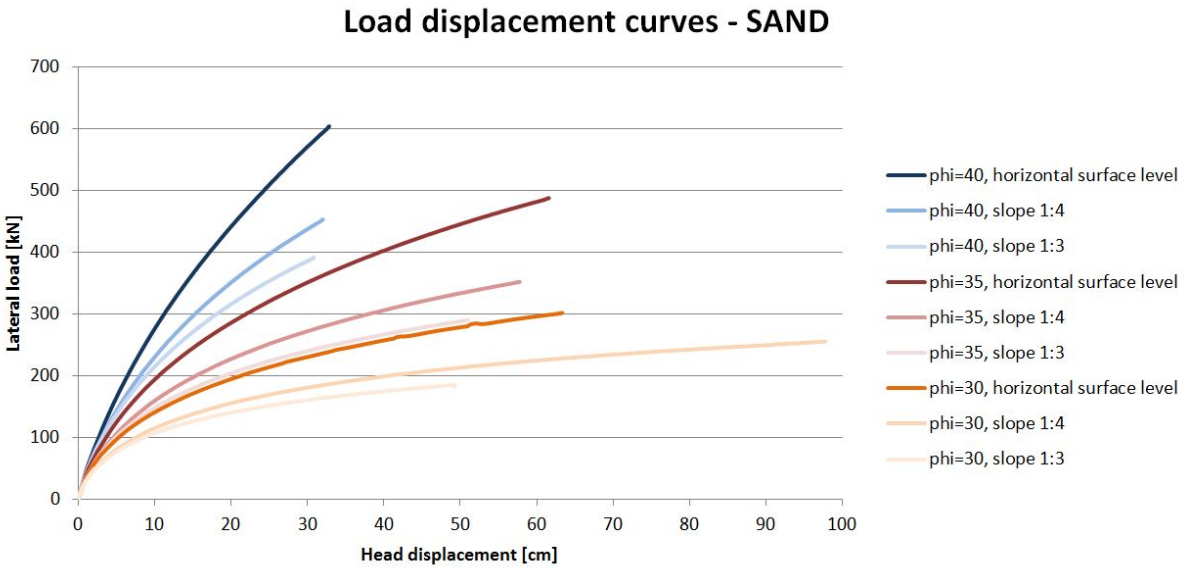

Figure 4-3: Load displacement curves of laterally loaded piles located in sand obtained from Plaxis 3D analysis

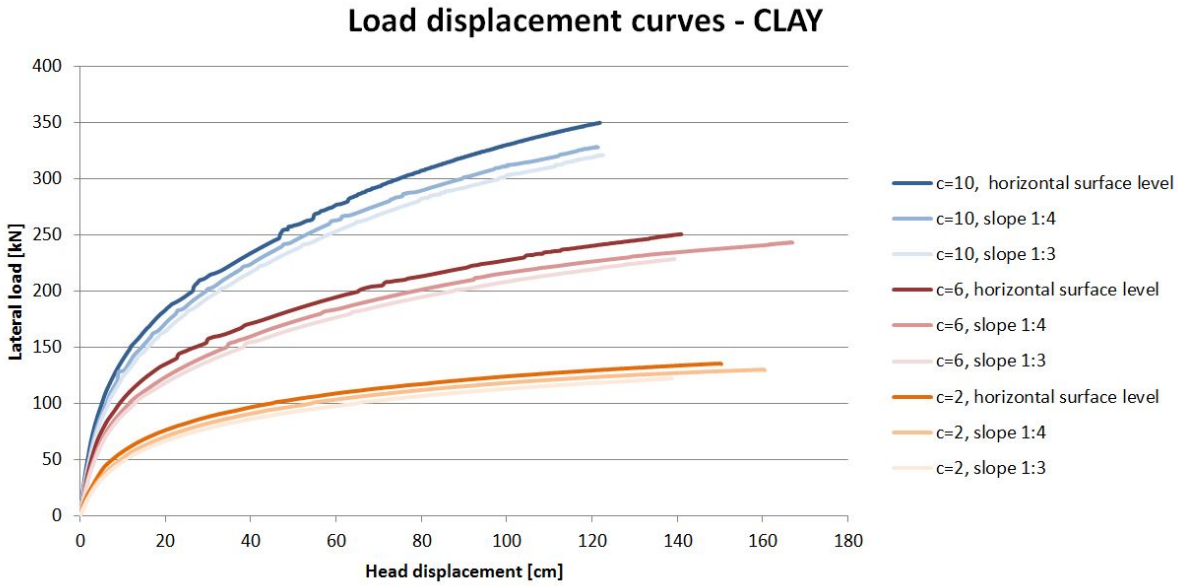

Figure 4-4: Load displacement curves of laterally loaded piles located in clay obtained from Plaxis 3D analysis

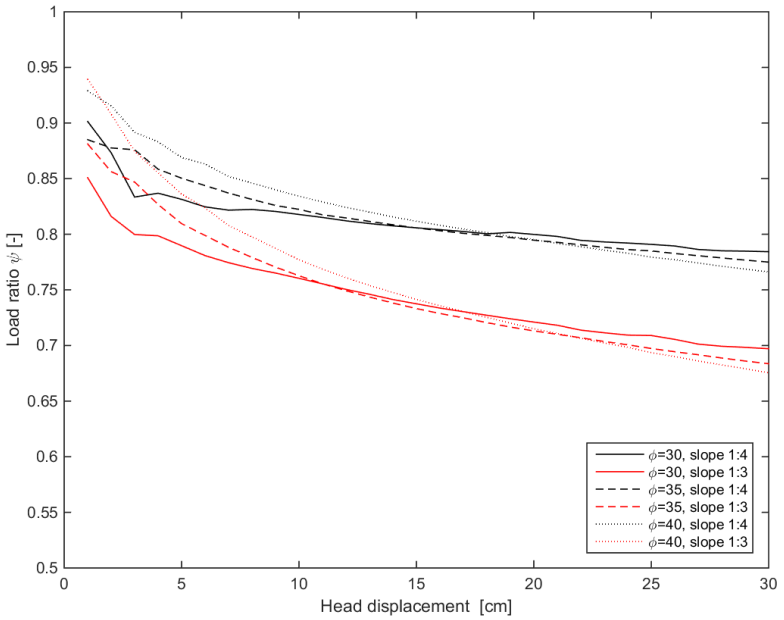

Figure 4-5: Overview of load ratios for sand obtained from Plaxis 3D analysis

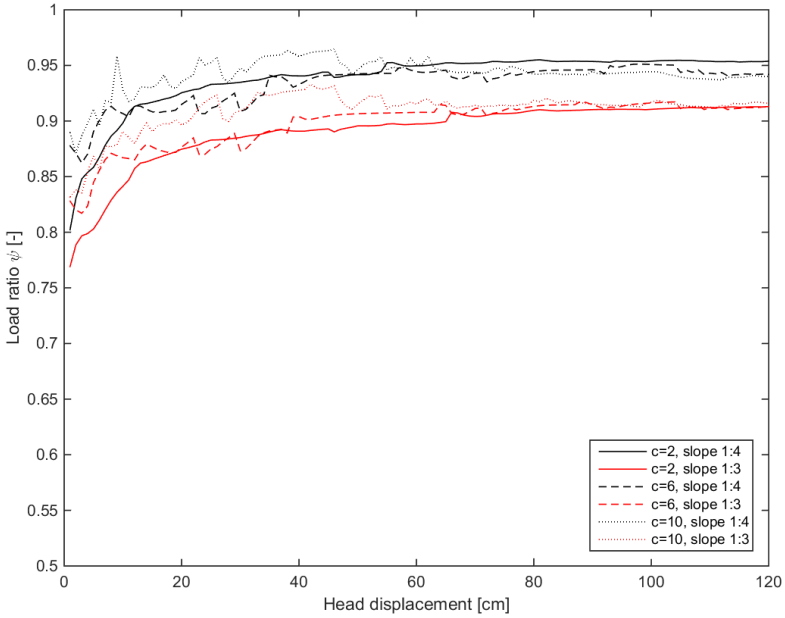

Figure 4-6: Overview of load ratios for clay obtained from Plaxis 3D analysis

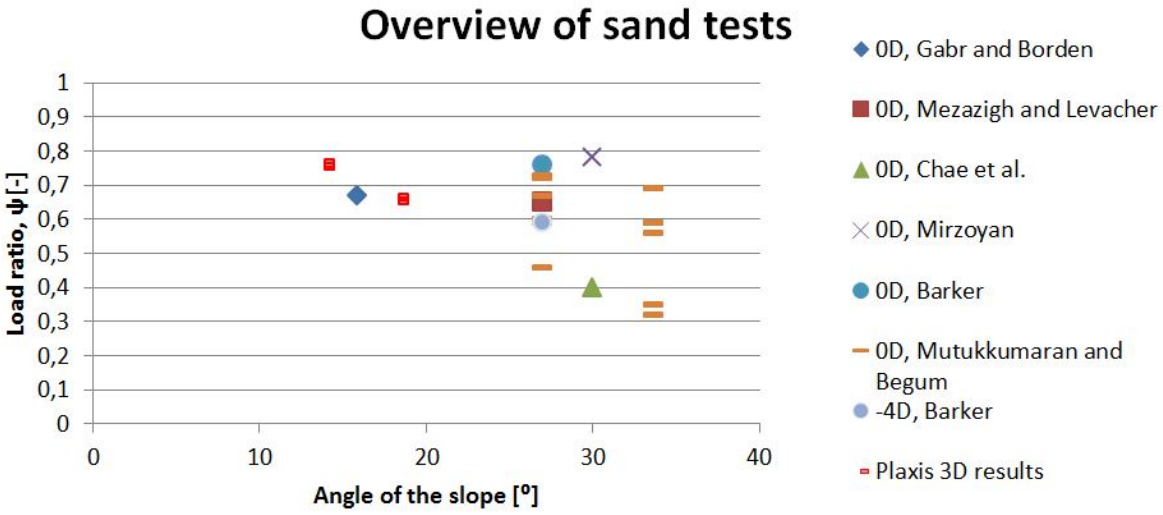

Figure 4-7: Overview of load ratios for sand from literature combined with Plaxis 3D analysis
NOTE: first term incicates location of tested pile with respect to slope crest. Plaxis 3D results were obtained from infinite slope

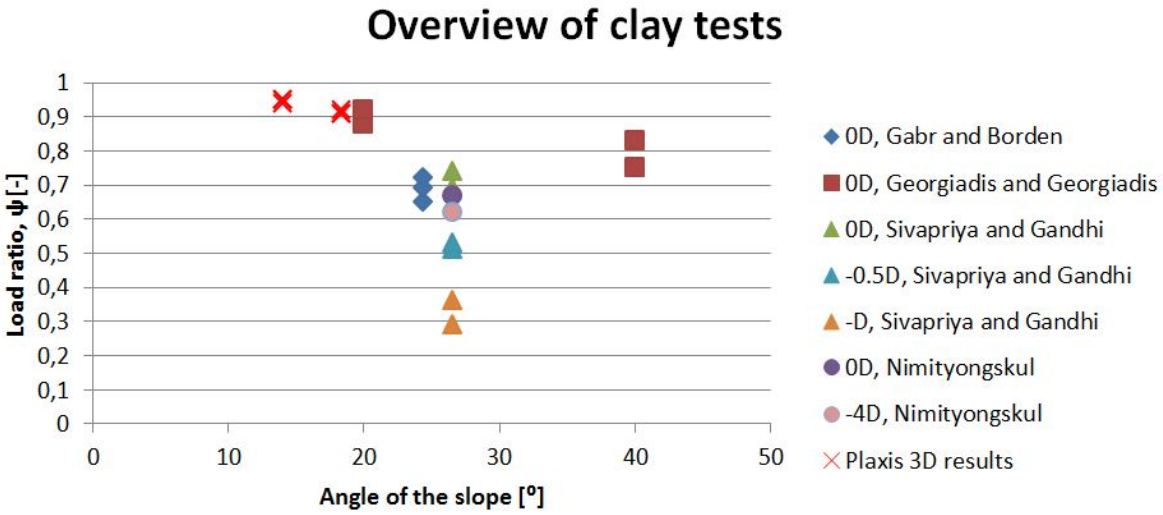

Figure 4-8: Overview of load ratios for clay from literature combined with Plaxis 3D analysis
NOTE: first term incicates location of tested pile with respect to slope crest. Plaxis 3D results were obtained from infinite slope

Pile variation along slope

Tests from literature showed that there can be a variation in load-displacement curves if the pile is located at different positions along the slope. It was observed in tests that as the pile moved downwards the slope, the lateral load capacity of the pile decreased. To qualify this effect an analysis has been performed with piles located at different positions along the slope, as schematized in Figure 4-2. This has been done for soil profile I, soil parameter set $\phi = 35$ and a slope angle of 1:4.

Surprisingly, the effect found in literature can not be recognized from the graph in Figure 4-9. This is explained by the fact that in this master's thesis for all calculations the embedded length of the pile and the height of load application remained constant. During other research where the pile location was varied along the slope, conducted by Sivapriya and Gandhi [7], Barker [4] and Nimityongskul [3], these lengths were not kept constant. In contrast, the embedded length decreased and the height of load application increased as the pile moved towards the slope, the advantage was that they could hold their loading equipment in the same position. But consequently, the lateral load capacity decreased. In Plaxis 3D one does not have that limitation, which explains the difference.

If one now examines again Figure 4-7 and 4-8, the 0D values are considered as most reliable. If one imagines the overviews without the values of the piles located in the slope (-0.5D to -4D), the variation in the graphs is much less and the trend improves.

It is also remarkable in Figure 4-9 that the pile located in the toe has a higher load capacity than the pile located in horizontal surface level. This demonstrates again that the active side does not negatively influence the lateral load capacity of a laterally loaded pile. The higher load capacity of the pile located in the toe is most likely be caused by the higher soil stresses behind the pile around the tip level, which prevents the pile to rotate.

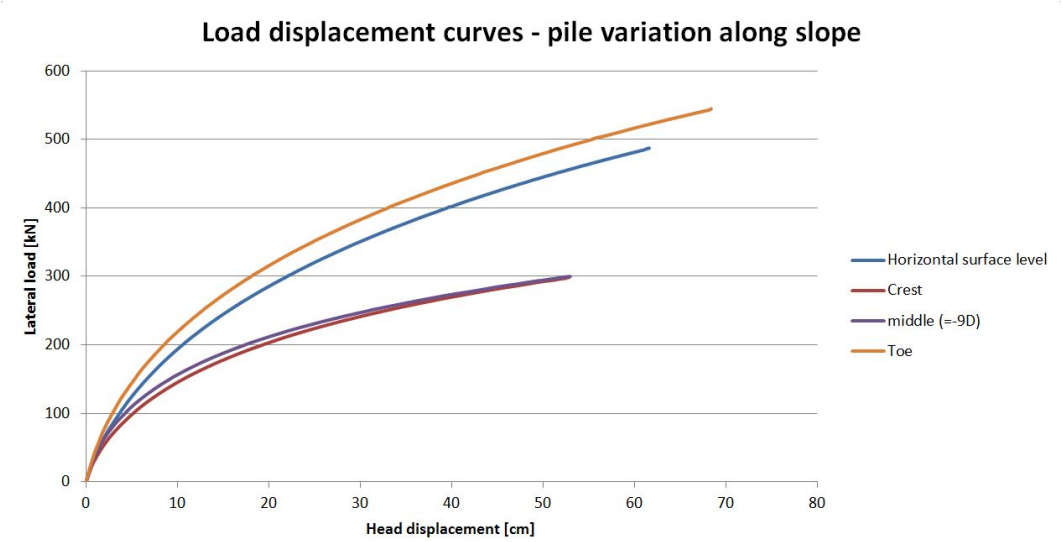

Figure 4-9: Load displacement curves for pile variation along slope with angle 1:4 for $\phi = 35$

Bending moments

In Figures F-1 to F-3 in Appendix F-2 the maximum bending moments for all the analyses are shown. Here can also be recognized that the effect of the slope on the pile in sand is larger than for the pile located in clay. Moreover, as well for the maximum bending moments the effect of the slope is different than one would expect by literature. In the research conducted by Sivapriya and

Gandhi [7], Barker [4] and Nimityongskul [3] the bending moments increased when the pile was located in sloping ground instead of horizontal surface level. For this analysis the effect was vice versa. As well for the pile variation, this is explained by the decrease in embedded length and increase in load application height in the tests by literature. While during the Plaxis 3D analyses the lengths kept constant.

Uphill loading direction

Two analyses have been performed for laterally loaded piles in sloping ground loaded in uphill direction. This has been done for the standard soil parameters sets of sand and clay and a sloping ground with a slope angle of 1:4. In Figure F-4 and F-6 in Appendix F the load-displacement curves are shown. Subsequently, the load ratios are shown in Figure F-5 and F-7 for respectively sand and clay. Only one analysis for both sand and clay have been performed, which means that it gives only an indication and no clear conclusions can be made. For the considered situation, the pile located in a sloping ground consisting of sand has a increased lateral load capacity of 40%, for clay the load capacity increases about 20%.

P-Y curves

In the engineering practice, p-y curves are frequently used for the design of laterally loaded piles. Deltares developed the software program D-Pile Group [16], which uses the p-y method as described in Section E-2. Unfortunatley, this program is not equipped to analyse laterally loaded piles in sloping ground. In the USA the software program LPILE has been developed [30], which uses also the p-y method. This program has the option to take sloping ground into account, however, it is not entirely validated yet. Since these software programs are a lot quicker and cheaper for design activities compared to Plaxis 3D in the present situation, it may be interesting to increase the knowledge of p-y curves for sloping ground. For these reasons, it is considered valuable to obtain the p-y curves from the Plaxis 3D calculations.

To derive the soil resistance, p, along the pile and the associated soil displacements, y, several steps should be taken. For each loading step, the bending moments along the laterally loaded pile as well as the associated soil displacement have been obtained. With help of a spreadsheet program the bending moments have been approximated by a sixth order polynomial, to obtain a function for the bending moments. By differentiating this function twice as defined by Formulas 4-1 and 4-2 the soil resistance can be determined. By coupling the derived soil resistance to the soil displacement of the corresponding bending moment, the p-y curves can be constructed. This is an extensive procedure, hence the help of a spreadsheet is required. The determined p-y curves are enclosed in Appendix F-2.

$$\frac{dM(z)}{dz} = S(z) \tag{4-1}$$

$$\frac{dS(z)}{dz} = p(z) \tag{4-2}$$

where

M	=	moment obtained from beam $[kNm]$
z	=	height along the pile $[m]$
S	=	shear force $[kN]$
p	=	soil resistance per unit pile length $[kN/m]$

If one examines the P-Y curves, it is again immediately notable that the P-Y curves of the sand profile are much more affected by the sloping ground than the p-y curves of the clay profile. Moreover, it is important to note that the ultimate resistance only increases up to z=-2D for sand. For clay the ultimate resistance increases till z=-4D. The quick reduction of the ultimate resistance is caused by the short embedded length of the piles. In Appendix F-2 representative

examples of the displacements along the pile for sand and clay are enclosed. For both sand and clay the laterally loaded pile has a rotation point, this is located at z=-6.5 m for clay and at z=-6 m for sand. This means that for clay the point of rotation is located at $13/15^{th}$ of the pile and for sand at $4/5^{th}$ of the pile. The P-Y curves below the point of rotation are not shown since this does not give any useful information.

Normalised P-Y curves

To better qualify the effect of the slope on the p-y curves, also the normalised p-y curves have been determined. As for the load-displacement curves, the normalised p-y curves have been derived with the help of the curve fitting app of Matlab [37]. First, the p-y curves have been approached with help of a Piecewise Cubic Hermit Interpolating Polynomical. Hereafter, the ratios, Ψ, have been calculated, defined as p_{slope}/p_{hor} and combined with the associated soil displacements. Again, it should be realised that the values for the p-y ratios must only be considered as an estimation, not as exact values. In Appendix G the normalised p-y curves have been enclosed.

When assessing the normalised p-y curves in Figures G-1 to G-8, the expected patterns from literature are clearly visible. The ratio increases slowly towards one if one examines the ratio lower down the pile for both clay and sand. This means that as expected the effect of the slope is largest in the upper soil layers and that the effect of the slope disappears at a certain depth below surface level. Unfortunately it can not be examined within this Plaxis 3D analysis, at which depth the sloping ground does not influence the p-y curves anymore, i.e. when the p-y ratio becomes equal to 1. This is caused by the short embedded length of the pile.

If one examines Figure G-8, it can be observed that the p-y ratio for clay at z=-3D are dropped slightly compared to the p-y ratios for clay at z=-2D. This can also be explained by the short embedded length of the piles. Since the pile rotates, above the point of rotation the soil reaction, and thus the p-y curve decreases. This effect is also visible for sand. For the same reasons, the p-y curves and p-y ratios beneath z=-3D are not shown. Around the point of rotation the soil reaction does not result into a characteristic p-y curve anymore. The obtained curves have been considered to be irrelevant to publish.

By examining the effect of the soil parameter sets on the p-y ratios of sand, the influence of the internal friction angle can be recognized. In general, the ratio Ψ decreases as the friction angle increases. This can again be explained by the stress-dependence of sand. When the confining stress reduces by the slope, sand with the largest strength, i.e. the largest internal friction angle will be affected most.

Moreover, in contrast to the load-displacement curves, the effect of the cohesion can be observed in Figures G-5 to G-8. When the cohesion increases, also the value of the p-y ratio increases. An explanation may be the stress-dependence of the stiffness in the HSsmall model in Plaxis 3D; an increase of the cohesion of clay means as well a higher stiffness of clay. It may be expected that a laterally loaded pile will be affected less by the presence of a slope when the stiffness of the soil increases.

Despite the fact that the effect of the soil parameters is visible, it is important to realize that the size of the slope angle has a dominant effect on laterally loaded piles in slopes.

Chapter 5

Design recommendation

In this chapter the existing methods to account for sloping ground will be reviewed, followed by a design recommendation. Since all recent published studies focus on the adoption of p-y curves to account for sloping ground, it is decided to build further on this knowledge. So far the studies that contain a recommendation for adoption of the p-y curves for sand are published by Mezazigh and Levacher [5] and Barker [4]. An adoption of p-y curves for clay is published by Nimityongskul [3] and Georgiadis and Georgiadis [10]. As stated earlier, the software programs D-Pile [16] and LPILE [30] use p-y curves for the analysis of a laterally loaded pile. LPILE contains already the option to consider a sloping ground, but that function is not validated yet. D-Pile does not have the option to consider a sloping ground. However, it has the option to manually enter p-y curves.

Sand

In Figure 5-1 recommended p-multipliers of previous studies are shown together with the obtained p-y ratios from the Plaxis 3D analysis in this master's thesis.

Since the p-y ratios derived from the Plaxis 3D analysis depend among others on the soil properties and the depth below the soil surface, the lower and upper bound ratios are shown in Figure 5-1. The discontinuities due to the approximation error in the first part of the graph are here ignored.

It should be noted that Mezazigh and Levacher's ratio in Figure 5-1 is obtained from Equation 2-19, and has therefore a value of 0.37 for a slope angle of 1:4, a value of 0.33 for a slope angle of 1:3 and a value of 0.25 for a slope angle of 1:2. As explained in Section 2-3-2 and based on Figure 2-15b in Chapter 2 one would expect a value which is at least larger than 0.5. The publication of Mezazigh and Levacher does not provide evidence about the discrepancy. With a value larger than 0.5, it approaches better the p-y ratios obtained from the Plaxis 3D analysis than it would with the values based on Equation 2-19. The values calculated according to Equation 2-19 can be considered as conservative.

The p-y ratio of Barker is obtained from one full scale test, so only a slope of 1:2 was tested. It is added however to this graphs, since it gives an indication. Barker recommends two different p-multipliers; one for a pile located at the crest of the slope and one for a pile located in the slope. In contrast, the Plaxis 3D analysis in this master's thesis did not reveal significant differences in load-displacement curves between these pile locations. As stated earlier, the difference in the p-multipliers of Barker may be explained by different heights of load application and embedded lengths. Since a constant height of load application in this study led to the same load-displacement curve, the highest ratio whereby the height of load application was equal to the pile in horizontal

level, namely 0.5, is considered as most valuable and reliable p-multiplier. If a p-y ratio of 0.5 for a slope of 1:2 is compared to the lower and upper bound values of the Plaxis 3D analysis, they seem to be in proportion and fall within the same range. The value of 0.3 of Barker does not fall within the range of the Plaxis 3D results and is considered to be conservative.

Clay

In Figure 5-2 the p-multipliers of previous studies for clay are shown combined with the obtained p-y ratios from the Plaxis 3D analysis.

Georgiadis and Georgiadis are at an advanced stage in the development of p-y curves for an undrained analysis of laterally loaded piles in clay slopes. In Section 2-4-3 the derivation of these p-y curves has been reported. To compare the p-y curves and obtain a p-y ratio for Figure 5-2, the p-y curve for an undrained analysis of a laterally loaded pile in clay has been plotted in a spreadsheet together with the adopted p-y curve for slopes of Georgiadis and Georgiadis. Hereafter, the p-y ratio has been derived according to the definition p_{slope}/p_{hor}. The p-y ratio of Georgiadis and Georgiadis differs a bit on the input parameters of the soilparameters, but the average value is given in Figure 5-2. The illustrated p-y ratio has been obtained at -1D below the ground surface.

If one compares the p-y ratios of Georgiadis and Georgiadis with the p-y ratios obtained from the Plaxis 3D analysis, the p-y ratios fall within the upper and lower bound of Plaxis 3D for a slope angle of 1:4. For a slope angle of 1:3 the p-y ratios coincides more or less with the upper bound ratio of the Plaxis 3D analysis. Also the p-y ratio of Georgiadis and Georgiadis for a slope angle of 1:2 has been added, this value seems to fall in the range of the upper bound Plaxis 3D results. The lower bound ratio primarily reflects the results of the analysis for the soil parameter set of c=2. This may indicate that the p-y curves of Georgiadis and Georgiadis may overestimate the capacity of laterally loaded piles in sloping ground consisting of soft clays for a slope angle of 1:3 and larger.

Reese et al. have developed the ratio $1/(1+\tan\theta)$ for the ultimate soil resitance, p_u, which only depends on the slope angle θ. This ratio is used in the software program LPILE [30] for the analysis of laterally loaded piles in sloping ground consisting of clay. Therefore it is added to the graph of Figure 5-2. If one compares it with the results of the Plaxis 3D analysis it will underestimate the capacity of the laterally loaded pile in the analysis. Reese et al. indicate that only for the upper part of the soil with a length of 10D, the p-y curves are effected by the sloping ground. For this length applies the ratio, hereafter the ratio becomes equal to 1.

Last, the p-multiplier of Nimityongskul is added to Figure 5-2. This p-y ratio is based on one full scale test, so only a slope of 1:2 was tested. It is immediately clear that this multiplier is not in proportion to the p-y ratios of Georgiadis and Georgiadis, Reese et al. and the Plaxis 3D analysis in this master's thesis. It considered to be very conservative. Part of the explanation may be the different field conditions, at Barker's test was the water table located at -2.1m below the surface level. However, this can not clarify the entire difference.

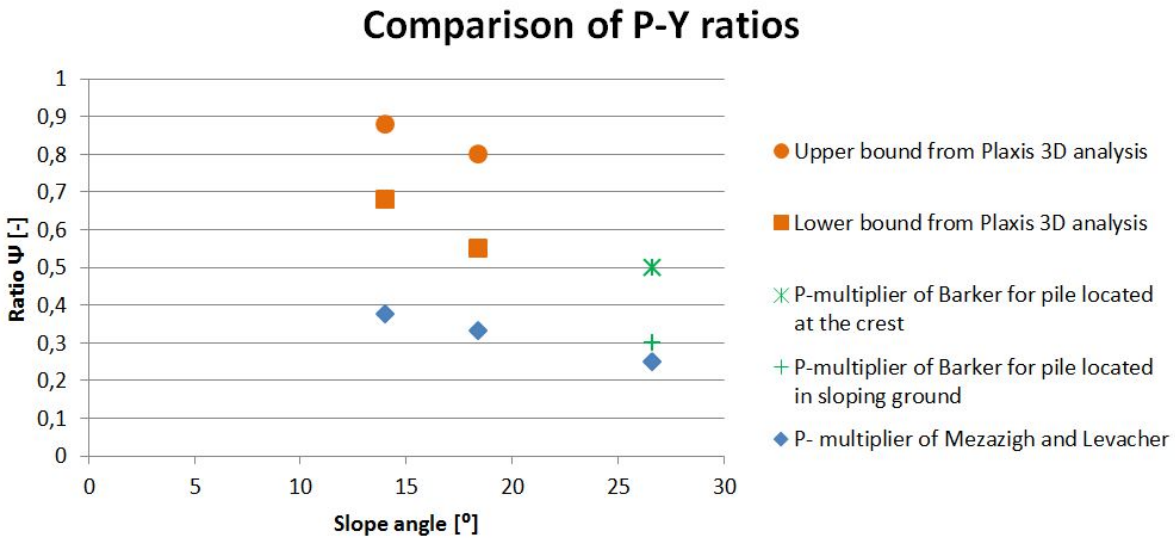

Figure 5-1: Comparison of recommended and measured P-Y ratios for sand

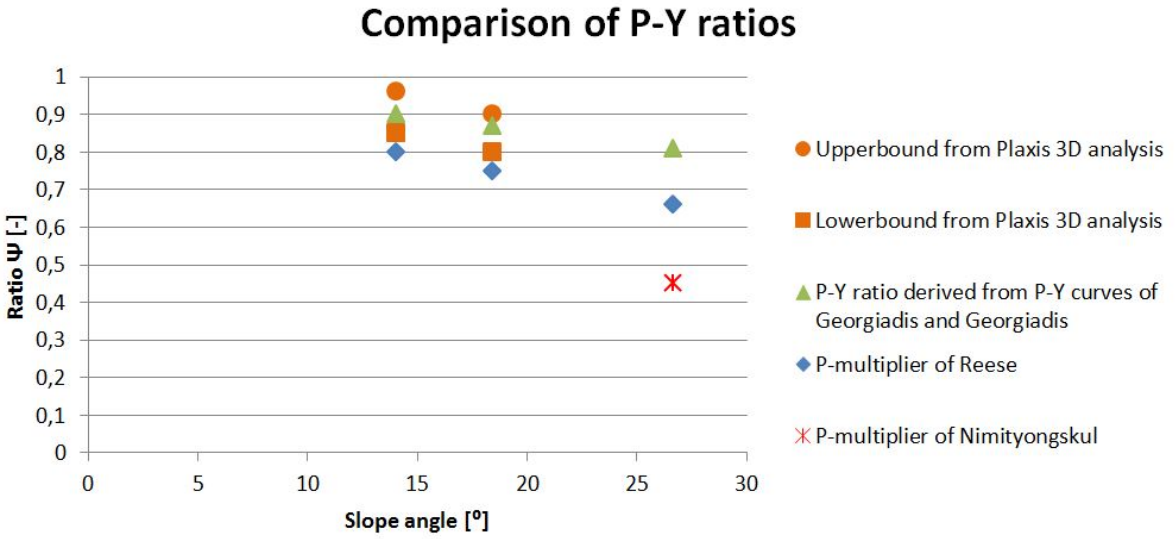

Figure 5-2: Comparison of recommended and measured P-Y ratios for clay

Design recommendation

As stated in the introduction of this chapter, all published studies regarding piles in slopes focus on the adoption of p-y curves to account for sloping ground. It is believed that expansion of the amount of performed full scale tests, small scale tests and finite element analyses eventually will lead to a complete set of p-y curves for laterally loaded piles in sloping ground. An extension of the software programs D-Pile Group and LPILE may also be included to facilitate the use of p-y curves in sloping ground.

Unfortunately, in the context of this master's thesis it was not possible to expand the series of developed p-y curves for sloping ground as Georgiadis and Georgiadis did for the undrained analysis in clay. The advantage of new developed p-y curves for sloping ground over the use of p-multipers, is the ease of use. Instead, it is considered that the best option for now is the application of p-multipliers on existing p-y curves for horizontal surface level.

Therefore, it is recommended to use a design flow chart as published earlier in the dissertation of Nimityongskul [3]. The design steps in the flow chart will then become:

1. Select the p-y curve for a laterally loaded pile in horizontal ground
2. Define with the help of Figures G-1 to G-8 in Appendix G appropriate p-multipliers
3. Construct the new p-y curve
4. Perform the analysis of the laterally loaded pile with the renewed p-y curves

The design chart of Nimityongskul was based on only one p-y ratio, which was concluded to be considerable conservative in the previous paragraph. The Plaxis 3D analysis of this master's thesis expanded the amount of available p-y ratios significantly.

In Table 5-1 p-multipliers are defined which correspond to the normalised p-y curves showed in Figures G-1 to G-8. Since the soil parameters play a subordinate role, only differentiation was made between the depth along the pile and the size of the slope angle. For the selected depth and slope angle, the presented value can be considered as the most conservative value. For a deeper insight, Figures G-1 to G-8 should still be consulted.

The p-y curves of Georgiadis and Georgiadis are not recommended for the undrained analysis of piles in clay slopes, since they seem to overestimate the capacity of laterally loaded piles in sloping ground consisting of soft clay for slope angles of 1:3 and larger. These conditions are typical for Dutch waterways, and therefore it is considered to be more reliable to use the p-y ratios derived from the Plaxis 3D analysis of this master's thesis.

Despite of the significant expansion of the available p-y ratios, this method has a number of limitations, which should be borne in mind during the design process. The p-y ratios presented in Appendix G are limited till a depth of z=-3D, due to the use of piles with a short embedded length it was not possible to elaborate p-y curves for lower depths. From literature it is known that around a depth of z=-10D, the p-y ratio becomes equal to 1. As mentioned earlier, for sand only a drained analysis is carried out. Therefore, it should be noted that the p-y ratio's of sand are only valid to analyse mooring dolphins. Moreover, limited parameters are considered. Only a pile diameter of 1.5 meter has been regarded, two slope angles of 1:3 and 1:4, and three soil parameter sets for both sand and clay. However, the selected parameters reflect the most common conditions a and has a wide range of application in Dutch conditions.

Unfortunately, there was no time left over to validate this design recommendation with the help of control calculations.

Sand ratios			**Clay ratios**		
z = 0	slope 1:4	0.67	z = 0	slope 1:4	0.88
	slope 1:3	0.55		slope 1:3	0.78
z = -1D	slope 1:4	0.72	z = -1D	slope 1:4	0.88
	slope 1:3	0.6		slope 1:3	0.78
z = -2D	slope 1:4	0.78	z = -2D	slope 1:4	0.91
	slope 1:3	0.63		slope 1:3	0.85
z = -3D	slope 1:4	0.78	z = -3D	slope 1:4	0.82*
	slope 1:3	0.69		slope 1:3	0.85*

Table 5-1: p-multipliers defined from the Plaxis 3D analysis

*these values are considered to be not realistic, but are caused by the short embedded length of the piles

Chapter 6

Conclusion and Recommendations

In this chapter the results of this master's thesis will be discussed in the light of the objectives that were defined in Chapter 1. Thereafter, recommendations for future research are formulated.

6-1 Conclusion

Literature review
With help of the literature review a complete picture could be formed of the knowledge about laterally loaded piles in sloping ground. The research so far, is merely focussed on laterally loaded piles located near sloping grounds or piles located at the crest of the slope. Moreover, the regarded slope angles in literature are larger than one encounters in Dutch waterways. The original model of the passive wedge to determine the ultimate soil resistance developed by Reese et al. has been adopted for the slope by three researchers; Gabr and Borden [1], Reese et al. [19] and recently by Mirzoyan [2]. A number of model tests have been conducted by Mezazigh and Levacher [5], Chae et al. [6], Sivapriya and Gandhi [7]. Four full scale tests have been conducted by Gabr and Borden [1], Mirzoyan [2], Nimityongskul [3] and Barker [4]. Moreover, finite element analysis have been performed by Chen and Martin [8], Begum and Mutukkumaran [9] and Georgiadis and Georgiadis [10].

These studies all conclude that reduction of the confining soil, due to a slope decreases the lateral capacity of the pile. Parameters that influence the amount of decline are the slope angle, θ, the soil parameters, the pile properties and the roughness of the pile-soil interface. Moreover, all the full scale tests demonstrate the formation of a gap, which is observed in both cohesive and cohesionless soil and opens further as the lateral load increases. The gap suggests that over the length of the gap there is no active pressure that does contribute to the pile-soil interaction. It can therefore be concluded that the size of the passive wedge and its offered resistance determine the pile-soil interaction. Another key finding is the fact that the lateral response of piles depends mainly on the soil properties of the soil layers in the first 8D-10D, where D is defined as pile diameter.

Scaling of the original p-y curves for piles located in horizontal level ground with a multiplier is the most common method recommended in literature to account for sloping ground in engineering practice. Several multipliers are suggested by the different studies. If one compares these, the study of Georgiadis and Georgiadis [10] is the most advanced method. They developed a completely renewed set of p-y curves for the analysis of undrained lateral pile response in sloping ground.

Validation

In Chapter 3 Nimityongskul's full scale test and Mezazigh and Levacher's model test have been modelled in D-Sheet Piling, D-Pile Group and Plaxis 3D to validate the software. There are some interesting results to note regarding Plaxis 3D. Firstly, modelling of Mezazigh and Levacher's test showed that the correlations developed by Brinkgreve et al. [34] for the $HSsmall$ model are appropriate to model a laterally loaded pile. To model the test in Plaxis 3D only the data of the internal friction angle was known, however, the correlations led still to considerably good results in Plaxis 3D. Moreover, by comparing the Plaxis 3D results of Nimityongskul with the Plaxis 3D results of this master's thesis, it became clear that the $HSsmall$ model is the most appropriate soil model for an undrained analysis of a laterally loaded pile in Plaxis 3D. The Plaxis 3D results of Nimityongskul, obtained with the soil model Mohr Coulomb, largely overestimated the stiffness of the load displacement curve and the lateral load capacity of laterally loaded piles in slopes. Last, the validation process demonstrated that it is sufficient to model only half of the problem, since the laterally loaded pile is a symmetrical problem. This conclusion can save a lot of calculation time in the future.

Plaxis 3D is at this moment more complicated and time-consuming compared with D-Pile Group and D-Sheet Piling. It is therefore understandable that the daily engineering practice calls for a design tool that simplifies the design process.

Parametric study in Plaxis 3D

To better qualify the influencing parameters within the pile-soil interaction, a parametric study has been conducted in Plaxis 3D. The starting point for this analysis were the conditions in Dutch waterways, to which the varied parameters are connected as much as possible. The study in Plaxis 3D have been performed for two different soil profiles; a homogeneous profile consisting of medium dense sand and a layered profile of a clay layer underlain by a deeper sand layer. Two different slope angles with infinite slope have been regarded, 1:3 and 1:4, as well as 3 different soil parameter sets for both profiles. At the end, an analysis has been performed with a finite slope, where the pile is located at the crest, in the middle and at the toe of the slope.

The most important conclusion of this analysis is the fact that the capacity of a laterally loaded pile in sand is much more affected by the angle of the slope than the capacity of a laterally loaded pile in clay. This can be explained by the fact that the strength of sand is stress-dependent and the cohesion of clay is not. The lateral load capacity of a pile in a clay slope is mostly decreased by reduction of the wedge. However, the lateral load capacity of a pile in sand is affected by both reduction of the wedge and reduction of the strength parameters of sand. After this observation, the effect of the slope on the load-displacement curves has been quantified with the help of load ratios. The reduction factor of the load-displacement curve for clay lies between 0.85 and 0.96, for sand this factor lies between 0.65 en 0.85. Hence, this is a significant difference in effect. Another key finding is the fact that after the distinction between cohesive and cohesionless soil has been made, the size of the slope angle is the dominating parameter in determining the effect of the slope on the laterally loaded pile.

Some large differences were shown in literature between load-displacement curves when the pile is located at different positions along the slope. However, the Plaxis 3D analysis in this master's thesis did not demonstrate this phenomenon. This disparity is explained by the fact that in this master's thesis for all calculations the embedded length of the pile and the height of load application was kept constant. During other studies, the embedded length decreased and the height of load application increased as the pile moved downwards the slope. This was caused by the necessity to keep the loading equipment in the same position.

From this analysis it can also be concluded that a pile located at the toe of the slope has a higher load capacity than a pile located in horizontal level ground. This proves once again that the active side of the pile does not influence the lateral load capacity negatively. The increase in lateral load capacity is most likely caused by the higher soil stresses behind the pile around the tip level, which prevents the pile to rotate.

Finally, p-y curves have been obtained from the Plaxis 3D analysis combined with the associated p-y ratios to quantify the effect of the slope. In the p-y ratios the effect of the sand and clay properties can clearly be recognized. The p-y ratio, Ψ, for sand decreases as the friction angle increases. For clay, this effect is vice versa, as the cohesion increases, also the value of the p-y ratio increases. Also this contrast is caused by the fact that the strength of sand is stress-dependent and the cohesion of clay is not.

Design recommendation

In Chapter 5 p-multipliers of previous studies have been compared with the p-y ratios derived from the Plaxis 3D analysis. From this comparison it can be observed that the recommended multiplier of Mezazigh and Levacher as well as the multiplier of Nimityongskul are very conservative. In contrast, the multiplier of Barker, derived from a full scale test with a slope of 1:2 falls within the range of the Plaxis 3D results. The multiplier of Reese et al. developed for piles located in clay slopes, is slightly conservative, but performs considerably better than the multiplier of Nimityongskul. Also the p-y ratios of Georgiadis and Georgiadis, derived from their developed p-y curves for the undrained analysis of piles in clay slopes, fall within the range of the Plaxis 3D results. However, the p-y ratios coincide merely with the upper bound results of the Plaxis 3D analysis. This may indicate that the p-y curves of Georgiadis and Georgiadis overestimate the capacity of laterally loaded piles in sloping ground consisting of soft clays for a slope angle of 1:3 and larger.

For these reasons, it is recommended to use a design chart as proposed by Nimityongskul. First, the original p-y curves for horizontal surface level need to be selected, followed by the selection of a p-multiplier from the normalised p-y curves in Figures G-1 to G-8. These can be combined to form new p-y curves to determine the pile-soil interaction of piles located in sloping ground. The main limitations of this method are the restricted amount of parameters considered in the Plaxis 3D analyses and the short embedded length of the piles, which led to a limited amount of p-multipliers.

6-2 Recommendations for future research

The recommendations for future research have been split up into two categories; one set recommendations focuses on dolphins and one set focuses on general research of laterally loaded piles in sloping ground.

Recommendations for future research regarding laterally loaded piles in sloping ground

- To expand the knowledge of laterally loaded piles in sloping ground and better understand the influence of all parameters, such as the slope angles, pile properties and soil properties, more tests should be executed. Both full scale tests, model tests and finite element analyses may contribute to a better understanding of the laterally loaded pile in sloping ground.
- A renewed set of p-y curves for the undrained analysis of piles in a slope is developed by Georgiadis and Georgiadis. However the p-y curves are not recommended in this thesis since the curves seem to overestimate the lateral load capacity of piles in soft clay, the aim should be in future research to develop renewed p-y curves for other analyses too. Advantages of redeveloped p-y curves are the ease of use, compared to multipliers. Expansion of the executed tests as described in the previous point will undoubtedly contribute to the development of renewed p-y curves.
- Plaxis 3D is at this moment too complicated and time-consuming and hence too expensive for the engineering practice to design a single pile. Therefore, it may be efficient, after the development of renewed p-y curves, to expand D-Pile Group and LPILE with the option to analyse a laterally loaded pile in sloping ground.
- It was concluded from the literature review that the pile diameter and the pile roughness influence the pile-soil interaction of a laterally loaded pile located in a slope. These factors have not been regarded in the Plaxis 3D analysis, since the amount of varied parameters had to be limited within this master's thesis. The influence of these parameters on laterally loaded piles in slopes should be examined in future research.
- For practical reasons, piles with a short embedded length are considered in the Plaxis 3D analysis. To obtain p-y ratio's which are characterizing for Dutch conditions at depths beneath z=-3D, an analysis should be performed with longer piles.

Recommendations for future research regarding dolphins in sloping ground

- The riverbanks are often covered with bed protection, to protect the banks. The influence of this on dolphins has not been regarded in this analysis and should be examined in further research. However, it may be expected that the effect of the bed protection is similar for dolphins located in horizontal level ground.
- As stated, the analysis of sand in Plaxis 3D is only valid for mooring dolphins, since the soil is modelled as drained. Another analysis with undrained sand should be performed to analyse the pile-soil interaction of breasting dolphins.

Appendix A

Derivation beam model Heteyeni

The derivation of Heteyeni, which provides a linear relationship between the pile deflection and the soil response, starts with the equilibrium of moments for an infinitely small element:

$$(M + dM) - M + P_x dy - V_v dx = 0 \tag{A-1}$$

or

$$\frac{dM}{dx} + P_x \frac{dy}{dx} - V_v = 0 \tag{A-2}$$

where

M	=	bending moment of the pile
P_x	=	axial load on the pile
y	=	lateral deflection of the pile
V_v	=	shear force in the pile

If one differentiates (A-2) with respect to x, the following equation is obtained:

$$\frac{d^2M}{dx^2} + P_x \frac{d^2y}{dx^2} - \frac{dV_v}{dx} = 0 \tag{A-3}$$

The following identities are noted:

$$\frac{d^2M}{dx^2} = E_p I_p \frac{d^4y}{dx^4} \tag{A-4}$$

$$\frac{dV_v}{dx} = p \tag{A-5}$$

$$p = E_{py} y \tag{A-6}$$

where

p	=	soil reaction per unit length
$E_p I_p$	=	bending stiffness of the pile
E_{py}	=	stiffness of the soil

Substituting equations (A-4) to (A-6) into equation (A-3) leads to the following formula:

$$E_p I_p \frac{d^4y}{dx^4} + P_x \frac{d^2y}{dx^2} + E_{py} y = 0 \tag{A-7}$$

To solve a number of practical problems it is convenient to add to the equation a distributed force per unit length, Q, along the upper part of the pile. The differential equation then becomes:

$$E_p I_p \frac{d^4y}{dx^4} + P_x \frac{d^2y}{dx^2} - p + Q = 0 \tag{A-8}$$

Other beam formulas from structural mechanics, which could be relevant in analysing piles subjected to lateral loads are:

$$E_p I_p \frac{d^3y}{dx^3} + P_x \frac{dy}{dx} = V \tag{A-9}$$

$$E_p I_p \frac{d^2y}{dx^2} = M \tag{A-10}$$

$$\frac{dy}{dx} = S \tag{A-11}$$

where

S = slope of the elastic curve defined by the axis of the pile

Appendix B

Derivation of Gabr and Borden

Gabr and Borden derived the ultimate lateral resistance of a $c-\phi$ soil for a pile in sloping ground. The force equilibrium of the wedge is shown in figure B-1a and B-1b [1]. The derivation of the wedge equilibrium is divided into two parts; the derivation of the resistance along plane EABF and the derivation of the resistance along the side planes EAD and FBC, from here the total ultimate lateral resistance will be derived.

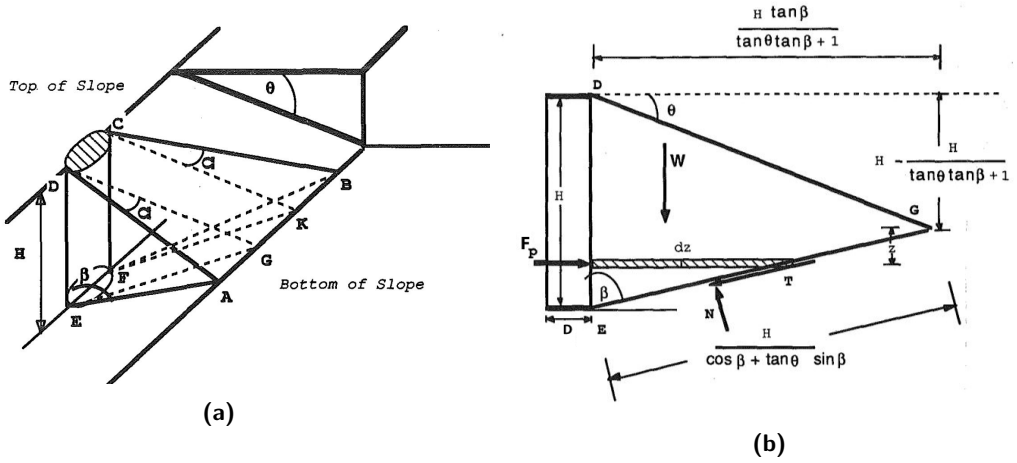

Figure B-1: (a) Assumed failure wedge with plane failure surface and (b) assumed wedge in equilibrium of Gabr and Borden [1]

Plane EABF

The slope angle of the ground surface is defined by θ, and the size of the displaced wedge is assumed to have angle Ω. Referring to figure B-1b the following parameters can be defined:

$$T = F_p \sin\beta - W\cos\beta \tag{B-1}$$

$$N = F_p \cos\beta + W\sin\beta \tag{B-2}$$

$$W = \frac{\gamma H^2 \tan\beta}{2(\tan\theta\tan\beta + 1)} \tag{B-3}$$

$$T = \frac{cH}{\cos\beta + \tan\theta\sin\beta} + N\tan\phi \tag{B-4}$$

where

T	=	friction force acting on the failure plane of the assumed wedge
N	=	normal force acting on the failure plane of the assumed wedge
W	=	weight of the assumed failure wedge
F_p	=	lateral load acting on the pile

Setting equation (B-4) equal to equation (B-1) and substituting W, P_p can be expressed as:

$$F_p = cHK_{pc} + \frac{\gamma H^2}{2}K_{p\phi} \tag{B-5}$$

where

$$K_{pc} = \frac{1}{(\tan\theta\sin\beta + \cos\beta)(\sin\beta - \cos\beta\tan\phi)} \tag{B-6}$$

$$K_{p\phi} = \frac{\tan\beta(\cos\beta + \sin\beta\tan\phi)}{(\tan\theta\tan\beta + 1)(\sin\beta\cos\beta\tan\phi)} \tag{B-7}$$

For the two accompanying areas EGA and FBK, the average failure stresses, σ_f and τ_f, will vary proportionally to the length of the failure plane. These stresses can be evaluated by dividing the resisting forces T and N by the length of the failure plane EG. For the mathematical simplification σ_f and τ_f are written as:

$$\sigma_f = c\lambda_1 + \gamma H\lambda_2 \tag{B-8}$$

$$\tau_f = c + \sigma_f\tan\phi = c(1 + \lambda_1\tan\phi) + \gamma H\lambda_2\tan\phi \tag{B-9}$$

where

$$\lambda_1 = K1K_{pc} \tag{B-10}$$

$$\lambda_2 = \frac{K1}{2}\left(K_{p\phi} + \frac{K2}{\cos\beta}\right) \tag{B-11}$$

$$K1 = \frac{\cos\beta(\tan\beta\sin\beta + \cos\beta)}{H} \tag{B-12}$$

$$K2 = \frac{\tan\beta\sin\beta}{\tan\theta\tan\beta + 1} \tag{B-13}$$

The force F_L is now defined as the force that resists the lateral movement of the pile. It can be evaluated by integrating the failure stresses, σ_f and τ_f, over the area of the inclined plane EABF:

$$F_L = \int_A \sigma_f\cos\beta dA + \int_A \tau_f\sin\beta dA \tag{B-14}$$

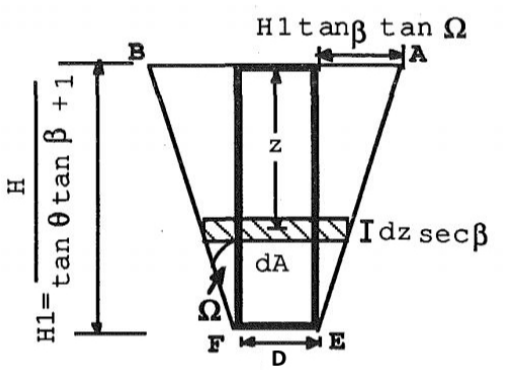

Figure B-2: Elevation view of inclined plane EABF of failure wedge by Gabr and Borden [1]

Referring to figure B-2, dA can be defined as:

$$dA = [D + 2\tan\Omega\tan\beta(H1 - z)]\sec\beta dz \tag{B-15}$$

If one now substitutes equation (B-8), (B-9) and (B-15) in equation (B-14), integrates this formula over dA, differentiates the resulting expression with respect to the depth, the lateral resistance per unit depth of the pile due to plane EABF can be expressed as:

$$f_L = \gamma H[HS_{1\phi} + bS_{2\phi}] + c[HS_{1c} + bS_{2c}] \tag{B-16}$$

where

$$S_{1\phi} = \frac{\lambda_2\tan\Omega\tan\beta}{(\tan\theta\tan\beta+1)^2}\Big[(\tan\theta\tan\beta+1)(3+4\tan\phi\tan\beta) - (2\tan\phi\tan\beta)\Big] \tag{B-17}$$

$$S_{2\phi} = \frac{2\tan\Omega\tan\beta}{\tan\theta\tan\beta+1}(1+\tan^2\phi) \tag{B-18}$$

$$S_{1c} = \frac{2\tan\Omega\tan\beta}{(\tan\theta\tan\beta+1)^2}\Big[\lambda_1(1+2\tan\theta\tan^2\beta+\tan\beta) + 2\tan\beta(\tan\theta\tan\beta+1) - \tan\beta\Big] \tag{B-19}$$

$$S_{2c} = \lambda_1 + \frac{1+\lambda_1\tan\phi}{\tan\theta\tan\beta+1} \tag{B-20}$$

Planes EAD and FBC

Similarly to the above derivation the resistance per unit depth for the two planes EAD and FBC can be derived:

$$f_s = 3\gamma K_o H^2 S_{3\phi} + 2cHS_{3c} \tag{B-21}$$

where

$$S_{3\phi} = (\tan\phi - \tan\Omega)\Big[\tan\beta - \frac{\tan^4\beta\tan^3\theta + \tan^3\beta\tan^2\theta}{(\tan\beta\tan\theta+1)^3}\Big] \tag{B-22}$$

$$S_{3c} = \tan\beta\frac{\tan^3\beta\tan^2\theta + \tan^2\beta\tan\theta}{(\tan\beta\tan\theta+1)^2} \tag{B-23}$$

Total lateral resistance

Now all the lateral resistances for the different planes are determined, the total lateral resistance can be derived. Summing the active earth pressure at the back of the pier together with the lateral resistance from the two side planes and the front plane, the total lateral resistance can be expressed by:

$$p_u = \gamma H[H(S_{1\phi} + 3K_o S_{3\phi}) + DS_{2\phi} - K_a D] + c[H(S_{1c} + S_{3c}) + DS_{2c} - 2DK_a^{0.5}] \tag{B-24}$$

For the angles β and Ω the values should be chosen such, that the critical failure wedge is obtained along which the total lateral resistance is the smallest.

Appendix C

Derivation of Mirzoyan

Derivation of the wedge weight

The derivation of the ultimate resistance starts with the derivation of the wedge weight. For the calculation is the wedge divided into two sections; one section above the virtual line Z_1, and one section beneath it, which is shown in figure C-2.

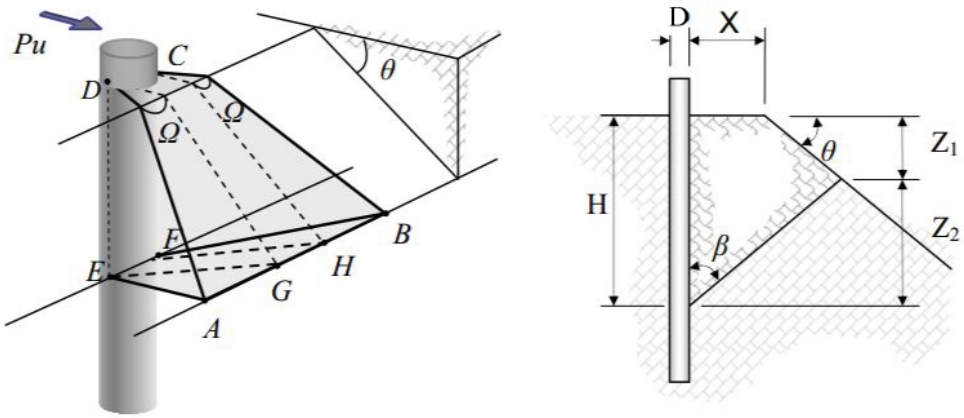

Figure C-1: Assumed failure wedge by Mirzoyan [2]

The incremental area of the first section can be expressed as:

$$A(z) = \frac{(D + D_2)x_z}{2} \tag{C-1}$$

where

$$x_z = X + z\tan(90 - \theta) \tag{C-2}$$

$$D_2 = D + 2x_z \tan\Omega \tag{C-3}$$

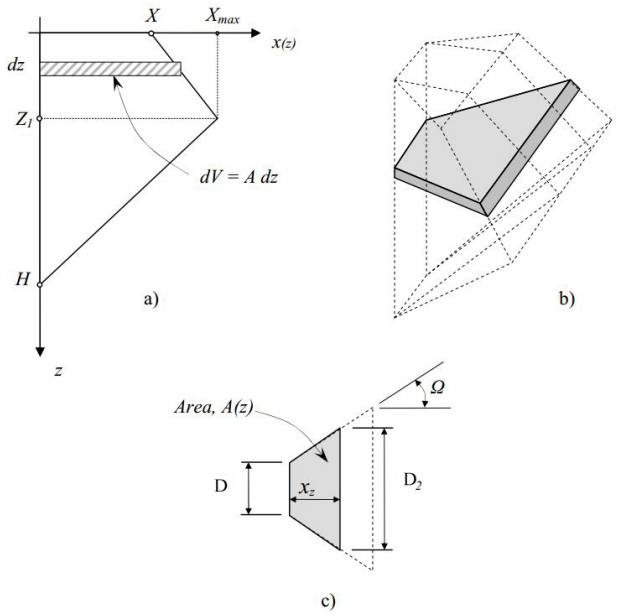

Figure C-2: Volume and area derivations by Mirzoyan [2]

Substituting these formula for x_z and D_2 in equation (C-1), the equation for $A(z)$ becomes:

$$A(z) = DX + X^2 \tan\Omega + 2zX \tan(90-\theta)\tan\Omega + zD\tan(90-\theta) + z^2\tan^2(90-\theta)\tan\Omega \quad \text{(C-4)}$$

Defining:

$$J_1 = \tan\Omega \quad \text{(C-5)}$$
$$J_2 = \tan(90-\theta)\tan\Omega \quad \text{(C-6)}$$
$$J_3 = \tan(90-\theta) \quad \text{(C-7)}$$
$$J_4 = \tan^2(90-\theta)\tan\Omega \quad \text{(C-8)}$$
$$Z_1 = \frac{H\tan\beta - X}{\tan(90-\theta)+\tan\beta} \quad \text{(C-9)}$$

The reduced formula for the area as function of the depth above the line Z_1 can then be expressed as:

$$A(z) = DX + X^2 J_1 + 2zXJ_2 + zbJ_3 + z^2 J_4 \quad \text{(C-10)}$$

Integrating the area over the depth leads to the volume of the failure wedge above the line Z_1:

$$V = Z_1 DX + Z_1 X^2 J_1 + Z_1^2 X J_2 + \frac{Z_1^2 D J_3}{2} + \frac{Z_1^3 J_4}{3} \quad \text{(C-11)}$$

For the second section the procedure can be repeated. The incremental area can now be expressed as:

$$A(z) = \frac{(D + D_2)x_z}{2} \tag{C-12}$$

where:

$$x_z = H \tan\beta - z \tan\beta \tag{C-13}$$
$$D_2 = D + 2x_z \tan\Omega \tag{C-14}$$

Substituting these formula's for x_z and D_2 in the equation, the area of the second section can be formulated as:

$$A(z) = DH \tan\beta + H^2 \tan^2\beta \tan\Omega - 2zH \tan^2\beta \tan\Omega - zD \tan\beta + z^2 \tan^2\beta \tan\Omega \tag{C-15}$$

Defining:

$$J_5 = \tan\beta \tag{C-16}$$
$$J_6 = \tan^2\beta \tan\Omega \tag{C-17}$$
$$Z_2 = H - Z_1 \tag{C-18}$$

The reduced formula for the area as function of the depth beneath the line Z_1 can then be expressed as:

$$A(z) = DHJ_5 + H^2 J_6 - 2zHJ_6 - zDJ_5 + z^2 J_6 \tag{C-19}$$

Integrating the area over the depth leads to the volume of the failure wedge beneath the line Z_1:

$$V = \Big(Z_2 H - \frac{H^2}{2} + \frac{Z_1^2}{2}\Big) DJ_5 + \Big(Z_2 H^2 + Z_1^2 H - \frac{2H^3}{3} - \frac{Z_1^3}{3}\Big) J_6 \tag{C-20}$$

The total volume of the wedge is then the sum of the two volumes:

$$\begin{aligned} V_{TOT} =& V_1 + V_2 \\ &= Z_1 DX + Z_1 X^2 J_1 + Z_1^2 X J_2 + \frac{Z_1^2 D J_3}{2} + \frac{Z_1^3 J_4}{3} \\ &+ \Big(Z_2 H - \frac{H^2}{2} + \frac{Z_1^2}{2}\Big) DJ_5 + \Big(Z_2 H^2 + Z_1^2 H - \frac{2H^3}{3} - \frac{Z_1^3}{3}\Big) J_6 \end{aligned} \tag{C-21}$$

Finally, the total weight of the wedge is:

$$W = \gamma V_{TOT} \tag{C-22}$$

Ultimate soil resistance

The ultimate soil strength, p_u, can be derived from the equilibrium of the wedge. The weight, W, the normal force, N, and the friction force, T, are acting on the failure wedge. Note that the friction force is assumed to come only from the bottom plan FEAB.

Force equilibrium in the x-direction:

$$\sum F_x = F_p - N\cos\beta - N\tan\phi\sin\beta \tag{C-23}$$

Force equilibrium in the y-direction:

$$\sum F_y = W - N\sin\beta + N\tan\phi\cos\beta \tag{C-24}$$

Solving for N:

$$N = \frac{W}{\sin\beta - \tan\phi\cos\beta} \tag{C-25}$$

Now solving for F_p, the force that resists the lateral movement of the soil:

$$F_p = N\cos\beta + N\tan\phi\sin\beta = \frac{W(\cos\beta + \tan\phi\sin\beta)}{\sin\beta - \tan\phi\cos\beta} \tag{C-26}$$

The ultimate resistance per unit length, p_{ult}, can be obtained by differentiating equation (C-26) with respect to the depth H. Due to the non-continuous geometry of the wedge, two equations are derived:

$$p_{ult} = \frac{\gamma H(bJ_5 + HJ_6)}{\tan(\beta - \phi)} \tag{C-27}$$

for $0 < H \leq (X/\tan\beta)$

and

$$p_{ult} = \frac{\gamma(X + HJ_3)(DJ_3J_5 + (DJ_5^2 + J_6(X + HJ_3)))}{(J_3 + J_5)^2\tan(\beta - \phi)} \tag{C-28}$$

for $H > (X/\tan\beta)$

Appendix D

Additional information to the full scale tests of Nimityongskul and Barker

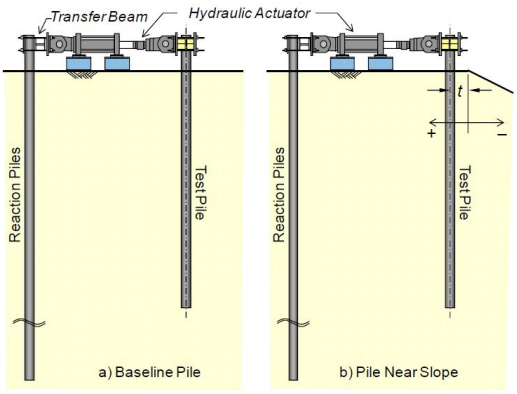

(a)

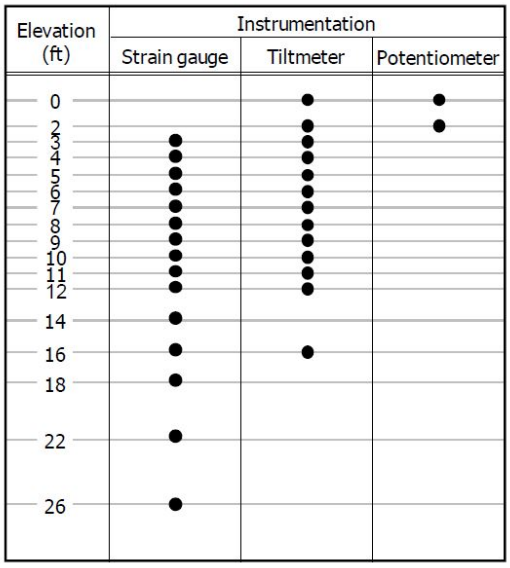

(b)

Figure D-1: (a) Side view of test set up and (b)instrumentation of Nimityongskul and Barker [3]

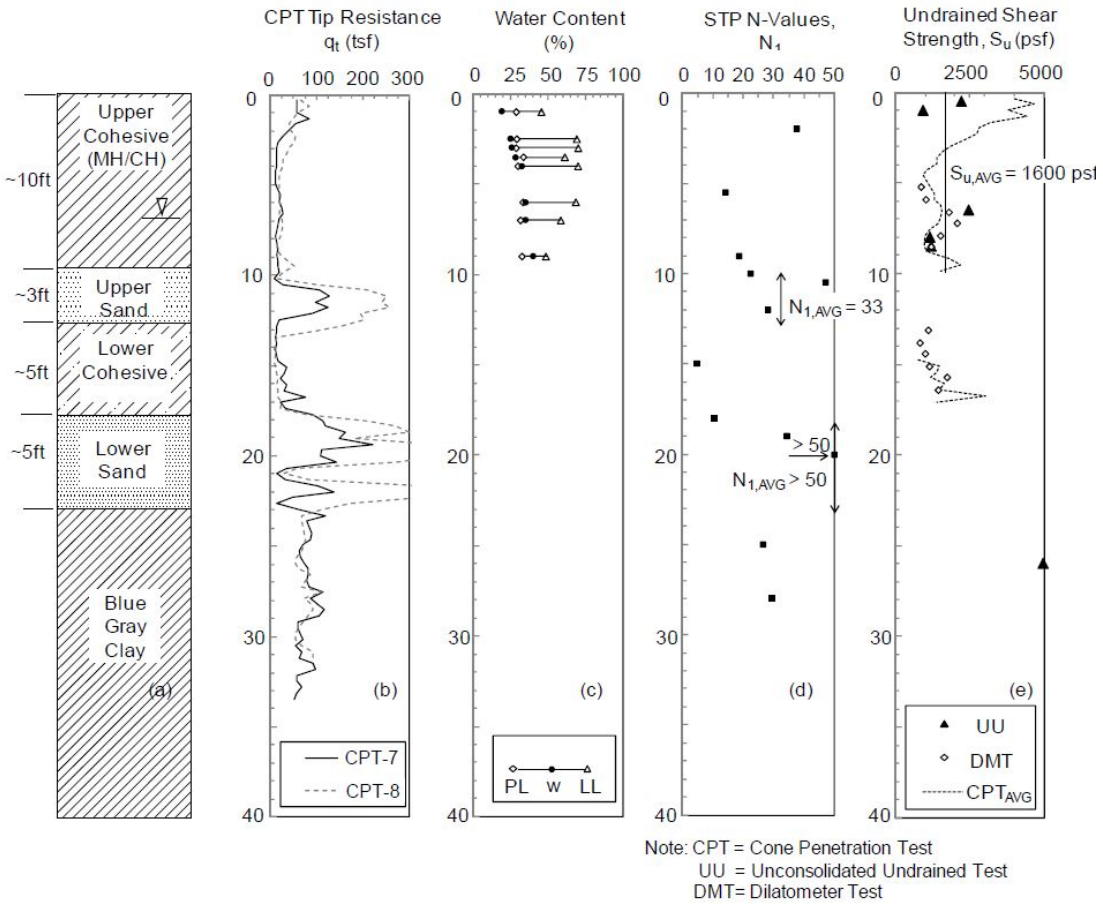

Figure D-2: Summary of the site specific explorations for the lateral pile loading tests of Nimityongskul citenimityongskul2010effects

Sample No.	Shipton #1	Shipton #2	Shipton #3	#101	#102
Type of Test	CU	CU	CU	CU	CU
Date of Testing	09/96	11/96	11/96	10/01	10/01
Sample Depth (ft)	10	15	16	8	48
Sample Length (in)	7.44	7.25	7.75	-	-
Sample Width (in)	2.75	2.75	2.75	-	-
Consolidation Pressure (psi)	50	56	65	27.77	40
Sample Pressure (psi)	43	45	54	7.5	20
Induced OCR	1.2	1.2	1.2	3.7	2.0
Strain Rate (mm/min)	0.096	0.096	0.096	0.048	0.021
Wet unit weight (pcf)	126	130	123.4	113.9	103.7
Water Content (%)	38.5	44.3	42.6	42	55.4
B-Parameter	0.987	0.987	0.971	-	-
Initial Void Ratio, e_0	-	-	-	1.14	-
$\Delta_{dev,max}$ (psi) @ Fail. Criteria 1	23	22	28	16	29.5
ε_{Axial} (%) @ Fail. Criteria 1	2.5	2	4	9.7	11.3
$\Delta_{dev,max}$ (psi) @ Fail. Criteria 2	-	-	-	12.25	26.8
ε_{Axial} (%) @ Fail. Criteria 2	-	-	-	5.2	10.2

Note: Failure criteria 1 - condition at which maximum deviator stress occurs
Failure criteria 2 - condition at which maximum principle stress ratio ($\sigma'_1/\sigma'_{3)}$ occurs

Figure D-3: Summary of TXCU tests from GEFRS report [3]

Sample No.	SH-2-3 (No. 1)	SH-2-3 (No. 2)	SH-2-3 (No. 3)	SH-5-6 (No. 1)	SH-5-5 (No. 2)	SH-5-5 (No. 3)	B-4-3 (No. 1)
Type of Test	CU	CU	CU	CU	CU	CU	CU
Date of Testing	10/03	10/03	10/03	11/03	11/03	11/03	04/02
Sample Depth (ft)	7.5-9	7.5-9	7.5-9	12.5-14.5	12.5-14.5	12.5-14.5	8.5
Sample Length (in)	5.56	5.72	5.56	5.69	5.7	5.65	6
Sample Width (in)	2.84	2.86	2.84	2.86	2.86	2.86	2.87
Cell Pressure (psi)	36	30	42	42	36	48	-
Sample Pressure (psi)	30	25	35	35	30	40	-
Induced OCR	1.2	1.2	1.2	1.2	1.2	1.2	-
Strain Rate (mm/min)	0.02	0.02	0.02	0.01	0.01	0.01	0.03
Dry Unit Weight (pcf)	82.2	81.3	82.2	83.8	84.8	83.8	79.6
Water Content (%)	38.9	38.9	38.9	35.9	35.9	35.9	40.6
Initial Void Ratio, e_0	1.05	1.04	1.05	0.97	0.97	0.97	1.12
% Saturation	99.9	99.5	99.9	97.8	99	97.8	97.9
$\Delta_{dev.max}$ (psi) @ Fail.	14.7	11.5	21.8	17.9	15.5	26.8	12.5
ε_{Axial} (%) @ Fail.	5	6.2	2	4.6	5.25	3.75	1.8
c (total stress), (psi)	1.97	1.97	1.97	2.84	2.84	2.84	-
ϕ (total stress), (psi)	20	20	20	21.7	21.7	21.7	-

Note: Failure criteria 1 - condition at which maximum deviator stress occurs
Only Sample No. B-4-3 from Kelly Engineering Center expansion project

Figure D-4: Summary of TXCU tests from Reser Stadium Expansion Project [3]

Table A-8 Summary of UUTX Tests from Caltrans Boring (B-12 and B-13)

Sample No. (Boring No.)	SH 1-15 (B-12)	SH-2-6 (B-13)	SH-2-5 (B-13)	SH-1-3* (B-12)	SH-1-5* (B-12)	SH-1-1 (B-12)	SH-1-1a (B-12)	SH-1-5a (B-12)
Type of Test	UU	UU	UU	UU	UU	UU	UU	UU
Date of Testing	1/21/10	1/26/10	1/28/10	2/2/10	2/4/10	2/9/10	2/9/10	2/11/10
Sample Depth (ft)	26-26.5	8.5-9	6.5-7	3.5-4	7.5-8	0-0.5	1-1.5	8-8.5
Sample Length (in)	6.02	6.11	6.07	5.69	6.01	6.67	5.93	6.05
Sample Width (in)	2.85	2.88	2.70	2.85	2.86	2.86	2.82	2.88
Cell Pressure (psi)	14.6	7.1	6.2	3.0	6.8	-	-	7.2
Strain Rate (%/min)	1	1	1	1	1	1	1	1
Unit Weight (pcf)	94	114	123	108	117	103	99	117
Water Content (%)	68	37	34	25	43	13	19	34
$(\sigma_1-\sigma_3)_{max}/2 = q_{max}$ (psi)	34.5	8.2	17	(4.91)	(1.8)	15.3	6.3	7.9
ε_1 @ q_{max} (%)	5.5	5.6	5.9	(9.2)	(8.6)	1.6	2.0	1.5
$\varepsilon_{50} = \varepsilon$ @ $q_{max}/2$ (%)	2.3	1.4	1.9	(0.55)	(0.11)	0.7	1	0.5
E_{50} (psi)	751	284	460	446	822	1137	326	849

Note: * = large amount of sample disturbance, results not included for analysis

Figure D-5: Summary of UUTX tests from Caltrans Boring [3]

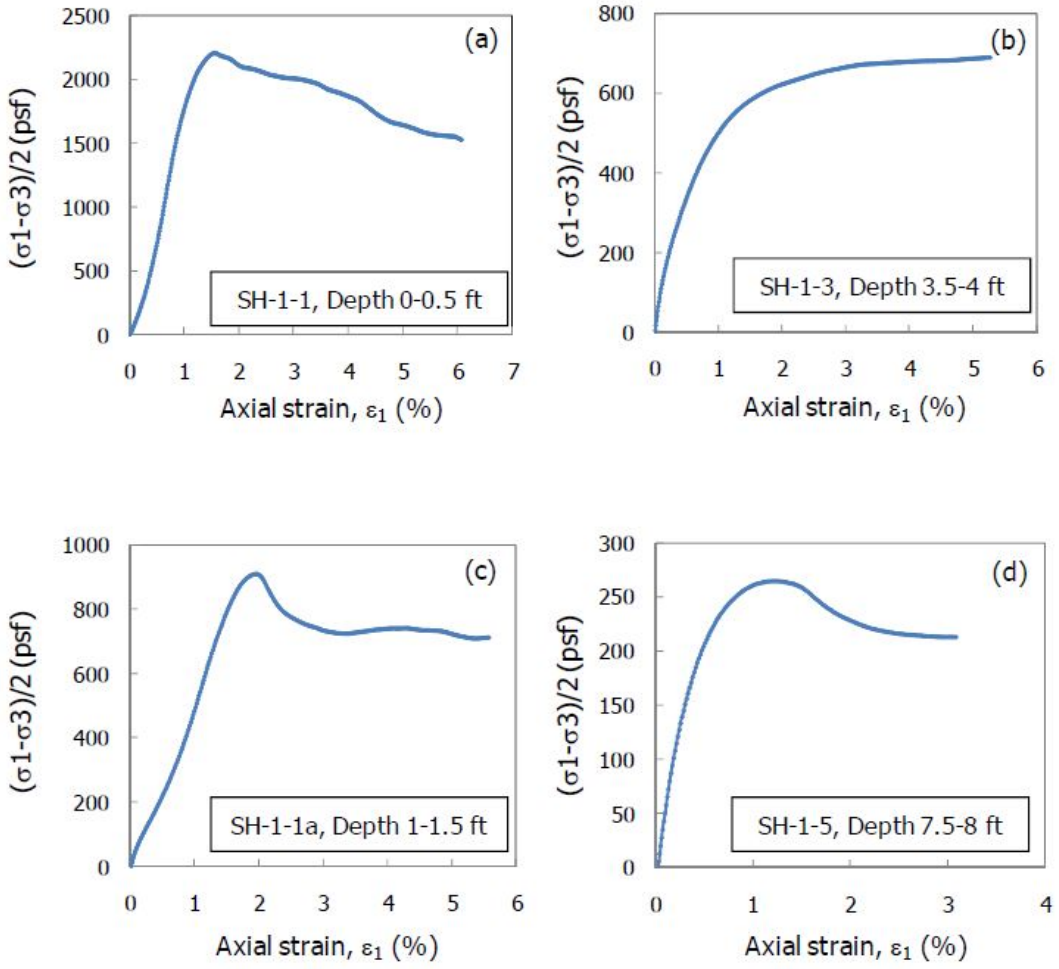

Figure D-6: Stress strain curves [3]

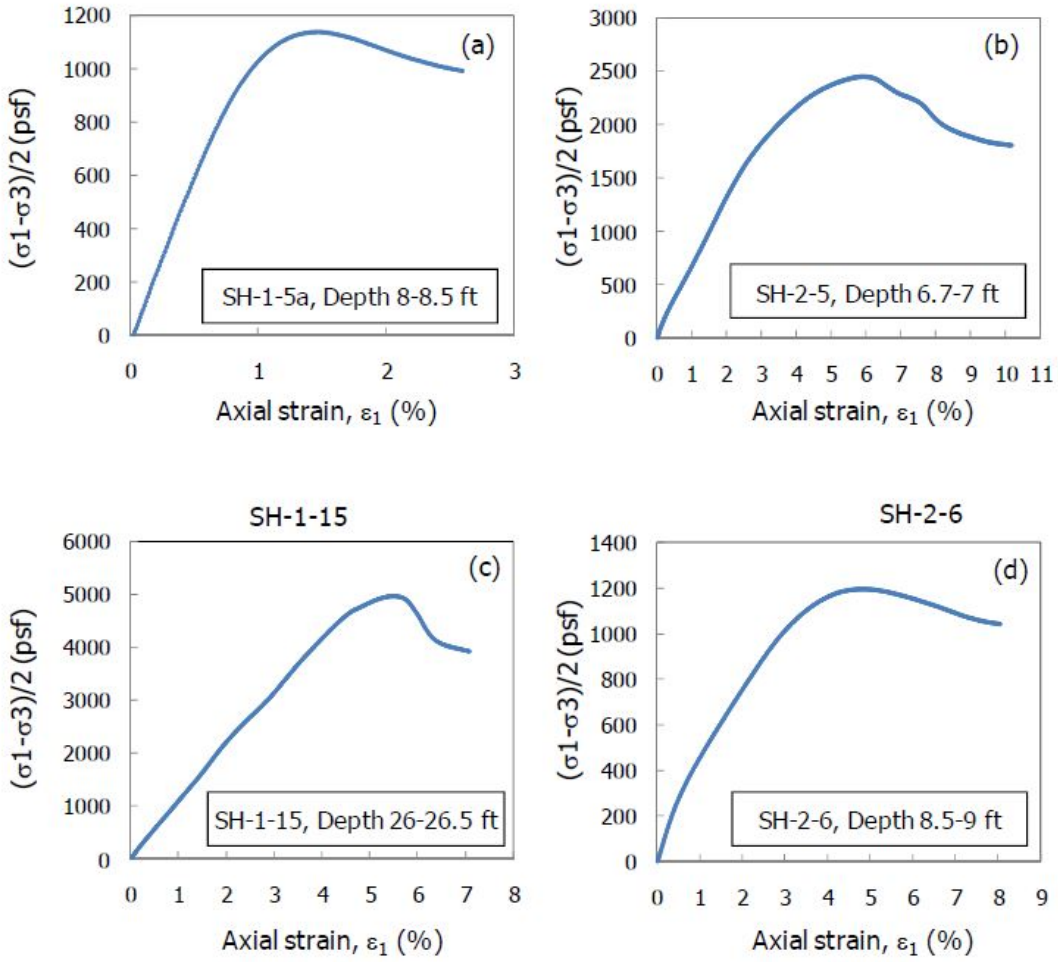

Figure D-7: Stress strain curves [3]

Appendix E

Software programs

E-1 D-Sheet Piling

D-Sheet piling version 9.3 is used to analyse a laterally loaded pile [38]. With the help of the single pile module one is able to determine the moments and displacements of the pile when the moment or the force at the head of the pile is given.

D-Sheet Piling is a spring model, the soil is modelled as a bilinear spring along the pile. The ultimate soil resistance is determined by Brinch Hansen[25] and the linear modulus of subgrade is determined by the formula of Ménard. The program attempts to find iteratively an equilibrium between the forces and/or moments on the pile and the soil springs.

Input parameters to derive the displacement and forces are the unit weight, cohesion, internal friction angle and the modulus of subgrade reaction of Ménard of the soil and the pile properties. These simple input parameters make it an easy and quick method, and therefore cheap method, to determine the pile-soil behaviour.

The main limitation of D-Sheet Piling is that the soil is modelled as a bilinear spring, which is not realistic for soil. Moreover, the stiffness of the soil is independent of stress and strain. However, this effect can be reduced by generating several layers for one soil layer with increasing elasticity along the depth. Also, it is not possible to model a sloping ground.

The formula by Brinch Hansen to determine the passive pressure behind the pile is defined as[25]:

$$\sigma_p = K_q * \sigma_v^{'} + K_c * c, \sigma_a = 0, \sigma_n = 0 \tag{E-1}$$

K_q and K_c are factors of Brinch-Hansen for the piles:

$$K_q = \frac{K_q^0 + K_q^\infty * \alpha_q * \frac{D}{B}}{1 + \alpha_q * \frac{D}{B}} \tag{E-2}$$

$$K_c = \frac{K_c^0 + K_c^\infty * \alpha_c * \frac{D}{B}}{1 + \alpha_c * \frac{D}{B}} \tag{E-3}$$

Where:

$$K_q^0 = e^{(\frac{\pi}{2}+\phi)*\tan\phi} * \cos\phi \tan(\frac{\pi}{4}+\frac{\phi}{2}) - e^{(-\frac{\pi}{2}+\phi)*\tan\phi} * \cos\phi \tan(\frac{\pi}{4}-\frac{\phi}{2})$$

$$K_c^0 = \left[e^{(\frac{\pi}{2}+\phi)*\tan\phi} * \cos\phi \tan(\frac{\pi}{4}+\frac{\phi}{2})\right] * \cot\phi$$

$$K_q^\infty = K_c^\infty * K_0 * \tan\phi$$

$$K_c^\infty = N_c * d_c^\infty$$

$$d_c^\infty = 1.58 + 4.09 * \tan^4\phi$$

$$N_c = \left[e^{\pi*\tan\phi} * \tan^2(\frac{\pi}{4}+\frac{\phi}{2}) - 1\right] * \cot\phi$$

$$K_0 = 1 - \sin\phi$$

$$\alpha_q = \frac{K_q^0}{K_q^\infty - K_q^0} * \frac{K_0 * \sin\phi}{\sin(\frac{\pi}{4}+\frac{\phi}{2}}$$

$$\alpha_c = \frac{K_c^0}{K_c^\infty - K_c^0} * 2\sin(\frac{\pi}{4}+\frac{\phi}{2})$$

The method according to Ménard [39] to determine the modulus of subgrade reaction of the soil is defined as:

$$\frac{1}{k_h} = \begin{cases} \frac{1}{3E_m}[1.3R_0(2.65\frac{R}{R_0})^\alpha + \alpha R] & if \quad R \geq R_0 \\ \frac{2R}{E_m} * \frac{4(2.65)^\alpha + 3\alpha}{18} & if \quad R < R_0 \end{cases} \tag{E-4}$$

where

k_h	=	the modulus of horizontal subgrade reaction
E_m	=	is the pressiometric modulus
R_0	=	constant, $R_0 = 0.3$
R	=	half width of the pile
α	=	rheological coefficient depending on the kind of the soil and the soil conditions

The correlation between the cone resistance and E_m is defined as [38]:

Peat	$E_m = (3 \text{ á } 4) * q_c$
Clay	$E_m = (2 \text{ á } 3) * q_c$
Loam	$E_m = (1 \text{ á } 2) * q_c$
Sand	$E_m = (0.7 \text{ á } 1) * q_c$
Gravel	$E_m = (0.5 \text{ á } 0.7) * q_c$

E-2 D-Pile Group

D-Pile Group is a software application that can be used to analyse single piles and pile groups. Version 5.1 is used in this master's thesis [16].

To analyse a laterally loaded single pile in D-Pile, the standard Poulos model in combination with the Cap module is required. Like D-sheet Piling, D-Pile group is based on a mass-spring model. However, in D-Pile Group the soil springs are non-linear and based on p-y curves calibrated by full scale tests. It has the possibility to use p-y curves recommended by the American Petroleum Institute (API) or to manually enter p-y curves. With the API p-y curves it is possible to do analysis for sand, both drained and undrained and analysis for undrained soft and stiff clay. These can be done for both static and cyclic lateral loading. The relevant p-y curves can be found in beneath.

The required input parameters for D-Pile Group are the cohesion, empirical constant J and $\epsilon_{50\%}$ for clay, the internal friction angle, cone resistance and K_0 for sand and unit weight for both sand and clay. Also, it is possible to model a pile that consists of different sections. Hence, D-Pile Group has more options than D-Sheet piling, but requires still an acceptable amount of input parameters to keep it an easy and cheap method to model the pile-soil behaviour. Moreover, it should model the soil behaviour more accurate than D-Sheet Piling since non-linear springs are used.

However, D-Pile Group has also limitations. K_0, the coefficient of horizontal earth pressure, is constant over depth within each soil layer. Moreover, lateral loads can only be applied at the top of the pile through the pile cap. Also, it is not possible to model a sloping ground.

p-y curve for sand

The p-y curve for sand according to the API is defined in equation E-5 and plotted in figure E-1.

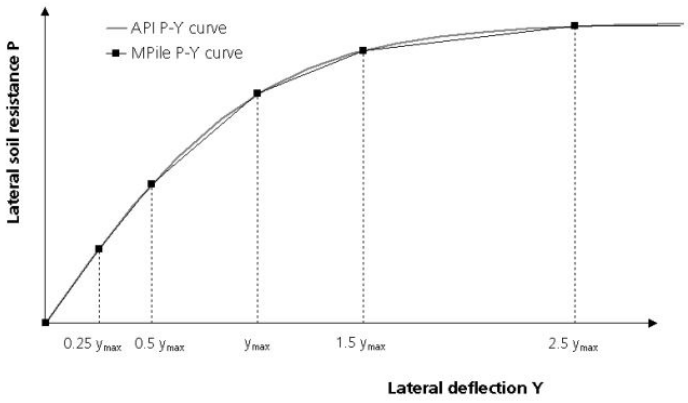

Figure E-1: Modelling of the p-y curve (API) for sand [16]

$$P = Ap_u \tanh\left(\frac{kH}{Ap_u}Y\right) \tag{E-5}$$

where

P	=	actual lateral soil resistance at depth H $[kN/m]$
A	=	factor to account for loading conditions [-]
k	=	initial modulus of subgrade reaction $[kN/m^3]$, in D-Pile determined by interpolation of table E-1
p_u	=	ultimate lateral soil resistance at depth H $[kN/m]$
H	=	depth below soil surface $[m]$
Y	=	actual lateral deflection $[m]$

and

$$A = 3 - 0.8\frac{H}{D} \geq 0.9 \quad forstaticloads \tag{E-6}$$

The ultimate resistance at depth H is the smallest value of p_{us} and p_{ud}

$$p_u = min(p_{us}; p_{ud}) \tag{E-7}$$

Angle of internal friction [°]	k (dry condition) $[kN/m^3]$	k (wet condition $[kN/m^3]$)
29	2715	2715
29.5	6109	5090
30	11199	8145
33	25453	16303
36	42761	25453
38	59051	32580
40	73541	41743

Table E-1: Values of k as function of ϕ in D-Pile

with

$$p_{us} = (C_1 H + C_2 D_H)\gamma` H \tag{E-8}$$

$$p_{ud} = C_3 D_H \gamma` H \tag{E-9}$$

where

p_{us}	=	ultimate lateral soil resistance at shallow depth $[kN/m]$
p_{ud}	=	ultimate lateral soil resistance at deep depth $[kN/m]$
C_1, C_2, C_3	=	coefficients of the API
D_H	=	Average pile diameter from surface to depth H $[m]$

The coefficients C1, C2 and C3 are defined as:

$$C_1 = \tan\alpha \tan\beta \left(\frac{\tan\beta}{\tan(\beta-\phi)} - K_0\right) + K_0 \sin\beta \tan\phi \left(\frac{\cot(\beta-\phi)}{\cos\alpha} + \tan\beta\right) \tag{E-10}$$

$$C_2 = \frac{\tan\beta}{\tan(\beta-\phi)} - K_a \tag{E-11}$$

$$C_3 = K_a(\tan^8\beta - 1) + K_0 \tan\phi \tan^4\beta \tag{E-12}$$

with

$$K_a = \tan^2(45° - \phi/2) \tag{E-13}$$

$$K_0 = 0.4 \tag{E-14}$$

$$\beta = 45° + \phi/2 \tag{E-15}$$

$$\alpha = \phi/2 \tag{E-16}$$

p-y curve for clay and static lateral loads
The p-y curve for clay and static lateral loads is not given as a curve by the API, but defined as a table. These points are part of the continuous curve in equation E-17 and plotted in figure E-2.

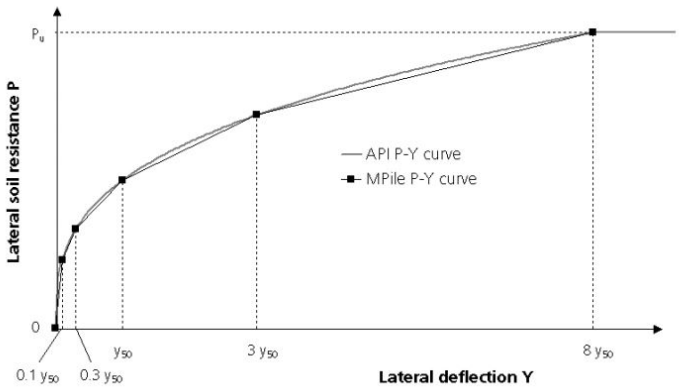

Figure E-2: Modelling of the p-y curve (API) for clay and static loading [16]

$$p = \begin{cases} 0.5 p_u (y/y_{50})^{1/3} & for \quad y < 8y_{50} \\ p_u & for \quad y \geq 8y_{50} \end{cases} \tag{E-17}$$

The ultimate resistance at depth H is the smallest value of p_{us} and p_{ud}, which is defined by the API for clay as:

$$p_{us} = 3c_u + \gamma^{`} H + J c_u \frac{H}{D} \tag{E-18}$$

$$p_{ud} = 9c_u \tag{E-19}$$

where
y_{50} = displacement which occurs at one-half the maximum stress on laboratory undrained compression tests of undisturbed soil samples
c_u = undrained shear strength $[kN/m^2]$
J = dimensionless empirical constant, value between 0.25 and 0.5 recommended

The parameter ϵ_{50} is also required for clay in D-Pile, this value can be determined from table E-2.

c_u $[kN/m^2]$	ϵ_{50} $[-]$
5-25	0.02
25-50	0.01
50-100	0.007
100-200	0.005
200-400	0.004

Table E-2: Determination of ϵ_{50} as a function of c_u

E-3 Plaxis 3D

Plaxis 3D is a 3D finite element program, developed for geotechnical modelling [40]. The advantages compared to D-Sheet Piling and D-Pile Group are that the continuity of the soil can be modelled and that it is feasible to investigate a lot of other aspects. The stress conditions in-situ can be considered, the effect of the construction sequence can be investigated and failure mechanisms can be examined. Several models are available in Plaxis 3D to model the soil behaviour, such as Mohr Coulomb, Hardening Soil and Hardening Soil Small Strains. For this master's thesis the Hardening Soil Small Strains model ($HSsmall$) is selected. Along the length of a laterally loaded pile both very large derformations (at the head of the pile) and very small deformations (lower down the pile) will appear. To model this correct, the Hardening Soil Small Strains model is considered to be the most appropriate. The advantage of this model over the Mohr-Coulomb model is the stress level dependency of the stiffness and the use of a hyperbolic stress-strain curve instead of a bi-linear curve, which is illustrated beneath.

Hardening Soil small strains

The $HSsmall$ model is an advanced model in Plaxis and is suitable to model both soft and stiff soils. In contrast to the Mohr Coulomb model the yield surface of the $HSsmall$ model is not fixed, but can expand. As a result it is possible to model soil hardening. Two types of hardening can be distinguished; shear hardening, which models irreversible strains due to primary deviatoric loading and compression hardening, which models irreversible plastic strains due to primary compression [41].

Since $HSsmall$ is an advanced model, a lot of soil parameters are required, in table E-3 they are shown with their function in the $HSsmall$ model.

symbol	description	function in $HSsmall$
m	power for stress-level dependency of stiffness	to model stress dependent stiffness
E_{50}^{ref}	reference stiffness modulus	to model plastic straining due to primary deviatoric loading
E_{oed}^{ref}	tangent stiffness for primary oedometer loading	to model plastic straining due to primary compression
E_{ur}^{ref}	reference Young's modulus fur unloading reloading	to model unloading/ reloading
ν_{ur}	poisson's ratio for unloading/ reloading	to model unloading/ reloading
G_0	initial shear modulus	to model variation of stiffness with strain
$\gamma_{0.7}$	shear strain level at which the secant shear modulus G_s is reduced to about 70% of G_0	to model variation of stiffness with strain
c	cohesion	to model MC failure criterion
ϕ	friction angle	to model MC failure criterion
ψ	angle of dilatancy	to model MC failure criterion

Table E-3: Model parameters in the HSsmall material model

The derivation of the model parameters is stated beneath.

Modelling of the pile

The pile is modelled as a plate element in Plaxis 3D. Characteristics of the plate that can be entered are the wall thickness, the unit weight, Young's modulus and poisson's ratio. The pile is modelled as an elastic material.

Interface

Around the pile, modelled as plate element, a positive and a negative interface can be activated.

These interface elements allow a proper modelling of the soil-structure interface. The roughness of the interface between the plate and the soil is characterised by the strength reduction factor R_{inter}. This factor relates the interface strength (wall friction and adhesion) to the soil strength (friction angle and cohesion).

Mesh

In Plaxis 3D, the soil is modelled as 10-node tetrahedral elements, the plate element of the pile consists of 6-node elements and 12-node interface elements are used to model the soil-structure behaviour.

Limitations

Regarding the soil behaviour, Plaxis 3D is the modelling program which approaches the best reality. However, the disadvantage is that a lot of soil parameters are required, which should be determined from laboratory research. Moreover, Plaxis 3D has large calculation times. Hence, it is time-consuming and expensive to use Plaxis 3D. For these reasons, Plaxis 3D is mainly used for research. For design activities D-Sheet Piling and D-Pile Group are often selected.

HSsmall model parameters

The Hardening Soil model is based on the hyperbolic relationship between the vertical strain, ϵ_1, and the deviatoric stress, q, which is observed in triaxial testing. The yield curve of a standard drained triaxial test can be described by the relation [42]:

$$-\epsilon_1 = \frac{q_a}{2E_{50}} \frac{\sigma_1 - \sigma_3}{q_a - (\sigma_1 - \sigma_3)} \quad for \quad q < q_f \tag{E-20}$$

The ultimate deviatoric stress, q_f, and the quantity q_a are defined as:

$$q_f = \frac{6 \sin \phi}{3 - \sin \phi}(p + c \cot \phi) \tag{E-21}$$

$$q_a = \frac{q_f}{R_f} \tag{E-22}$$

Since it are triaxial loading conditions, $\sigma_2^{'} = \sigma_3^{'}$ and $\sigma_1^{'}$ is the effective major compressive stress. If the deviatoric stress becomes equal to the ultimate deviatoric stress, the Mohr Coulomb failure criterion is satisfied and perfectly yielding occurs. The hyperbolic relationship is shown in figure E-3a. The failure ratio, R_f, has a default setting of 0.9 in Plaxis 3D.

With the hyperbolic relationship in figure E-3a of a standard drained triaxial test the stiffness modulus for primary loading, E_{50}, and the stiffness modulus for unloading and reloading, E_{ur} can be derived. From here the reference stifness moduli corresponding to the reference stress p_{ref}, which have to be entered in Plaxis 3D for the $HSsmall$ model, can be derived:

$$E_{50} = E_{50}^{ref} \left(\frac{c \cos \phi - \sigma_3^{'} \sin \phi}{c \cos \phi + p^{ref} \sin \phi} \right)^m \tag{E-23}$$

$$E_{ur} = E_{ur}^{ref} \left(\frac{c \cos \phi - \sigma_3^{'} \sin \phi}{c \cos \phi + p^{ref} \sin \phi} \right)^m \tag{E-24}$$

The reference oedometer stiffness can be determined from equation E-25 and is as indicated in figure E-3b.

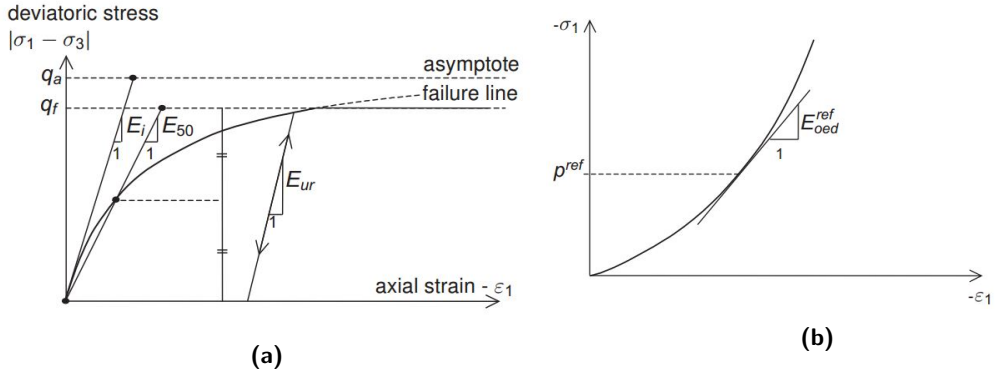

Figure E-3: (a) Hyperbolic stress-strain relation in primary loading for a standard drained triaxial test [41] and (b) Definition of E_{oed}^{ref} in oedometer test results [41]

$$E_{oed} = E_{oed}^{ref} \left(\frac{c\cos\phi - \frac{\sigma_3^{`}}{K_0^{nc}} \sin\phi}{c\cos\phi + p^{ref}\sin\phi} \right)^m \tag{E-25}$$

The additional parameters for the hardening soil model with small-strain stiffness with respect to the hardening soil model are the initial or very small-strain shear modulus, G_0, and the shear strain level $\gamma_{0.7}$ at which the secant shear modulus G_s is reduced to about 70% of G_0. These parameters are relevant to model very small strains. At very small strains, the soil behaves stiffer. As the strain increases, the stiffness reduces. This effect is included by the $HSsmall$ model by the parameters $\gamma_{0.7}$ and G_0. The parameter G_0 is for this master thesis's more important than the parameter $\gamma_{0.7}$, since that parameter is used for calculating the stiffness in un- and reloading phase.

Santos and Correia [43] have proposed that the stress-strain curve for small strains can be described by a hyperbolic law:

$$\frac{G_s}{G_0} = \frac{1}{1 + 0.385|\frac{\gamma}{\gamma_{0.7}}|} \tag{E-26}$$

The reference shear modulus for small strains can be derived from the equation:

$$G_0 = G_0^{ref} \left(\frac{c\cos\phi - \sigma_3^{`}\sin\phi}{ccos\phi + p^{ref}\sin\phi} \right)^m \tag{E-27}$$

Appendix F

Parametric study

F-1 Overview Plaxis 3D calculations

SUM	Soil profile	Location pile	Slope angle	Loading direction
SAND	**Aim: variation slope**			
1	sand standard	H	-	downhill
2	sand standard	S	1:4	downhill
3	sand standard	S	1:3	downhill
	Aim: variation soil parameters			
4	sand variation 1	H	-	downhill
5	sand variation 1	S	1:4	downhill
6	sand variation 1	S	1:3	downhill
7	sand variation 2	H	-	downhill
8	sand variation 2	S	1:4	downhill
9	sand variation 2	S	1:3	downhill
	Aim: variation loading direction			
10	sand standard	S	1:4	uphill
	Aim: variation location pile			
11	sand standard	crest, middle, toe	1:4	downhill
CLAY	**Aim: variation slope**			
12	clay standard	H	-	downhill
13	clay standard	S	1:4	downhill
14	clay standard	S	1:3	downhill
	Aim: variation soil parameters			
15	clay variation 1	H	-	downhill
16	clay variation 1	S	1:4	downhill
17	clay variation 1	S	1:3	downhill
18	clay variation 2	H	-	downhill
19	clay variation 2	S	1:4	downhill
20	clay variation 2	S	1:3	downhill
21	clay standard	S	1:4	uphill

Table F-1: Overview of calculations in Plaxis 3D for parametric study

F-2 Plaxis 3D results

Bending moments

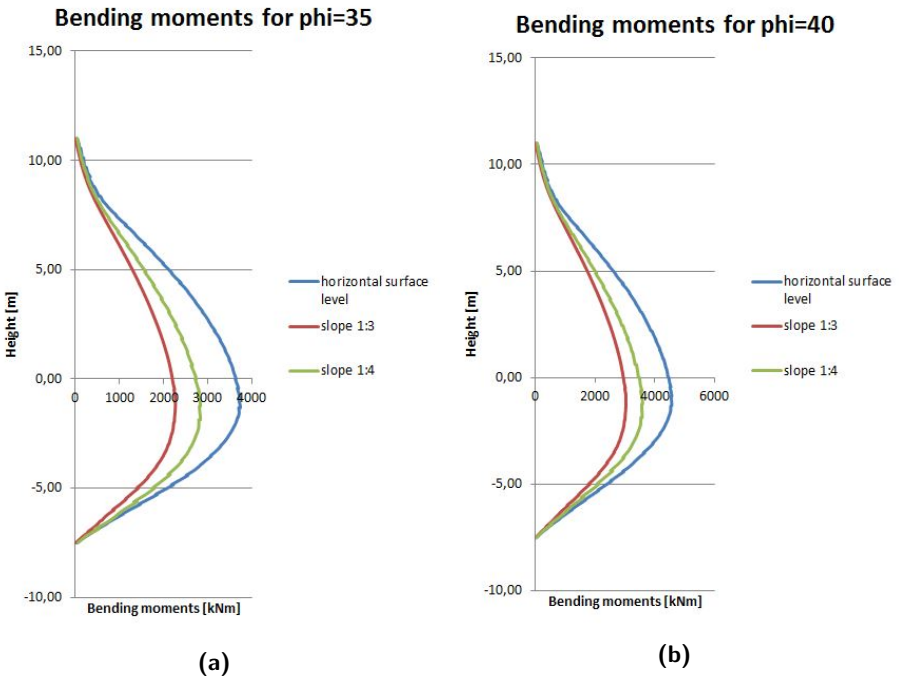

Figure F-1: Maximum bending moments obtained from Plaxis 3D analysis

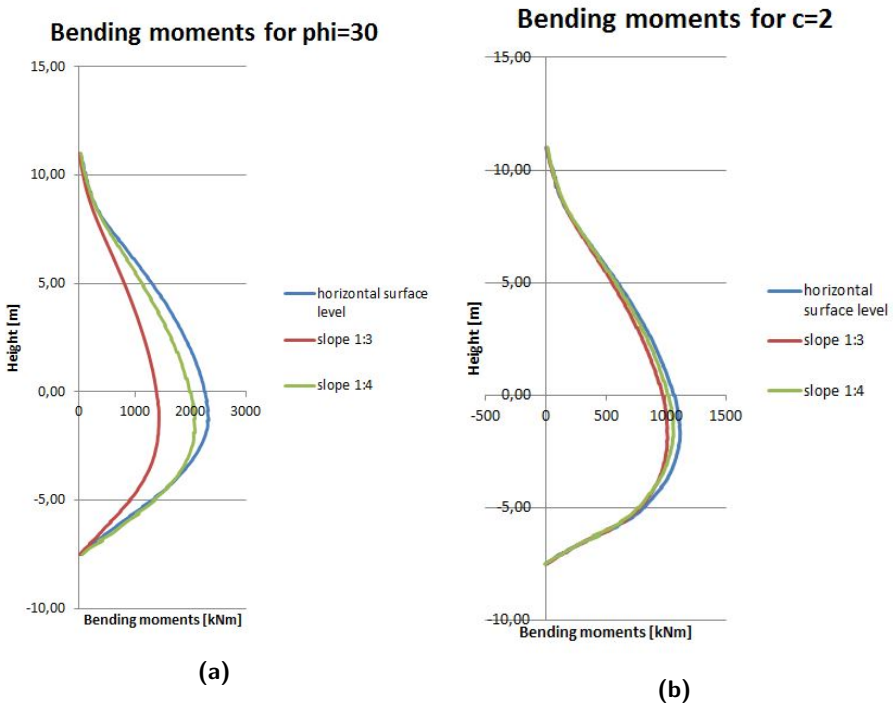

Figure F-2: Maximum bending moments obtained from Plaxis 3D analysis

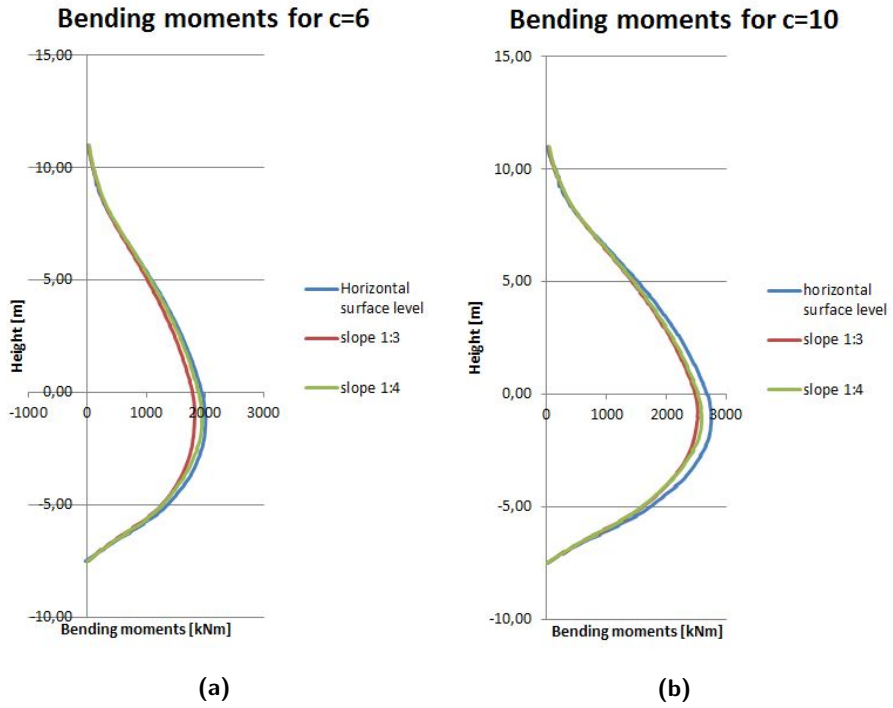

Figure F-3: Maximum bending moments obtained from Plaxis 3D analysis

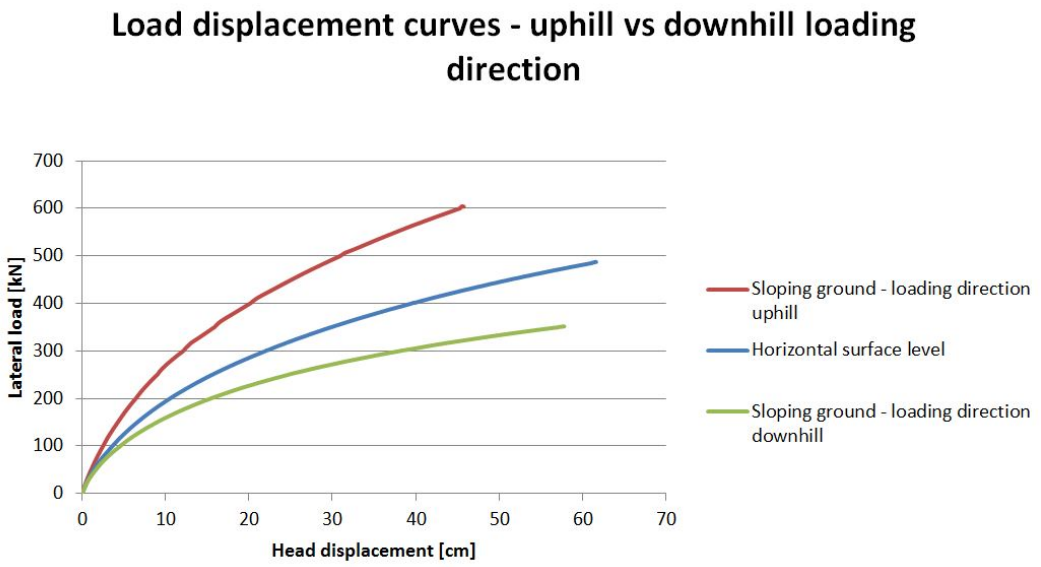

Figure F-4: Load displacement curves of uphill and downhill loading direction for a laterally loaded pile in sand slope

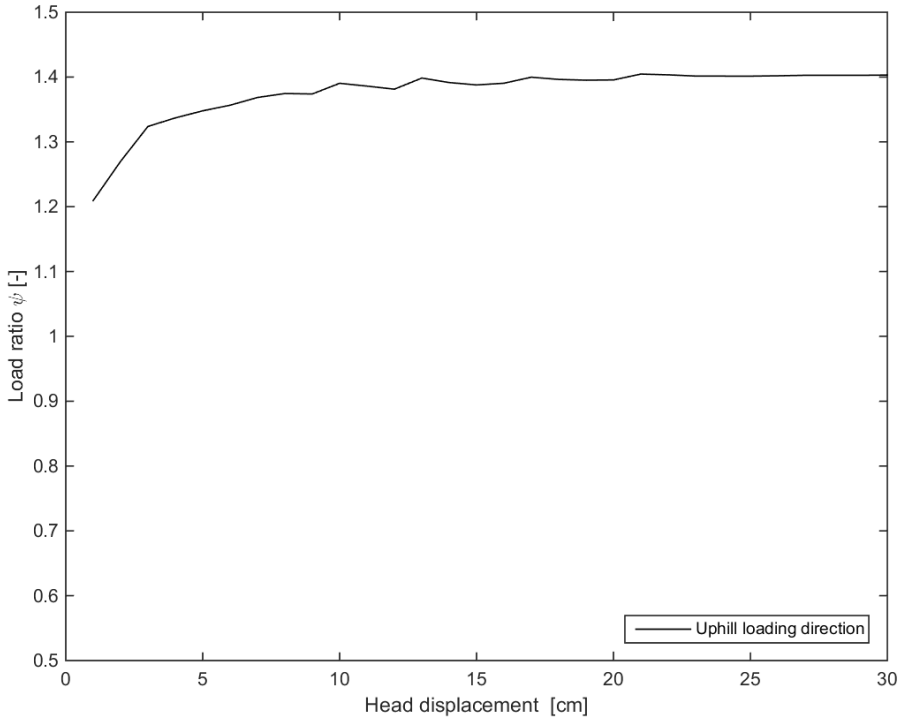

Figure F-5: Load ratio for uphill loading direction for sand, $\phi = 35$, slope 1:4

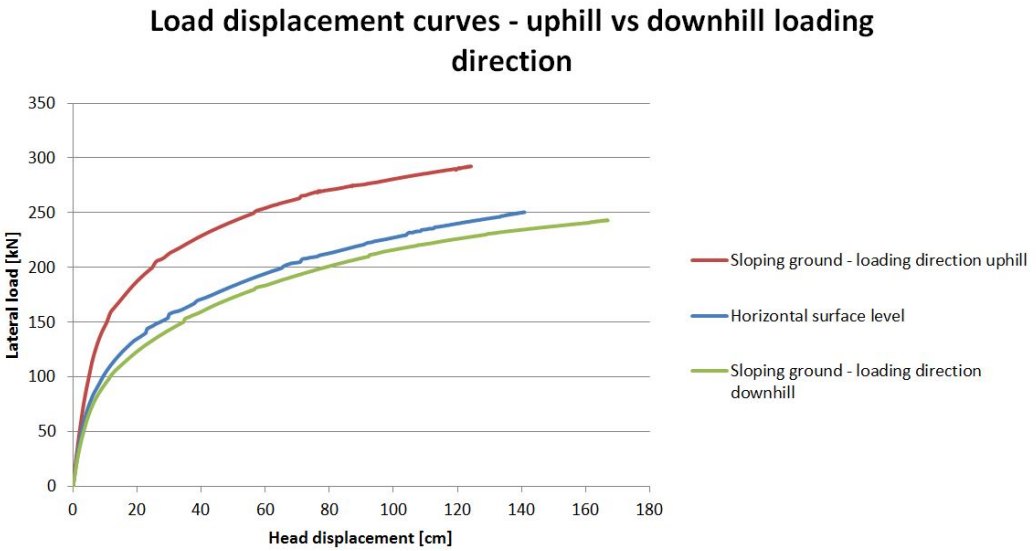

Figure F-6: Load displacement curves of uphill and downhill loading direction for a laterally loaded pile in clay slope

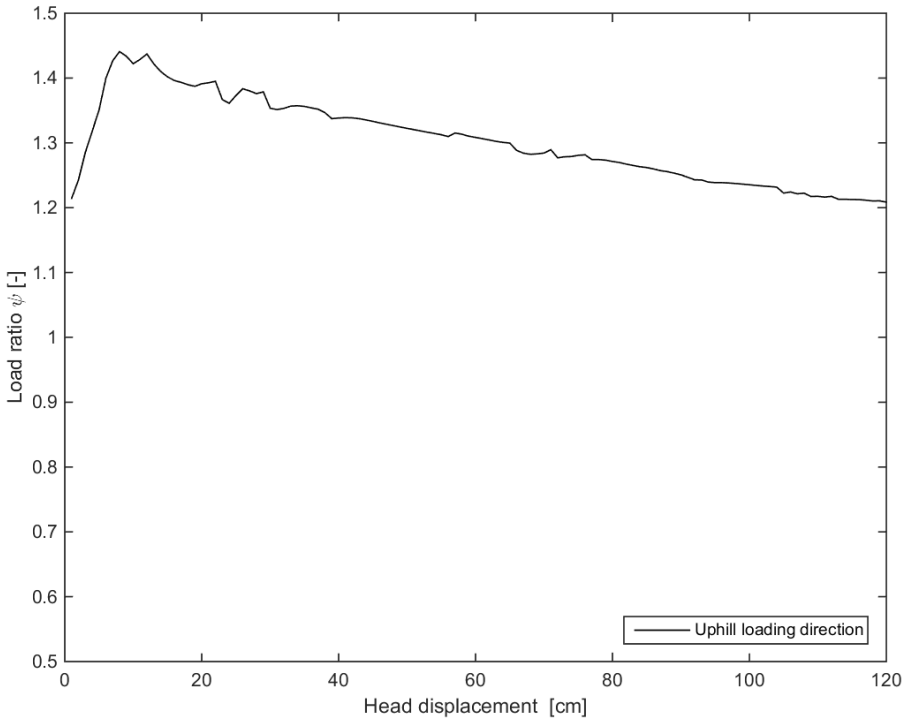

Figure F-7: Load ratio for uphill loading direction for clay, $c = 6$, slope 1:4

P-Y curves

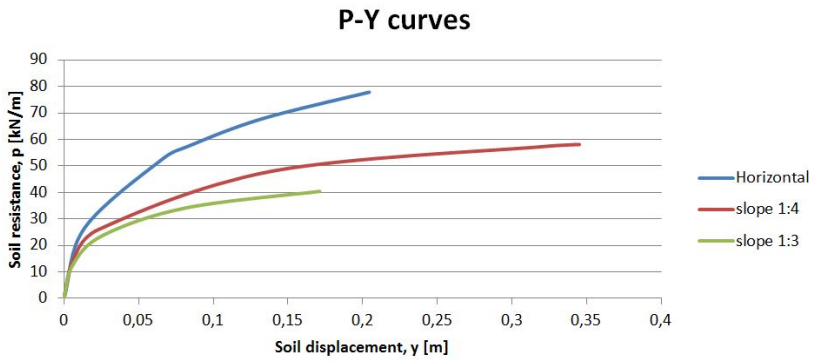

Figure F-8: P-Y curves for sand at z=0 for $\phi = 30^\circ$ obtained from Plaxis 3D analysis

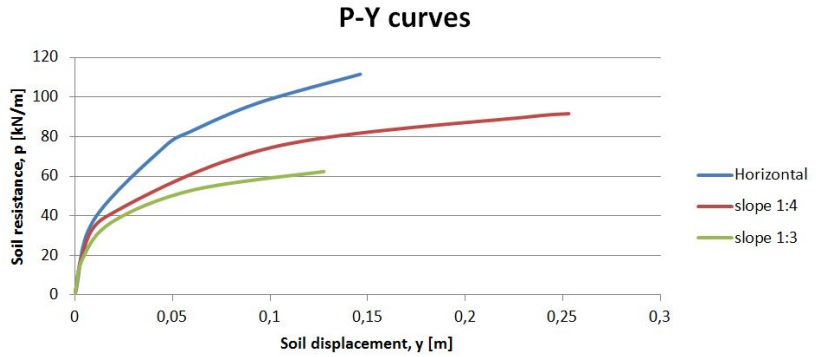

Figure F-9: P-Y curves for sand at z=-1D for $\phi = 30^\circ$ obtained from Plaxis 3D analysis

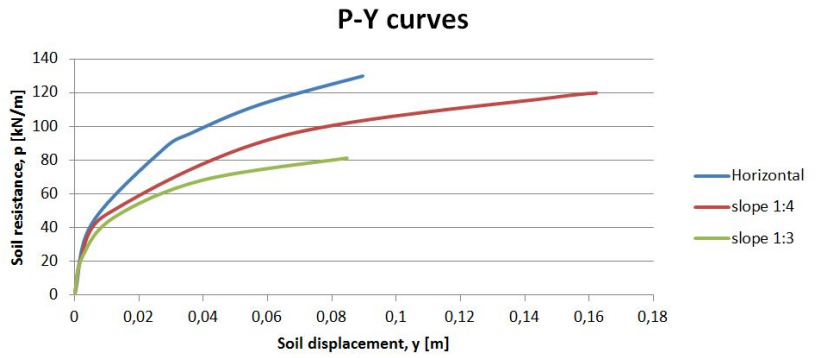

Figure F-10: P-Y curves for sand at z=-2D for $\phi = 30^\circ$ obtained from Plaxis 3D analysis

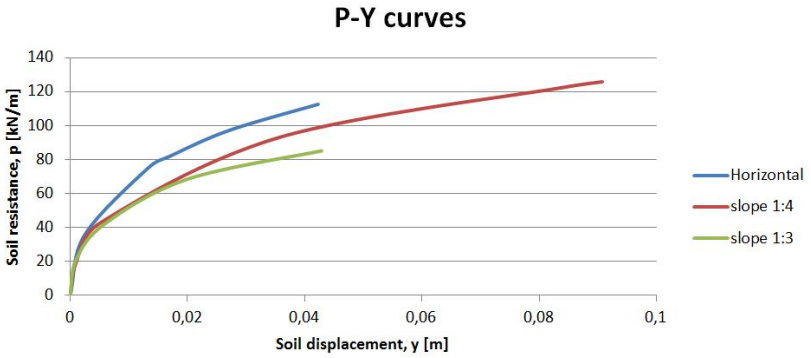

Figure F-11: P-Y curves for sand at z=-3D for $\phi = 30^{\circ}$ obtained from Plaxis 3D analysis

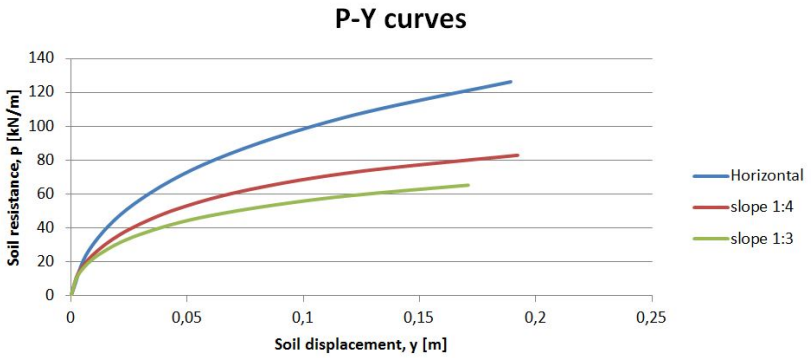

Figure F-12: P-Y curves for sand at z=0 for $\phi = 35^{\circ}$ obtained from Plaxis 3D analysis

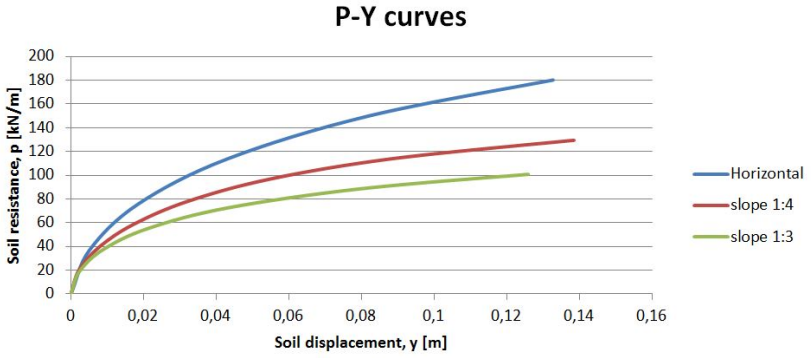

Figure F-13: P-Y curves for sand at z=-1D for $\phi = 35^{\circ}$ obtained from Plaxis 3D analysis

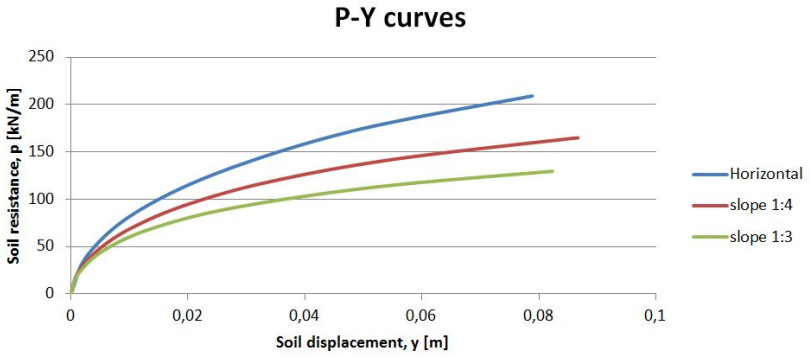

Figure F-14: P-Y curves for sand at z=-2D for $\phi = 35^{\circ}$ obtained from Plaxis 3D analysis

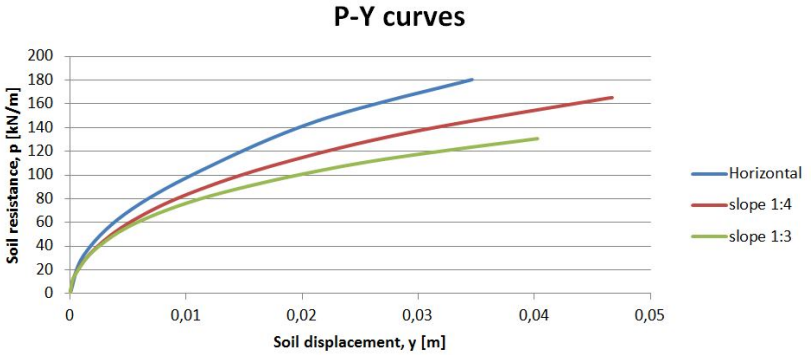

Figure F-15: P-Y curves for sand at z=-3D for $\phi = 35^{\circ}$ obtained from Plaxis 3D analysis

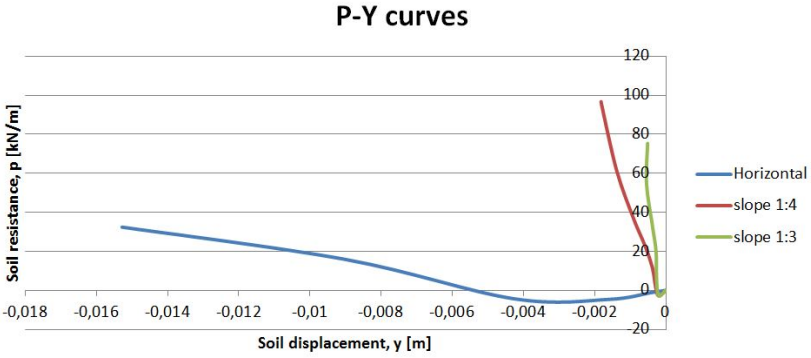

Figure F-16: P-Y curves for sand at z=-4D for $\phi = 35^{\circ}$ obtained from Plaxis 3D analysis

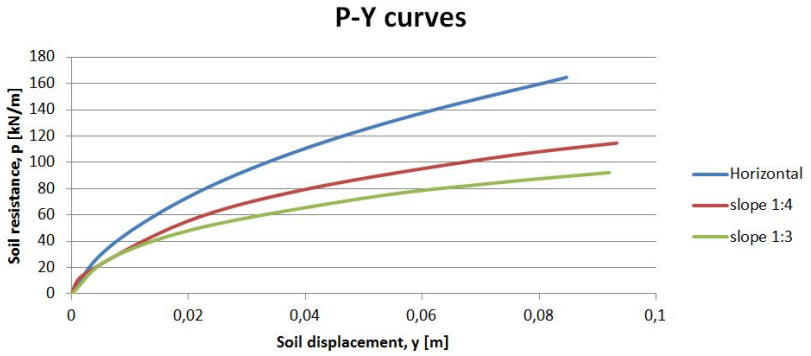

Figure F-17: P-Y curves for sand at z=0 for $\phi = 40^{\circ}$ obtained from Plaxis 3D analysis

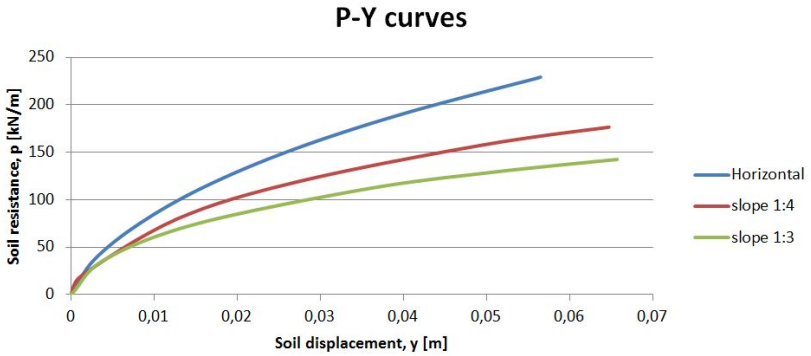

Figure F-18: P-Y curves for sand at z=-1D for $\phi = 40^{\circ}$ obtained from Plaxis 3D analysis

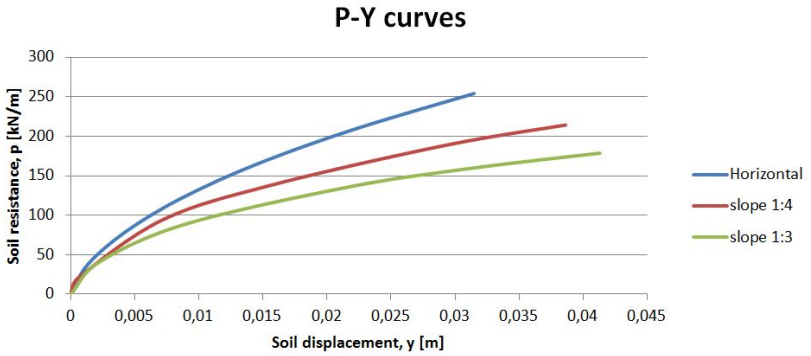

Figure F-19: P-Y curves for sand at z=-2D for $\phi = 40^{\circ}$ obtained from Plaxis 3D analysis

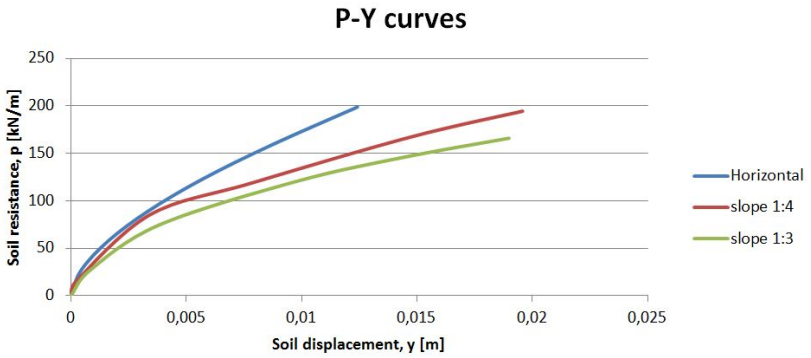

Figure F-20: P-Y curves for sand at z=-3D for $\phi = 40^{\circ}$ obtained from Plaxis 3D analysis

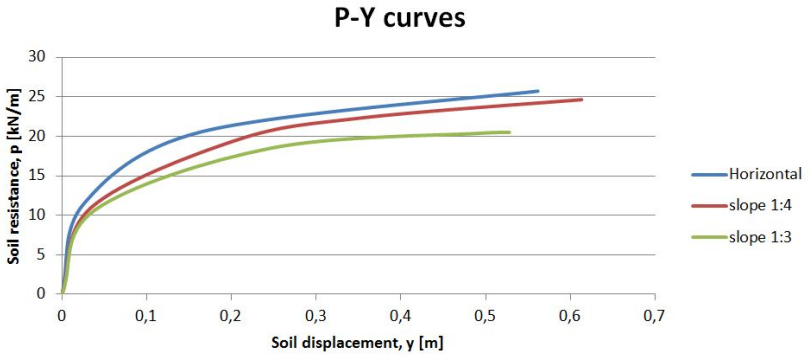

Figure F-21: P-Y curves for clay at z=0 for c=2 obtained from Plaxis 3D analysis

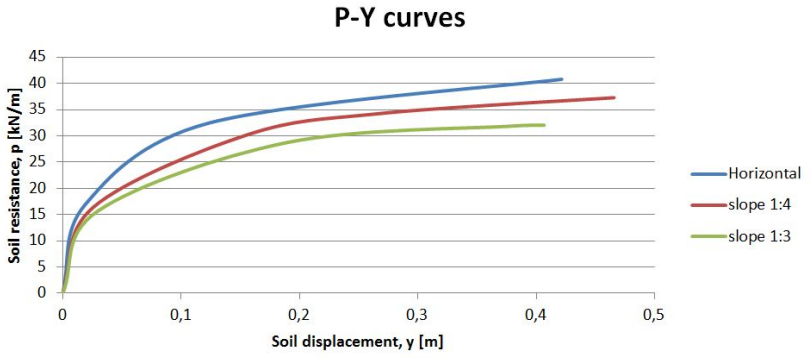

Figure F-22: P-Y curves for clay at z=-1D for c=2 obtained from Plaxis 3D analysis

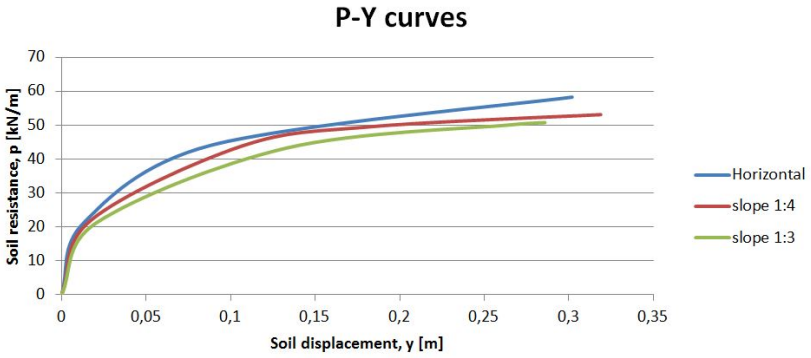

Figure F-23: P-Y curves for clay at z=-2D for c=2 obtained from Plaxis 3D analysis

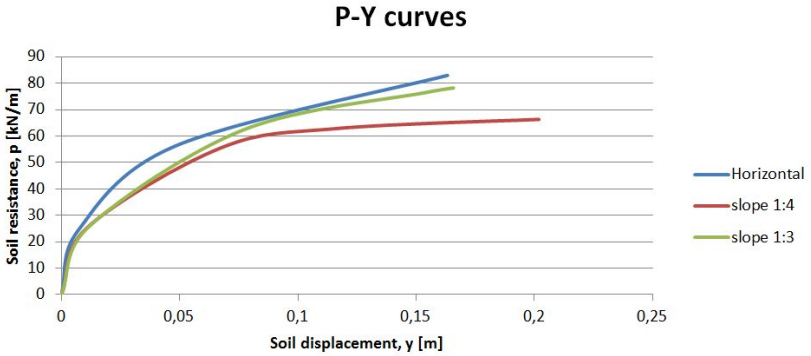

Figure F-24: P-Y curves for clay at z=-3D for c=2 obtained from Plaxis 3D analysis

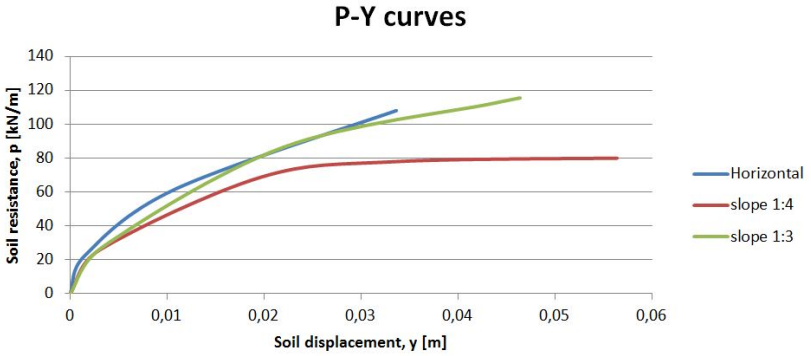

Figure F-25: P-Y curves for clay at z=-4D for c=2 obtained from Plaxis 3D analysis

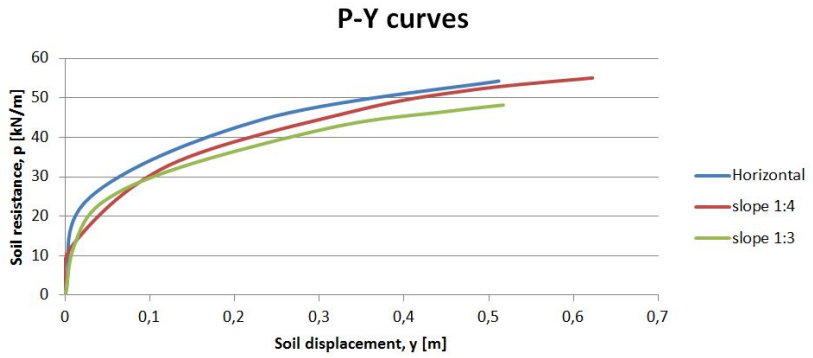

Figure F-26: P-Y curves for clay at z=0 for c=6 obtained from Plaxis 3D analysis

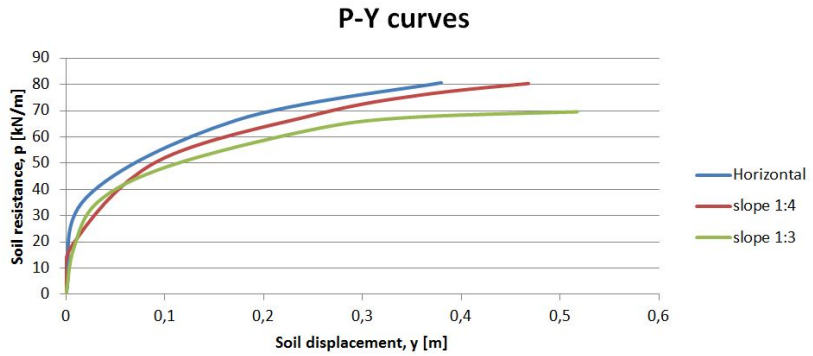

Figure F-27: P-Y curves for clay at z=-1D for c=6 obtained from Plaxis 3D analysis

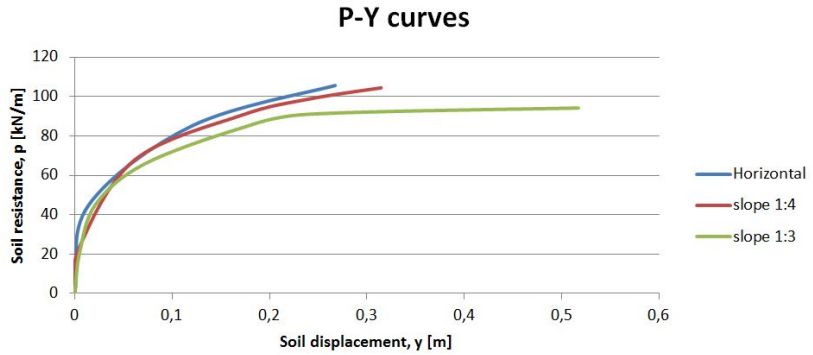

Figure F-28: P-Y curves for clay at z=-2D for c=6 obtained from Plaxis 3D analysis

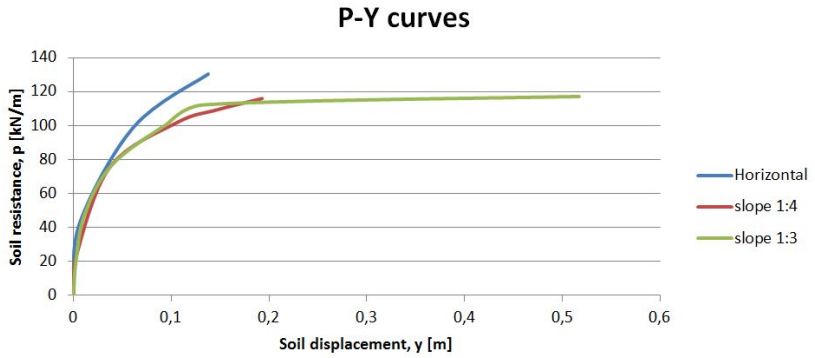

Figure F-29: P-Y curves for clay at z=-3D for c=6 obtained from Plaxis 3D analysis

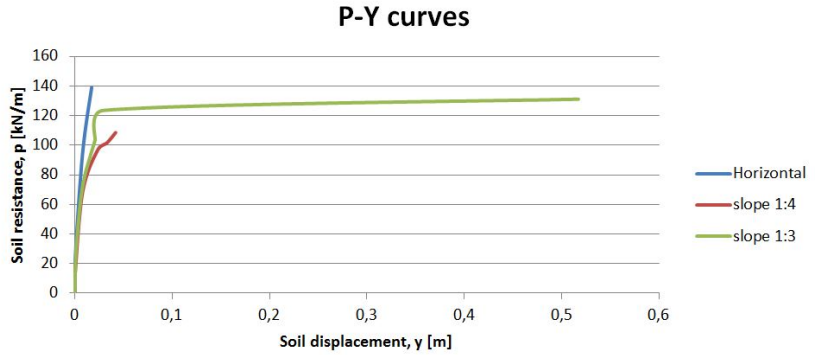

Figure F-30: P-Y curves for clay at z=-4D for c=6 obtained from Plaxis 3D analysis

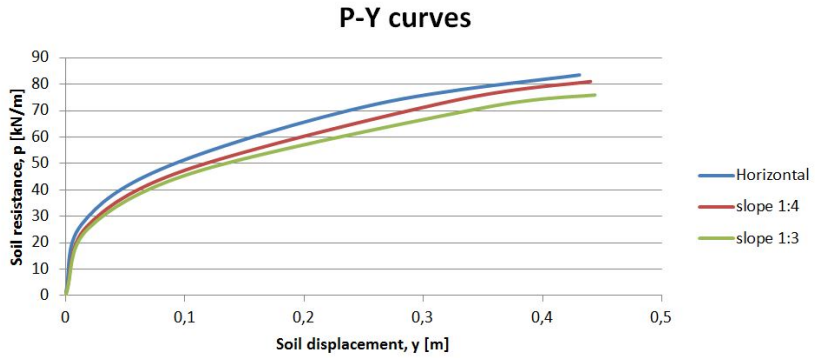

Figure F-31: P-Y curves for clay at z=0 for c=10 obtained from Plaxis 3D analysis

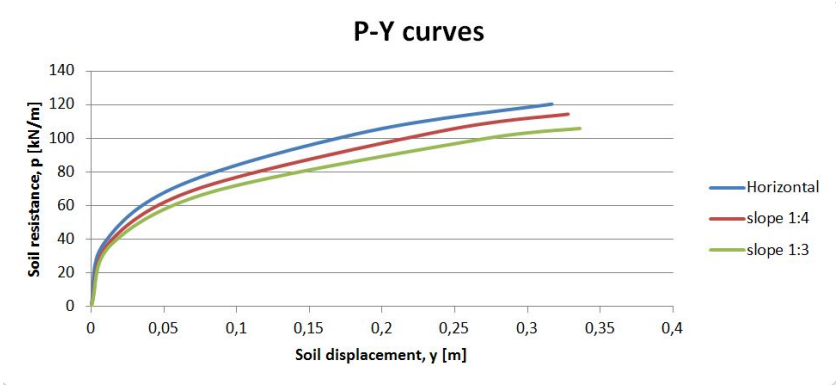

Figure F-32: P-Y curves for clay at z=-1D for c=10 obtained from Plaxis 3D analysis

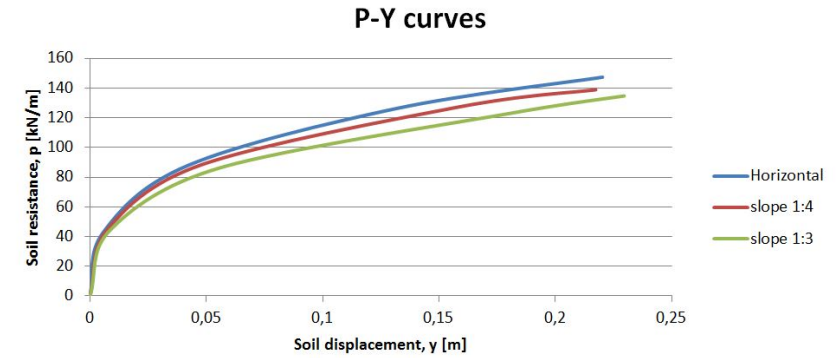

Figure F-33: P-Y curves for clay at z=-2D for c=10 obtained from Plaxis 3D analysis

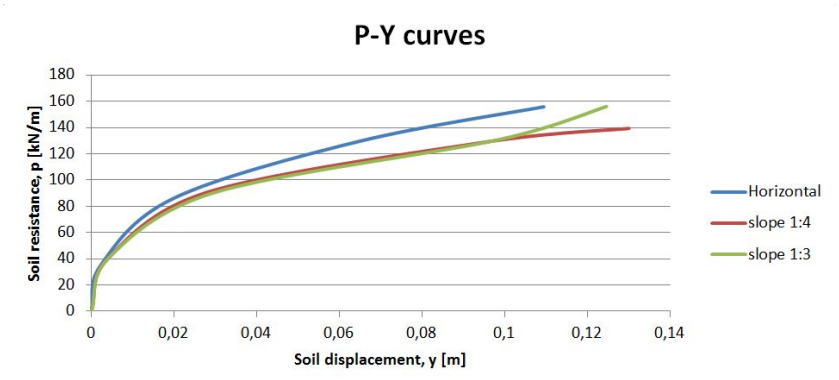

Figure F-34: P-Y curves for clay at z=-3D for c=10 obtained from Plaxis 3D analysis

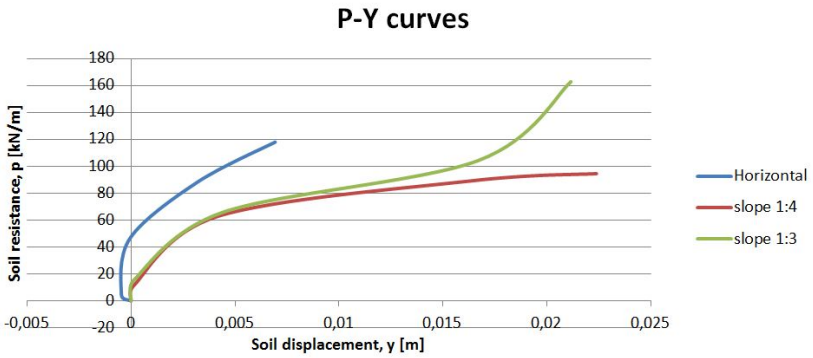

Figure F-35: P-Y curves for clay at z=-4D for c=10 obtained from Plaxis 3D analysis

Illustrations from Plaxis 3D

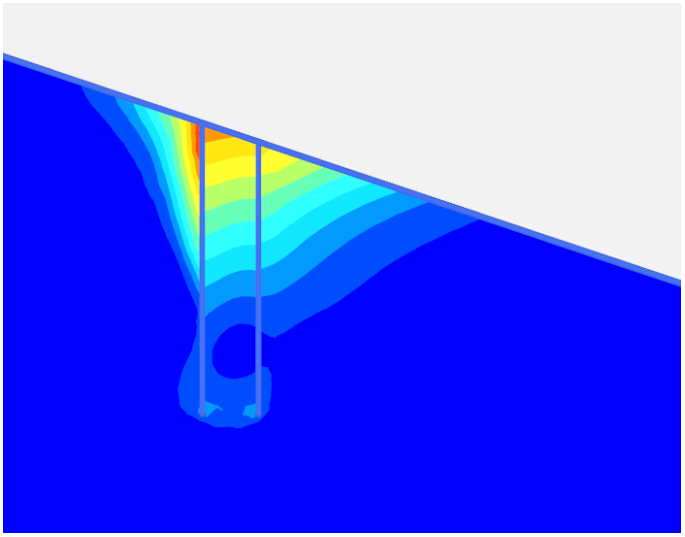

(a)

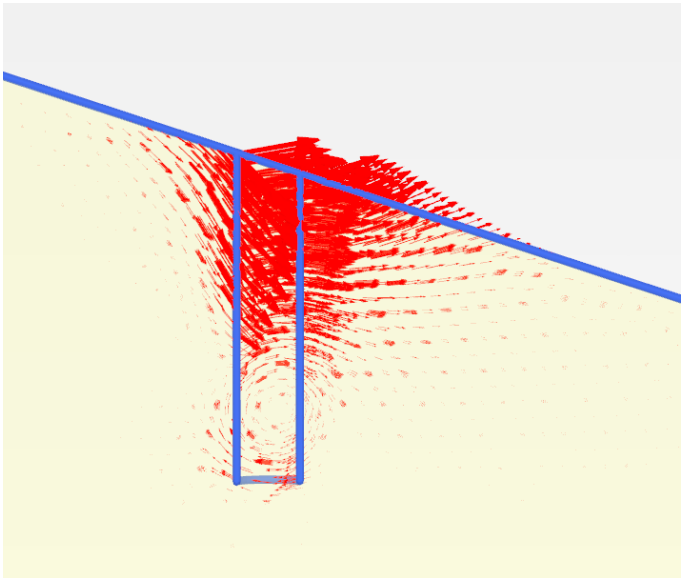

(b)

Figure F-36: Soil failure in Plaxis 3D of sand for soil parameterset of $\phi = 35$ and slope 1:4

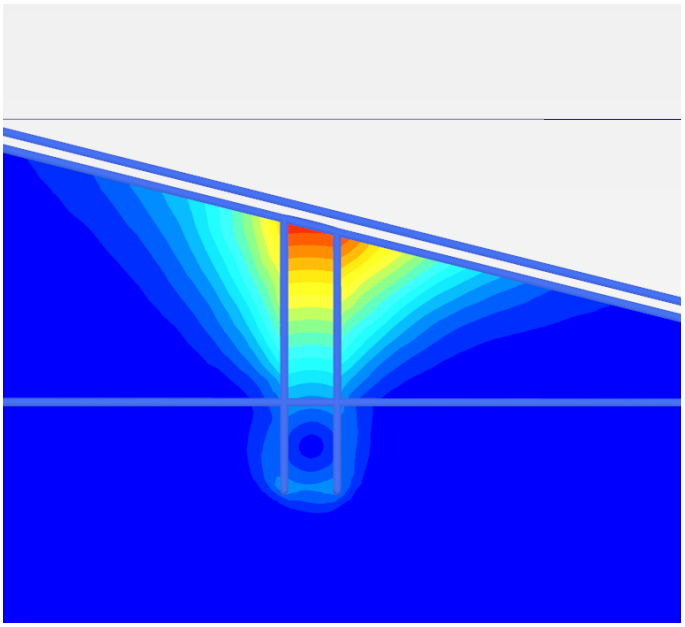

(a)

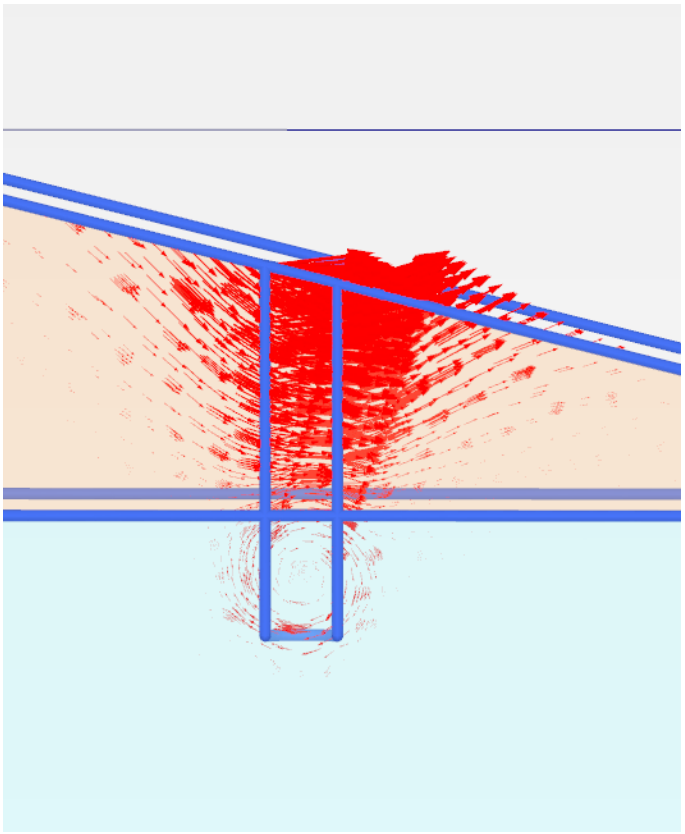

(b)

Figure F-37: Soil failure in Plaxis 3D of clay for soil parameterset of $c = 6$ and slope 1:4

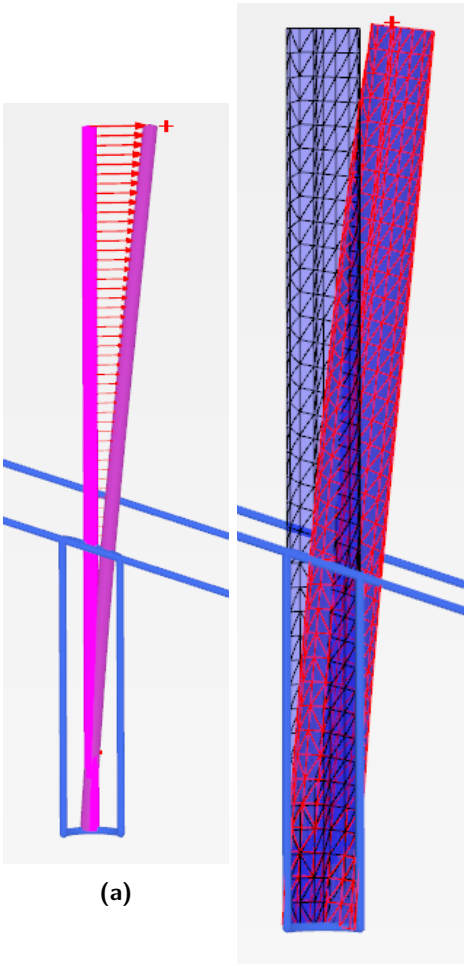

Figure F-38: Displacements of the pile in Plaxis 3D for sand calculation for soil parameterset of $\phi = 35$ and slope 1:4

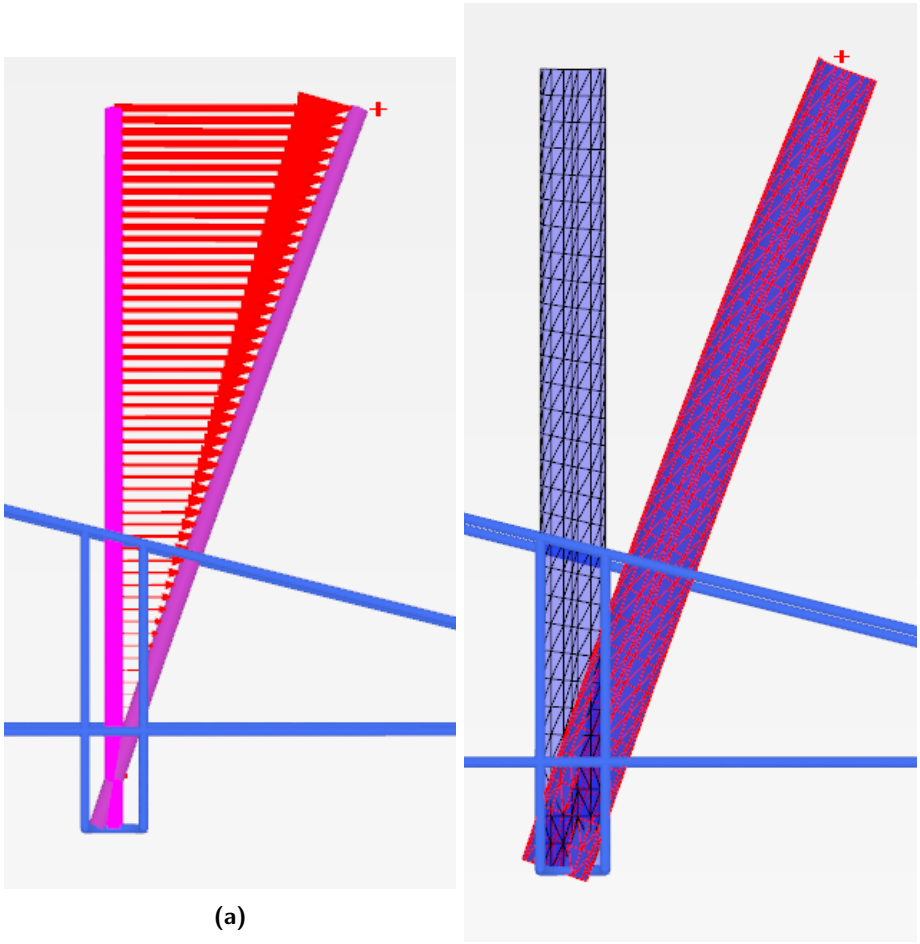

(a) (b)

Figure F-39: Displacements of the pile in Plaxis 3D for clay calculation for soil parameterset of $c = 6$ and slope 1:4

Appendix G

P-Y ratios obtained from Plaxis 3D analysis

Sand

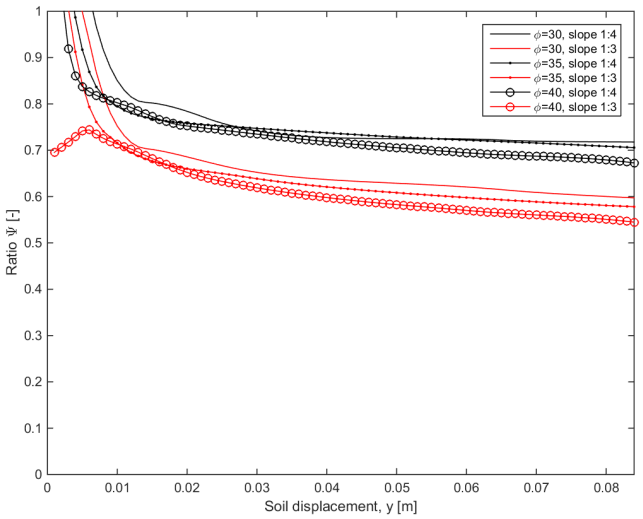

Figure G-1: P-Y ratios at z=0 for sand obtained from Plaxis 3D analysis

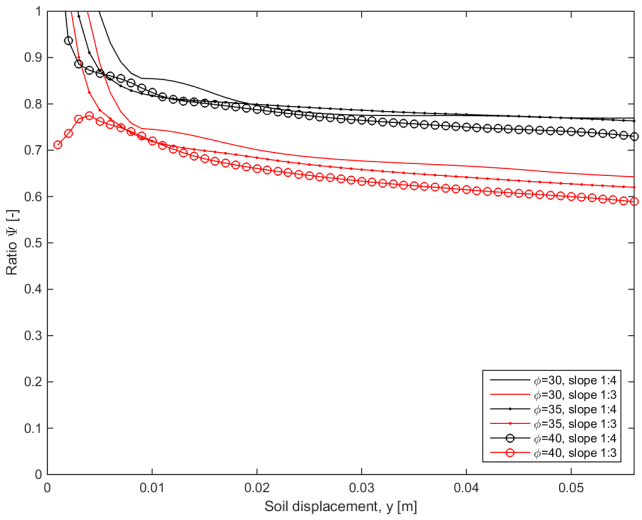

Figure G-2: P-Y ratios at z=-1D for sand obtained from Plaxis 3D analysis

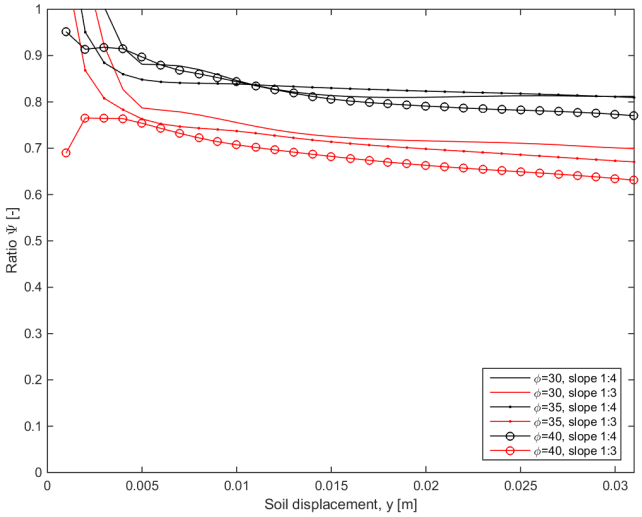

Figure G-3: P-Y ratios at z=-2D for sand obtained from Plaxis 3D analysis

Clay

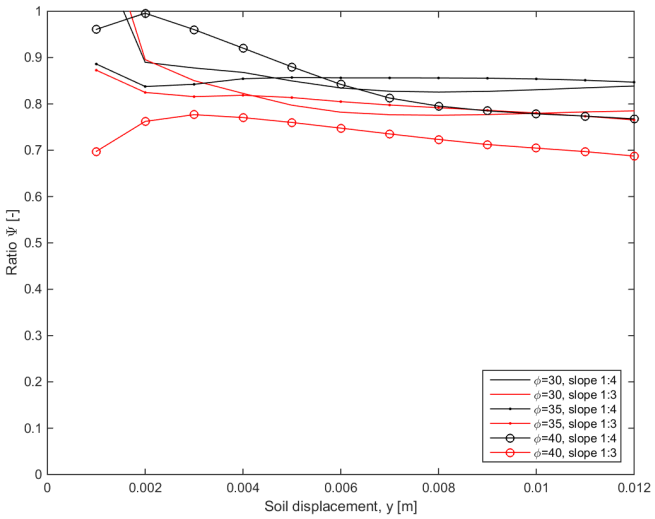

Figure G-4: P-Y ratios at z=-3D for sand obtained from Plaxis 3D analysis

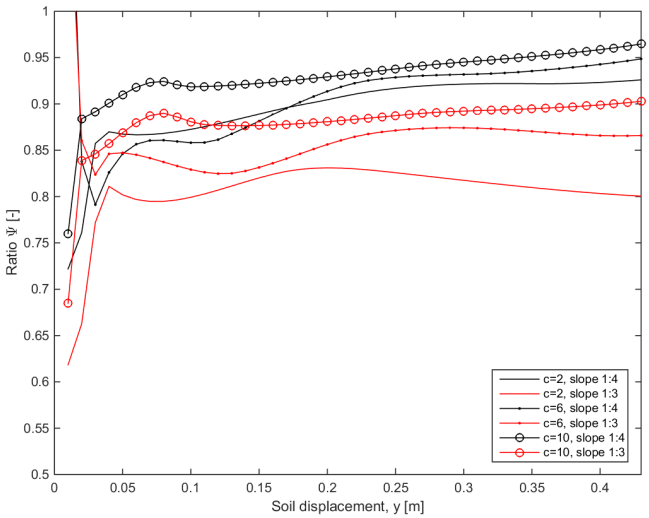

Figure G-5: P-Y ratios at z=0 for clay obtained from Plaxis 3D analysis

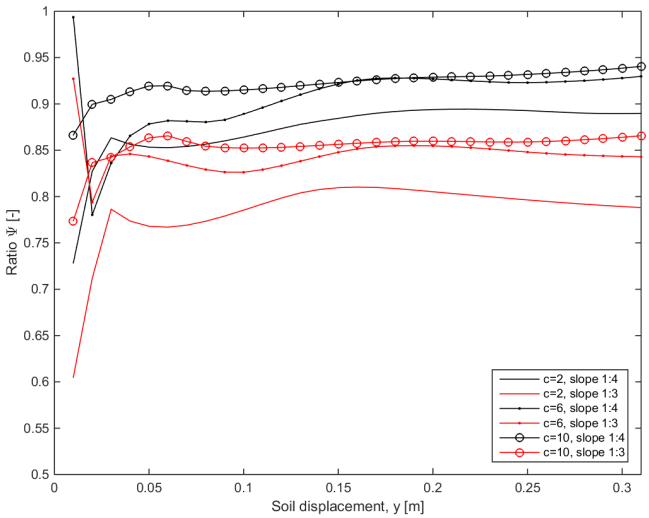

Figure G-6: P-Y ratios at z=-1D for clay obtained from Plaxis 3D analysis

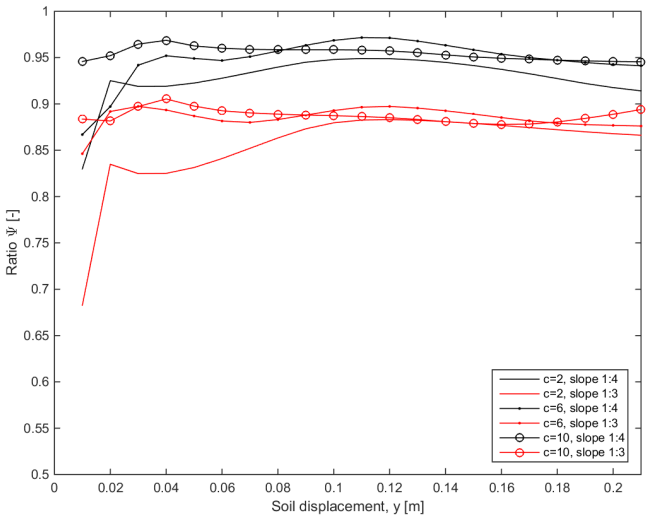

Figure G-7: P-Y ratios at z=-2D for clay obtained from Plaxis 3D analysis

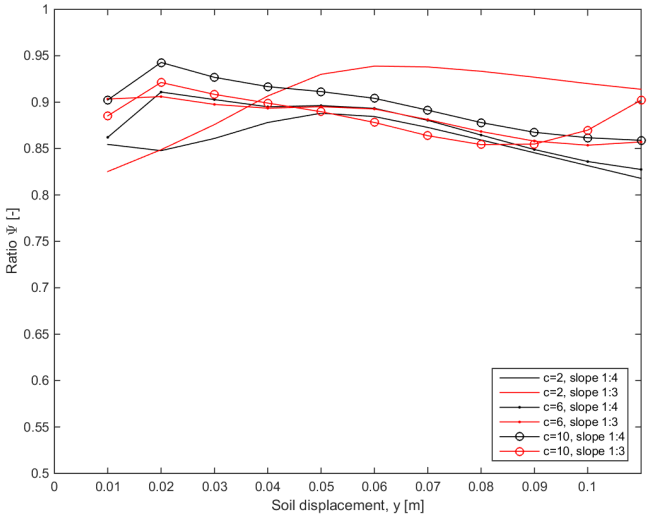

Figure G-8: P-Y ratios at z=-3D for clay obtained from Plaxis 3D analysis

Bibliography

[1] M. A. Gabr and R. H. Borden, "Lateral analysis of piers constructed on slopes," *Journal of Geotechnical Engineering*, vol. 116, no. 12, pp. 1831–1850, 1990.

[2] Mirzoyan, *Lateral resistance of piles at the crest of slopes in sand*. Brigham Young University, 2007 (Master's thesis).

[3] N. Nimityongskul, *Effects of soil slope on lateral capacity of piles in cohesive soils*. Oregon State University, 2010 (Dissertation).

[4] Barker, *Effects of soil slope on lateral capacity of pilesin cohesionless soils*. Oregon State University, 2012 (Master's thesis).

[5] S. Mezazigh and D. Levacher, "Laterally loaded piles in sand: slope effect on p-y reaction curves," *Canadian geotechnical journal*, vol. 35, no. 3, pp. 433–441, 1998.

[6] K. Chae, K. Ugai, and A. Wakai, "Lateral resistance of short single piles and pile groups located near slopes," *International Journal of Geomechanics*, vol. 4, no. 2, pp. 93–103, 2004.

[7] S. Sivapriya and S. Gandhi, "Behaviour of single pile in sloping ground under static lateral load," in *Proceedings of Indian Geotechnical Conference*, pp. 199–202, 2011.

[8] C. Chen and G. Martin, "Effect of embankment slope on lateral response of piles," in *FLAC and numerical modeling in geomechanics: proceedings of the second International FLAC Symposium*, pp. 205–213, A.A. Balkema, 2001.

[9] N. A. Begum and K. Muthukkumaran, "Numerical modeling for laterally loaded piles on a sloping ground," in *Proceedings of the 12th International Conference of International Association for Computer Methods and Advances in Geomechanics,(IACMAG), Goa, India*, pp. 1–6, 2008.

[10] K. Georgiadis and M. Georgiadis, "Undrained lateral pile response in sloping ground," *Journal of geotechnical and geoenvironmental engineering*, vol. 136, no. 11, pp. 1489–1500, 2010.

[11] K. Fleming, A. Weltman, M. Randolph, and K. Elson, *Piling engineering*. CRC Press, 2008.

[12] L. C. Reese, W. M. Isenhower, and S. T. Wang, *Analysis and design of shallow and deep foundations*. Wiley Hoboken, NJ, 2006.

[13] J. Ruigrok, *Laterally Loaded Piles, Models and Measurements*. Delft University of Technology, 2010 (Master's thesis).

[14] K. Georgiadis and M. Georgiadis, "Development of p-y curves for undrained response of piles near slopes," *Computers and Geotechnics*, vol. 40, pp. 53–61, 2012.

[15] K. Georgiadis, M. Georgiadis, and C. Anagnostopoulos, "Lateral bearing capacity of rigid piles near clay slopes," *Soils and Foundations*, vol. 53, no. 1, pp. 144–154, 2013.

[16] J. L. Bijnagte and H. L. Luger, *D-Pile group version 5.1, 3D modelling of single piles and pile groups*. Deltares, 2010.

[17] http://www.sbrcurnet.nl/over-sbr/wie-zijn-we. [Online; accessed 10-January-2015].

[18] H. Davidson, *Laterally loaded drilled pier research*, vol. 1. The Institute, 1982.

[19] L. C. Reese and W. F. Van Impe, *Single piles and pile groups under lateral loading*. CRC Press, 2000.

[20] M. Hetenyi, *Beams on elastic foundation*. The University of Michigan Press, Ann Arbor, Michigan, 1946.

[21] L. C. Reese and H. Matlock, *Non-dimensional solutions for laterally-loaded piles with soil modulus assumed proportional to depth*. Association of Drilled Shaft Contractors, 1956.

[22] "API RP 2A-WSD, Recommended practice for planning, designing and constructing fixed offshore platforms–working stress design–," 21st edition, 2000.

[23] M. F. Randolph and G. Houlsby, "The limiting pressure on a circular pile loaded laterally in cohesive soil," *Geotechnique*, vol. 34, no. 4, pp. 613–623, 1984.

[24] Blum, *Wirtschaftliche dalbenformen und deren berechnung*. Bautechnik, Heft 5, 1932.

[25] J. B. Hansen and N. Christensen, *The Ultimate Resistance of Rigid Piles Against Transversal Forces; Model Tests with Tranversally Loaded Rigid Piles in Sand*. Geoteknisk Institut, 1961.

[26] B. B. Broms, "Lateral resistance of piles in cohesive soils," *Journal of the Soil Mechanics and Foundation division*, vol. 90, no. 2, pp. 123–156, 1964.

[27] R. Frank, J. Brangratz, and M. Kutniak, "Programme de calcul d'un pieu isolé soumis à des efforts de flexion en tê et àdes poussées latérales de sol," *Laboratoire des Ponts et Chaussées, Paris*, p. 69, 1990.

[28] H. Matlock, "Correlations for design of laterally loaded piles in soft clay," *Offshore Technology in Civil Engineering's Hall of Fame Papers from the Early Years*, pp. 77–94, 1970.

[29] L. C. Reese, W. R. Cox, and F. D. Koop, "Analysis of laterally loaded piles in sand.," in *Offshore Technology in Civil Engineering's Hall of Fame Papers from the Early Years*, pp. 95–105, ASCE, 1974.

[30] L. C. Reese, W. M. Isenhower, S.-T. Wang, and J. A. Arrellaga, *LPLILE Plus – Version 5. A program for the analysis of piles and drilled shafts under lateral loads*. ENSOFT, Austin, Tex, 2004.

[31] D. Wu, B. B. Broms, and V. Choa, "Design of laterally loaded piles in cohesive soils using p-y curves," *Soils and foundations*, vol. 38, no. 2, pp. 17–26, 1998.

[32] J. M. Duncan, L. T. Evans Jr, and P. S. Ooi, "Lateral load analysis of single piles and drilled shafts," *Journal of geotechnical engineering*, vol. 120, no. 6, pp. 1018–1033, 1994.

[33] D. S. Christensen, *Full scale static lateral load test of a 9 pile group in sand*. Brigham Young University, 2006 (Master's thesis).

[34] R. Brinkgreve, E. Engin, and H. Engin, "Validation of empirical formulas to derive model parameters for sands," *Numerical Methods in Geotechnical Engineering Numge*, pp. 137–142, 2010.

[35] R. Brinkgreve and W. Swolfs, *Plaxis 3D foundation version 2 user's manual*. Plaxis 3D B.V., Netherlands, 2007.

[36] D. A. Brown and C. F. Shie, "Some numerical experiments with a three dimensional finite element model of a laterally loaded pile," *Computers and Geotechnics*, vol. 12, no. 2, pp. 149–162, 1991.

[37] "MATLAB R1014b, Interactive Curve and Surface Fitting." http://nl.mathworks.com/help/curvefit/interactive-curve-and-surface-fitting-.html, 2014. [Online; accessed 7-January-2015].

[38] *D-Sheet Piling 9.3, Design of diaphragm and sheet pile walls, User Manual*. Deltares, 2013.

[39] L. Ménard, G. Bourdon, and M. Gambin, "Methode generale de calcul d'un rideau ou d'un pieu sollicite horizontalement en fonction des resultats pressiometriques.," *Sols Soils*, vol. 6, no. 22/23, 1971.

[40] *Plaxis 3D, Reference Model*. Plaxis 3D B.V., 2013.

[41] *Plaxis 3D, Material Models Manual*. Plaxis 3D B.V., 2013.

[42] T. Schanz, P. Vermeer, and P. Bonnier, "The hardening soil model: formulation and verification," *Beyond 2000 in computational geotechnics*, pp. 281–296, 1999.

[43] J. Dos Santos, A. Correia, *et al.*, "Reference threshold shear strain of soil. its application to obtain an unique strain-dependent shear modulus curve for soil.," in *Proceedings of the Fifteenth International Conference on Soil Mechanics and Geotechnical Engineering, Istanbul, Turkey, 27-31 August 2001. Volumes 1-3.*, pp. 267–270, AA Balkema, 2001.

Glossary

Nomenclature

β	Angle of the inclined plane with the vertical	$[°]$
ϵ_1	Vertical strain	$[-]$
γ	Unit weight of the soil	$[kn/m^3]$
$\gamma_{0.7}$	Shear strain at which $G_s = 0.722G_0$	$[-]$
κ	Reduction factor for shearing resistance along the face of the pile	$[-]$
$\lambda_1 - \lambda_2$	Parameters in the analytical derivation of Gabr and Borden	$[-]$
ν_{ur}	Poisson's ratio for unloading-reloading	$[-]$
Ω	Angle of the side flanks of the failure wedge	$[°]$
ϕ	Internal friction angle of the soil	$[°]$
ψ	Angle of dilatancy	$[°]$
σ_f	Failure stress	$[kN/m^2]$
τ_f	Failure shear stress	$[kN/m^2]$
θ	Angle of the slope	$[°]$
$A(z)$	Incremental area in derivation of Mirzoyan	$[m^2]$
c	Cohesion of the soil	$[kN/m^2]$
c_a	Average undrained shear strength	$[kN/m^2]$
D	Diameter of the pile	$[m]$
D_2	Width of the wedge in derivation of Mirzoyan	$[m]$
e	Height of load application above surface level	$[m]$
E_pI_p	Bending stiffness of the pile	$[kNm^2]$
E_{50}^{ref}	Secant stiffness in standard drained triaxial test	$[kN/m^2]$
E_{oed}^{ref}	Tangent stiffness for primary oedometer loading	$[kN/m^2]$
E_{py}	Stiffness of the soil	$[kN/m^2]$
E_{ur}^{ref}	unloading/ reloading stiffness at engineering strains	$[kN/m^2]$
F_L	Force that resists the lateral movement of the pile	$[kN]$
f_L	Lateral resistance per unit depth of the pile due to plane EABF	$[kN/m]$
F_p	Lateral load acting on the pile	
f_s	Lateral resistance per unit depth of the pile due to plane EAD and FBC	$[kN/m]$
G_0	Reference shear modulus at very small strains	$[kN/m^2]$

H	Height of the wedge along the pile	$[m]$
H_u	Lateral bearing capacity	$[kN]$
$J_1 - J_6$	Parameter in the analytical derivation of Mirzoyan	$[-]$
$K1 - K2$	Parameters in the analytical derivation of Gabr and Borden	$[-]$
K_0	Coefficient of earth pressure at rest	$[-]$
K_a	Coefficient of active earth pressure	$[-]$
$K_{p\phi}$	Parameter in the analytical derivation of Gabr and Borden	$[-]$
K_{pc}	Parameter in the analytical derivation of Gabr and Borden	$[-]$
L	Embedded pile length	$[m]$
M	Bending moment of the pile	$[kNm]$
m	Power for stress-level dependency of stiffness in the $HSsmall$ model	$[-]$
N	Normal force acting on the failure plane of the assumed wedge	$[kN]$
p	Soil reaction per unit length	$[kN/m]$
p^{ref}	Reference stress	
p_u	Ultimate resistance per unit length along the pile	$[kN/m]$
P_x	Axial load on the pile	$[kN]$
Q	Distributed load along the length of the pile	$[kN/m]$
q	Deviatoric stress	$[kN/m^2]$
q_a	Asymptotic deviatoric stress	$[kN/m^2]$
q_f	Ultimate deviatoric stress	$[kN/m^2]$
R_f	Failure ratio of the deviatoric stress	$[-]$
S	Slope of the elastic curve defined by the axis of the pile	$[^\circ]$
$S_{1\phi} - S_{3\phi}$	Parameters in the analytical derivation of Gabr and Borden	$[-]$
$S_{1c} - S_{3c}$	Parameters in the analytical derivation of Gabr and Borden	$[-]$
T	Friction force acting on the failure plane of the assumed wedge	$[kN]$
V_v	Shear force in the pile	$[kN]$
W	Weight of the assumed failure wedge	$[kN]$
X	Distance between the pile and the crest in derivation of Mirzoyan	$[m]$
x_z	Width of the wedge in derivation of Mirzoyan	$[m]$
y	Lateral deflection of the pile	$[m]$
z_0	Depth of rotation	$[m]$
$Z_1 - Z_2$	Parameter in the analytical derivation of Mirzoyan	$[-]$
P	Actual lateral soil resistance at depth h	$[kN/m]$